PHYSICAL OCEANOGRAPHIC MEASUREMENTS IN THE KLONDIKE AND BURGER SURVEY AREAS OF THE CHUKCHI SEA: 2008 - 2010

Prepared for

ConocoPhillips, Inc.
P.O. Box 100360
Anchorage, AK 99510-0360

Shell Exploration & Production Company
3601 C Street, Suite 1334
Anchorage, AK 99503

and

Statoil USA E&P, Inc.
2700 Gambell Street
Anchorage, AK 99507

FINAL REPORT

Prepared by

Thomas Weingartner, Seth Danielson, Liz Dobbins, and Rachel Potter

Institute of Marine Science
University of Alaska
Fairbanks, AK 99775

November 2011

Introduction

The Chukchi and Beaufort seas are the northernmost shelves bordering Alaska. Although properly a part of the western Arctic Ocean, both shelves are linked, atmospherically and oceanographically, to the Pacific Ocean. These connections profoundly influence the wind and wave regimes, the seasonal distribution of sea ice, the regional hydrologic cycle, and the water masses and circulation characteristics of the Chukchi shelf (**Figure 1**). The atmospheric connection is primarily via the Aleutian Low, whose time-varying position and strength and interactions with polar air masses affects regional meteorological conditions. The oceanographic link is via the mean northward flow through Bering Strait, which draws water from the Bering Sea shelf and basin, and which is sustained by a large-scale pressure gradient between the Pacific and Atlantic oceans [*Coachman et al.*, 1975; *Aagaard et al.*, 2006].

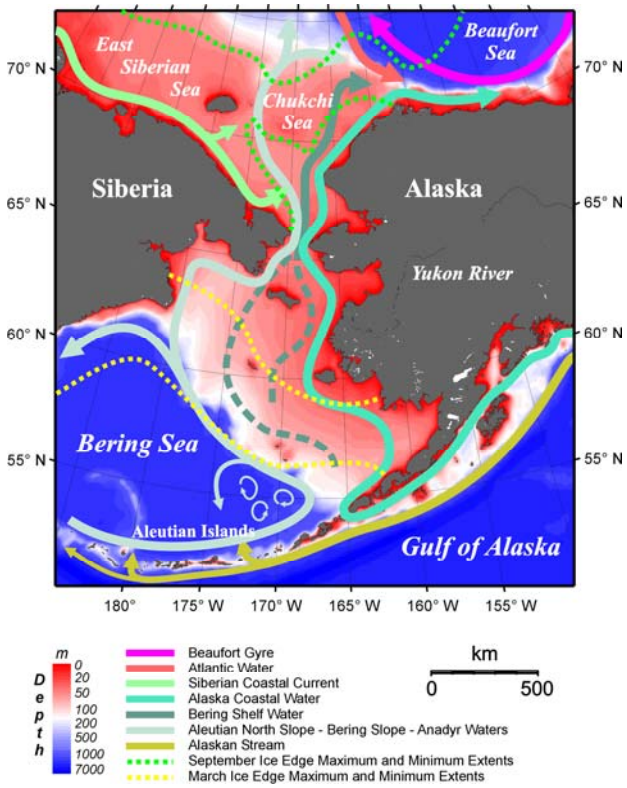

Figure 1. Schematic circulation map of the Bering-Chukchi-Beaufort shelves.

The northward flux of mass, heat, nutrients, carbon, and organisms through the strait bequeath the Chukchi shelf with physical and ecological characteristics that are unique among arctic shelves. For example, the spring retreat of ice occurs earlier and fall ice formation is delayed in comparison to most other arctic shelves because of the northward heat flux through the strait. *Woodgate et al*. [2006] estimate that summer Pacific waters provide a heat source capable of melting nearly the entire (~640,000 km^2) 2-m thick ice cover of the Chukchi Sea and *Shimada et al.* [2006] contend that this flux may be an important source of interannual variability in the ice cover. Similarly, the enormous biological productivity of this shelf [*Walsh et al.*, 1989; *Grebmeier and McRoy*, 1989; *Springer and McRoy*, 1993], including its ability to support large and diverse marine mammal populations, is due to the carbon and nutrient loads carried through Bering Strait.

The water properties of the strait throughflow reflect the time-varying output of physical processes occurring over the Bering shelf and northern North Pacific. These fluxes are a result of the net effects of upwelling from the deep Bering Sea basin and areally integrated heat and freshwater fluxes [*Aagaard et al.*, 2006], including the freezing and melting of sea ice [*Danielson et al.*, 2006], river runoff, atmospheric moisture and heat fluxes, and heat and freshwater contributions from the Gulf of Alaska [*Weingartner et al.*, 2005a], all of which ultimately affect the heat and salt budgets of the Chukchi Sea shelf [*Coachman et al*., 1975; *Woodgate et al.*, 2005b]. The remainder of the introduction summarzies our present understanding of the northeast Chukchi Sea shelf.

Much of our understanding of the Chukchi shelf derives from the early syntheses of the modeling and theoretical work of [*Gawarkiewicz and Chapman*, 1995], and the sea-ice studies of *Muench et al*. [1991], *Liu et al*. [1994], and.

Mean Circulation

The shallow (~50m) Chukchi Sea shelf extends ~800 km northward from Bering Strait to the shelfbreak at about the 200 m isobath. The mean flow over much of the shelf is northward *Weingartner and Proshutinsky* [1998], *Weingartner et al.* [1998], *Weingartner et al*. [2005] due to the Pacific-Arctic pressure gradient and opposes the prevailing winds, which are from the northeast This pressure gradient propels the Bering Strait throughflow along three principal pathways that are associated with distinct bathymetric features (**Figure 2**); Herald Valley, the Central Channel, and Barrow Canyon. Herald Shoal separates Herald Valley from the Central Channel, and Hanna Shoal is between Barrow Canyon and the Central channel. The recent MMS Chukchi Sea lease sales lie on the northeast shelf between the Central Channel and Barrow Canyon and south of Hanna Shoal (**Figure 2**).

As sketched in **Figure 1**, a western branch flows northwestward from the strait and exits the shelf through Herald Valley [*Coachman et al*., 1975; *Walsh et al.*, 1989; *Hansell et al.*, 1993]. While most of this outflow probably descends through Herald Valley, some of it may spread eastward across the central shelf. A second branch flows northward through the Central Channel *Paquette and Bourke* [1974], *Weingartner et al.* [2005b] and then probably splits; with some water continuing eastward toward the Alaskan coast along the south flank of Hanna Shoal while the remainder flows northeastward toward the continental slope [*Johnson* 1989; *Weingartner and Proshutinsky*, 1998; *Münchow and Carmack*, 1997] Some of this water likely rounds the northern flank of Hanna Shoal and then turns southward toward the head of Barrow Canyon *Winsor and Chapman*, 2002; *Spall*, 2007]. The third branch flows northeastward along the Alaskan coast towards Barrow Canyon at the junction of the Chukchi and Beaufort shelves [*Mountain et al.* 1976; *Paquette and Bourke*, 1981; *Ahlnäes and Garrison*, 1984]. In summer this flow includes the northward extension of the Alaskan Coastal Current (ACC) that originates south of Bering Strait [*Aagaard et al.*, [1985], *Aagaard* [1988],*Münchow et al.* 2000]. At the head of Barrow Canyon the ACC is joined by waters flowing eastward from the central shelf *Weingartner et al*. [2005], with the merged flow then continuing downcanyon as a narrow, but strong, coastal jet *Aagaard and Roach* [1990], *Pickart et al.* [2005].

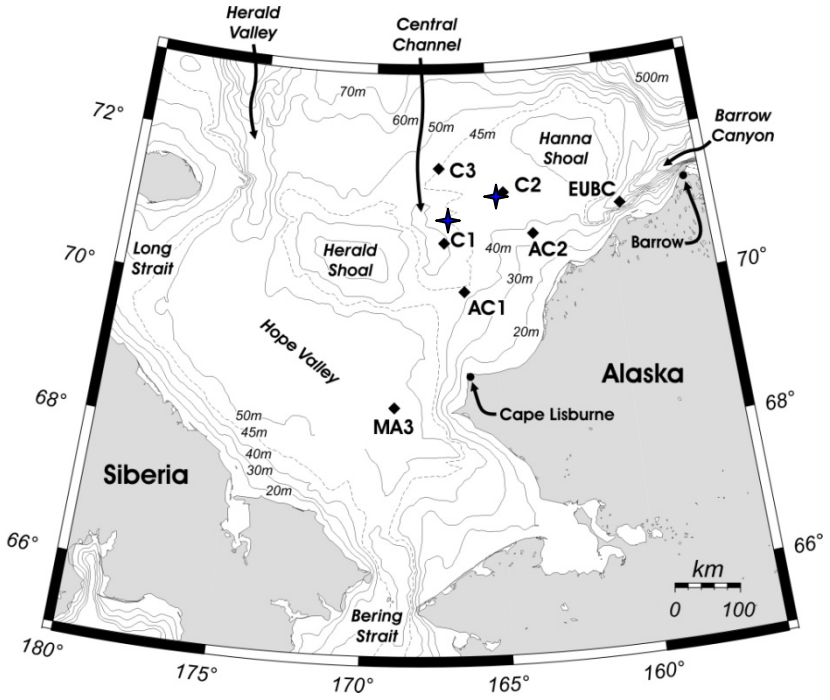

Figure 2. Bathymetric map of the Chukchi Sea shelf showing the Herald Valley, Central Channel, Barrow Canyon and two prominent shoals: Herald and Hanna. Also shown are the locations of current meter moorings deployed from 1994-1995. The blue stars are the approximate locations of the Klondike and Burger leases.

Mean current speeds within the Herald and Barrow canyons are swift (~25 cm s^{-1}), more moderate in the Central Channel (~10 cm s^{-1}), and generally ≤5 cm s^{-1} elsewhere (**Figure 3**). Long-term transport estimates for these three pathways are very approximate at best and suggest that the flow through the Central Channel is ~200,000 m^3 s^{-1}, while the branches in both Herald Valley and Barrow Canyon carry ~300,000 m^3 s^{-1} [*Woodgate et al.*, 2005b]. Estimates of transit time from Bering Strait to Barrow Canyon are from 3 – 4 months in summer and longer in winter [*Weingartner et al*., 2005; *Woodgate et al.*, 2005b]. Mean current vectors suggest that some of the Barrow Canyon outflow proceeds eastward along the Beaufort continental slope [*Weingartner et al*., 2005]. Water mass analyses and current meter measurements clearly show that this is indeed the case, but apparently not all of the mass transported down the canyon is captured by the slope flow [*Pickart,* 2004, *Steele et al.*, 2004, *Nikoloupolis et al.*, 2009; *Pickart et al*., in press]. Instead some of the outflow is entrained into shelfbreak eddies that drift into the deep basin [*Pickart et al.*, 2005; *Spall et al.*, 2008], some appears to spill over onto the inner Beaufort shelf when winds from the northeast are sufficiently weak [Okkonen, pers. comm.], and some appears to drift northwestward from the canyon's mouth and into the Arctic basin [*Shimada et al*., 2006]. The mean flow outlined from observations is similar to that produced by numerical circulation models of the Chukchi shelf [*Weingartner and Proshutinsky*, 1998; *Winsor and Chapman*, 2004; *Spall* 2007]. Of importance to this study are that some of the model results suggest that waters over Hanna Shoal are trapped by this bank and are only mixed slowly with adjacent shelf waters. The models also predict that flow through the Central Channel continues northeastward around the northern flank of Hanna Shoal, then turns southward at ~72°N (between Hanna Shoal and Barrow Canyon) before turning eastward to enter Barrow Canyon at

~71°N. We are unaware of any observations that confirm the clockwise flow around Hanna Shoal, but it is dynamically consistent with barotropic, geostrophic dynamics. An implication from the models is that materials discharged southwest of Hanna Shoal may be advected around the northern and eastern sides of the shoal and then swept down Barrow Canyon.

The influence of the three main flow pathways is evident, in summer and fall, by the formation of perennial "melt-back embayments" [*Paquette and Bourke*, 1981] that indent the ice edge. The embayments reflect accelerated melting by the warm Bering Sea summer waters that are channeled northward along these pathways. The routes and transit times by which Bering water ultimately enters the Arctic Ocean affects the distribution of hydrographic properties across the Chukchi Sea shelf and gives rise to complex shelf hydrographic structures as discussed next and as found in the measurements reported herein.

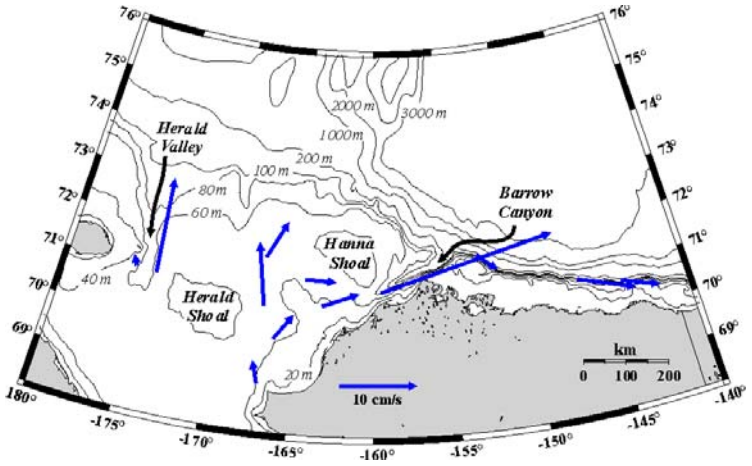

Figure 3. Mean flow vectors (blue arrows) from moorings deployed in the Chukchi Sea and Beaufort slope deployed between 1990-1995 and with record lengths exceeding 9 months.

In general, relatively warm (>2°C), salty (salinity >32.4) and nutrient-rich "summer" water from Bering Strait is found in Herald Valley and the Central Channel [*Coachman et al.,* 1975; *Hansell et al.,* 1993; *Cooper et al.* 1997; *Weingartner et al.;* 2005b; *Münchow et al.*, 1999; *Codispoti et al.*, 2005]. Warm, but fresher (salinity <32.2), Alaskan Coastal Water, also of Bering Sea origin, flows along the coast and occupies the eastern wall of the head of Barrow Canyon [*Coachman et al.*, 1975; *Weingartner et al.,* 2005b; *Pickart et al.,* 2005]. Ice tends to remain over Herald and Hanna shoals longer than elsewhere [*Drucker and Martin*, 1997] due to topographic obstruction of the flow and so cold, dilute waters, derived from ice melt, often lie within the upper 20 meters atop Herald Shoal, Hanna Shoal, and between the Central Channel and Barrow Canyon [*Drucker and Martin*, 1997; *Weingartner et al.,* 2005b]. The region south of Hanna Shoal, between the Central Channel and Barrow Canyon, is often strongly stratified with the water column having a 2-layer structure [*Weingartner et al.,* 2005b]. The stratification increases from spring through summer and then erodes in fall as strong winds, cooling, and freezing enhance vertical mixing. The bottom half of the water column usually contains relatively cold, salty water remnant from the previous winter, whereas the surface layer consists of ice melt, and/or mixtures of Alaskan Coastal Water or water flowing through the Central Channel. Seasonal changes in stratification may possibly lead to different surface velocity responses to winds. In addition to its spatial

complexity, the hydrographic structure can vary considerably on seasonal and storm time scales as well as from year-to-year.

Wind-Forced Variability

The mean circulation is due to the large scale oceanographic pressure field between the Pacific and Arctic oceans and opposes the mean winds, which are from the northeast at ~ 4 m s^{-1} on average. The winds are, however, the principal cause of flow variations [*Weingartner et al.,* 2005b], which can be substantial. Wind forcing varies seasonally with the largest variations being in fall and early winter and the smallest being in summer. Over the northeast Chukchi Sea shelf, current fluctuations are coherent with wind velocity variations over spatial scales of at least 300 km, with currents responding to wind variations in something less than a day [*Weingartner et al.,* 2005b]. These circulation adjustments reflect wind-induced modifications to the shelf pressure field. Although the adjustment envelopes a broad area, the magnitude of the current response varies over the shelf. In particular both the wind-forced (and mean) currents are more vigorous in regions of strong bathymetric gradients (e.g., Central Channel and Barrow Canyon) than in areas of gentler bottom relief. On occasion, and most frequently in fall and winter, strong storm winds from the northeast can reverse the shelf flow field or even re-distribute the flow from one of the main flow pathways to another.

There are, in addition, mesoscale flow variations associated with frontal instabilities, which have not been studied extensively in the Chukchi Sea. In summer and fall there are particularly prominent along ice-edge fronts [*Muench*, 1990; *Liu et al.*, 1994]. In winter, they are likely associated with the cross-shelf spreading of cold, saline water formed in the coastal polynyi along the northwest coast of Alaska [[*Cavalieri and Martin,* 1994; *Gawarkiewicz and Chapman*, 1995; *Gawarkiewicz et al*., 1998].

The current measurements discussed above were obtained from current meters installed ~10 m above the seabed in depths $\geq$40 m. However, these measurements may not reflect currents in the upper 3 m since near-surface currents are difficult to measure from year-round moorings with present technology. Although there are no direct measurements of surface currents on the Chukchi Sea, ice drift measurements suggest that ice drifts westward (and downwind) over the outer Chukchi shelf [*Muench et al.,* 1991]. In addition, several passive acoustic recorders prematurely released in summer 2008 drifted westward out of the lease sale area [C. Rea, pers. comm., 2009]. These few observations suggest that the flow in a “thin” surface layer, which absorbs the bulk of the momentum imparted by the wind to the water column, may differ from the deeper flow measured by current meters. The thickness of this wind-shear layer will likely vary due to wind velocity, ice, bathymetry, and stratification. We note that a joint industry-government program is presently underway to address this issue. That program involves the combined use of shore-based, radars that map the surface currents and upward looking Acoustic Doppler Current Profilers (ADCPs), moored within the radar mask, to measure flow to within ~3 m of the surface.

In the following sections we discuss separately the 2008 and 2009 variations in the winds and sea ice fields during the survey periods and then examine the water property distributions. These presentations are then followed by a brief discussion of the differences between the two years. The water property distributions are based on 1-meter averages of the CTD data collected at the various stations established in each prospect.

Methods

The sampling discussed in this report was concentrated in selected areas of the northeast Chukchi Sea. In 2008 and 2009, sampling was conducted in the Klondike and Burger study areas (**Figure 4**). Both of these areas were surveyed again in 2010 along with stations in the Statoil study area (**Figure 4**). Slightly different grids were occupied during each survey and the station distributions are shown in the discussions pertinent to each year. Note that the Klondike box lies to the east of the Central Channel, whereas Statoil is along the southwest flank of Hanna Shoal and Burger is on the southern flank of this shoal. Water depths in the region are ~40 – 45 m.

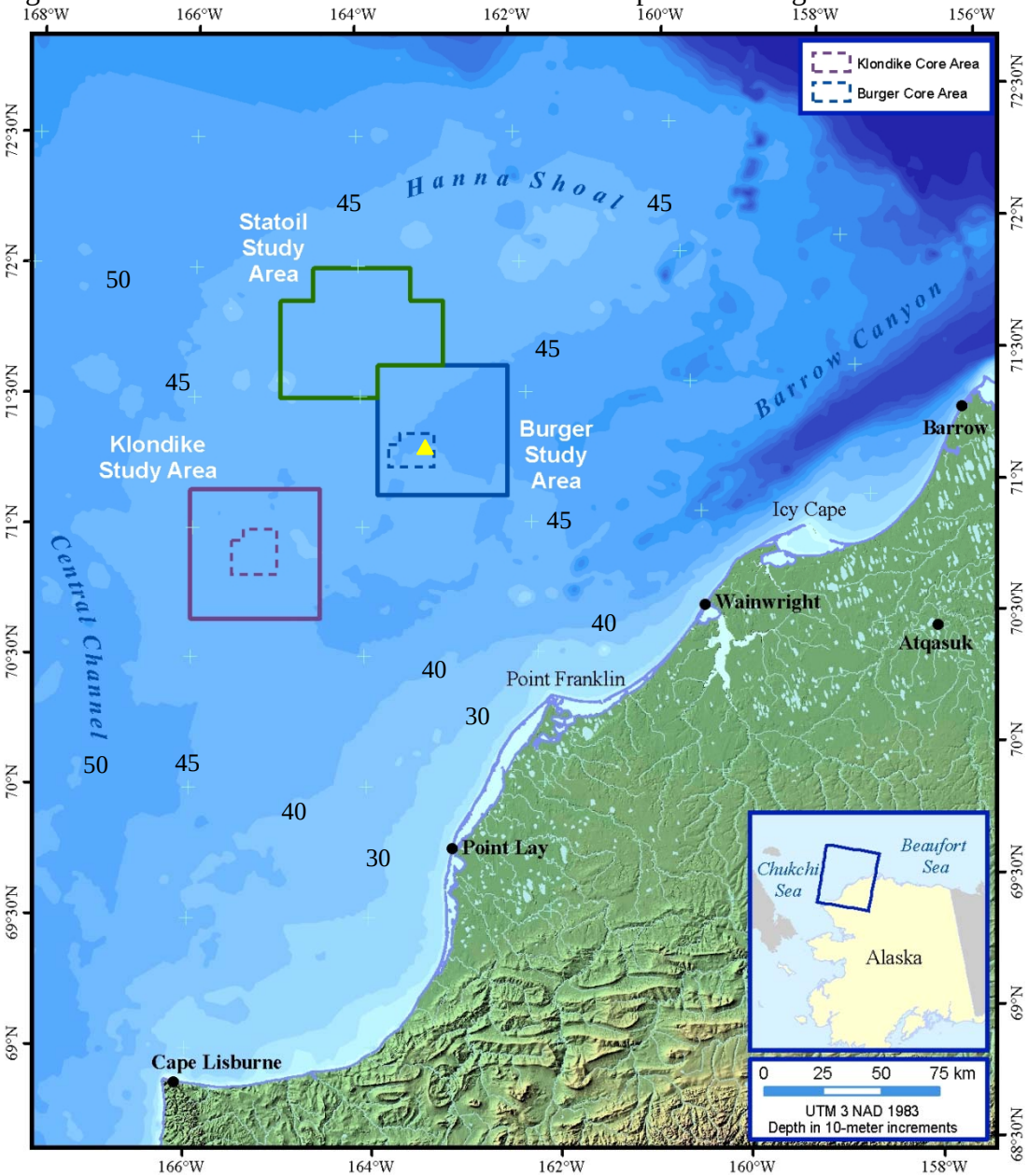

Figure 4. Map showing locations of the Klondike, Burger, and Statoil study areas in relation to the Alaskan coast. The yellow triangle shows the location of the NCEP wind point averaged between 162.5° and 165°W and 70°N and 72.5°N.

Data were collected with a Seabird, Inc. SBE-19+V2 CTD sampling at 4 Hz. The instrument was lowered throughout the water column at a rate of ~0.5m min^{-1} so that ~480 samples m^{-1} were obtained. Measured variables include pressure, temperature, conductivity, beam attenuation, beam transmission, and fluorescence. Derived variables include depth, salinity, density and speed of sound. Data were processed according to the manufacturer's recommended procedures [provided in the SBE Data Processing manual) and further screened for anomalous spikes, dropouts and density inversions. Data are averaged to 1 decibar (approximately 1 meter) vertical profiles. Post-season calibrations of the temperature and conductivity cells are performed at the manufacturer's calibration facility. Comparison of the pre- and post-calibration values indicate that the temperature data are accurate to better than 0.005 °C and salinity to 0.02.

ADCP data quality and processing summary:

A 600-KHz Teledyne-RDI acoustic Doppler current profiler (ADCP) was operated during the 2010 Chukchi field season. Setup, operating parameters, transformations and error-screening procedures are listed in the **Tables 1** and **2**. Through the course of the field season and including transit data collections, 35 deployments of the ADCP system resulted in valid data.

Overall data quality appears fairly good, although a few instances of computer/adcp system down time and bad bottom-track pings (likely resultant from rough seas) resulted in periods of unusable or missing data (**Figure 5**). The largest data gap (~ 15 days in late September) corresponds to the period when the vessel worked in the Beaufort Sea. The second-largest gap (~ 3 days in mid August) corresponds to a period when the ADCP data files and navigation files were not synchronized with one another. It appears the problem started on August 16, was identified on August 18 (when twenty-eight computer re-starts over the course of 17 hours were attempted), with normal data collection resuming on August 19. Gaps where data was collected, but of poor quality, mostly correspond to periods of high winds where a rough sea state presumably caused bubble entrainment below the transducer. Vessel speed and orientation with respect to direction of the surface wave field may also impact data quality. In general, data quality decreases if the vessel is heading into heavy seas.

Initial data screenings were performed in the TRDI software package VmDAS. Final data assessment and transformations were made in the MATLAB programming language with custom software. Data QA/QC parameters are listed in **Table 3**. After evaluating each 1-minute ensemble, consisting of 60 1-second pings, the data were averaged into 6-hour bins and plotted. In order to form a 6-hour average at least 25% of the ensembles collected during that 6-hour period had to have had good data. Time series of the percent good, error and vertical velocity time series as a function of depth and 6-hour averaged ensemble are shown in **Figure 6**. Inspection of these data suggested that the first depth bin which yielded reliably acceptable data was 11m below the surface. Velocities were also depth-averaged into 2-m deep bins.

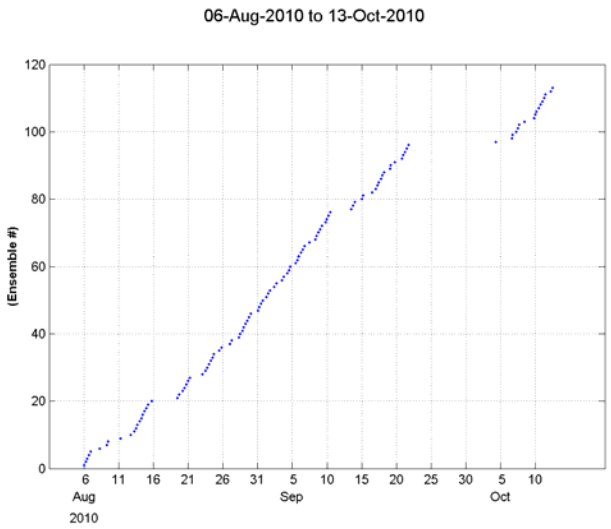

Figure 5. Temporal distribution of final averaged data. The largest data gap in August is due to computer issues; the largest data gap in September is because the vessel was in the Beaufort Sea.

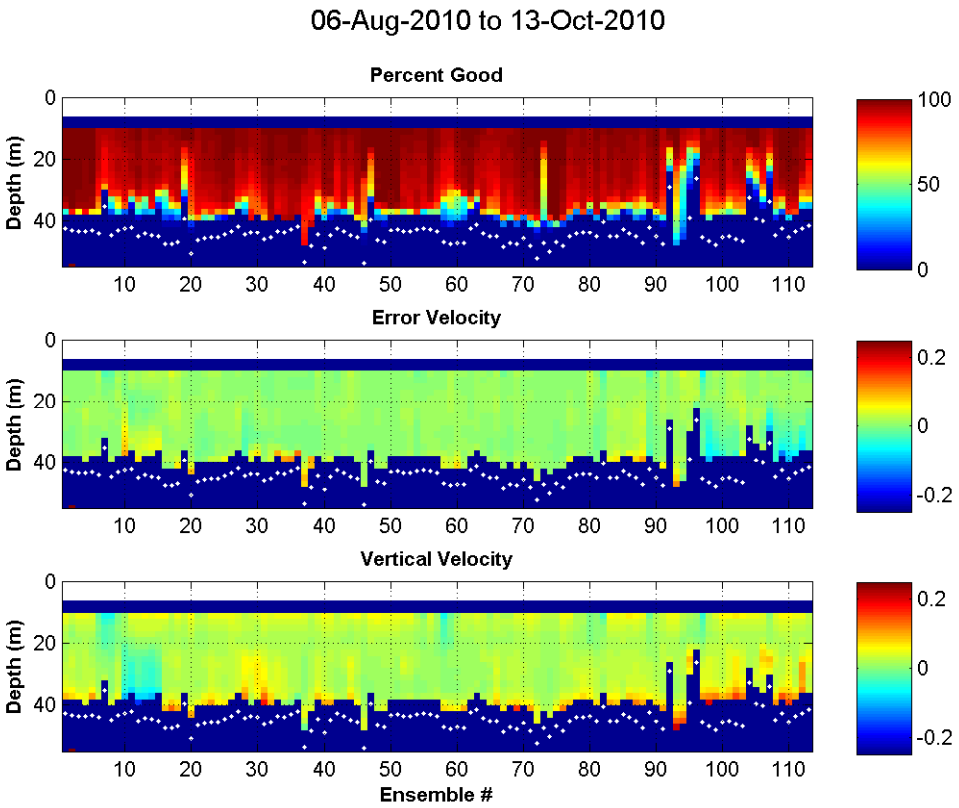

Figure 6. Percent good, error velocity and vertical velocity of the 6-hourly averaged ensembles.

Table 1. ADCP Setup and Navigation parameters.

System	Teledyne RDI Workhorse
Frequency	600KHz
Installation	Vessel-attached pole-mount
Orientation	Downward
Operating mode	Broadband
Bottom Track	Yes
Time per ping	1 s
Number of bins:	25
Bin size	2 m
Blanking Distance	2 m
Transducer Depth	3m
Ship position	NMEA1 GGA
Ship speed	NMEA2 VTG
Tilt source	ADCP internal tilt sensor
Heading source:	NMEA2 HDT
Alignment Error:	40.38^{o}

Table 2. VmDAS averaging and data screening thresholds.

STA average interval	60s
Profile Ping Normalization reference layer	Bins 3 - 10
Water Current Profile Received Signal Strength Indicator	80 counts
Water Current Profile Correlation	180 counts
Water Current Profile Error Velocity	1 m/s
Water Current Profile Vertical Velocity	1 m/s
Water Current Profile Fish target	50 counts
Water Current Profile Percent Good	50%
Bottom Track Received Signal Strength Indicator	30 counts
Bottom Track Correlation	220 counts
Bottom Track Error Velocity	1 m/s
Bottom Track Fish:	50 counts
Bottom Track Vertical Velocity	1 m/s
Bottom Track Percent Good	50%

Table 3. QA/QC thresholds and corrections applied to 1-minute STA ensembles.

Minimum correlation	64
Minimum percent-good 4-beam + 3-beam solutions	50%
Minimum percent-good bottom track pings	25%
Blanking above bottom (% of distance to transducer)	6%
Maximum heading standard deviation	3
Maximum change in speed	0.2 m/s
Minimum speed	1.5 m/s
Maximum vertical velocity	0.1 m/s
Maximum error velocity	0.05 m/s
Minimum good fraction of water profile allowed	2/3
Individual ensemble cross-track magnitude/direction corrections	Yes
Transducer mis-alignment correction	-0.49°
Ensembles removed with unrealistically large mean velocity (> 2 m/s)	Yes
Removed adjacent ensembles with unrealistically large change in velocity	Yes
Truncated bins based on largest/smallest	0.25% outliers

Heat Budget

We computed the heat content (Q) in each survey area based on the CTD temperature data between the surface and bottom:

$$Q = \int_{dA} \int_{-h}^{0} \rho C_p T dz dA$$

where ρ_w is the water density (1023 kg m^{-3}), C_p is the specific heat of seawater (= 3985 J kg^{-1} ^{o}K^{-1}), T is temperature, dA is the area of each survey site, and h is the water depth. The variable Q, effectively represents the mean temperature of each site. The areas of each survey box were constant and Q was pro-rated to the area of each survey site. We also examined the changes in heat content between each survey and attempt to ascribe the causes in these variations based on the following heat budget:

$$\underbrace{\frac{\Delta Q}{\Delta t}}_{\text{heat gain or lost per unit time}} = \underbrace{(1-\alpha)Q_{solar}}_{\text{albedo corrected solar radiation}} + \underbrace{Q_{net\ longwave}}_{\text{incoming+outgoing longwaveradiation}} + \underbrace{\left(Q_{latent} + Q_{sensible}\right)}_{\text{heat loss or gain by the ocean due to evaporative cooling/heating (latent) and sensible heat exchange with the atmosphere}} + \underbrace{Q_{oceanic}}_{\text{heat added or lost due to transport by ocean currents or horizontal mixing}}$$

The radiation terms are the dominant terms amongst the first four terms on the right hand side. Both long and short-wave terms are sensitive to the cloud cover, which is poorly modeled by NCEP (*Walsh et al.*, 2009). For our analyses we use hourly incoming solar radiation

measurements obtained at the Barrow Atmospheric Radiation Measurement (ARM) site operated by the Department of Energy. The net longwave radiation was estimated following from *Bignami et al.* (1991) and includes longwave loss from the sea surface and longwave emittance from the atmosphere:

$$Q_{net\ longwave} = \varepsilon\sigma T_s^4 \left[\left(0.344 - 6.66x10^{-3} e_a\right)\left(1 - 0.42C\right) \right]$$

Where ε=0.98 is the emissivity of seawater, e_a is the vapor pressure in miilibars, C is cloud cover (in tenths), σ= 5.6704 x 10^{-8} W m^{-2} K^{-4}, is the Stefan-Boltzmann constant, and T_s is the sea surface temperature (taken from the CTD data). The vapor pressure is calculated using the mean monthly air temperature (at Barrow) and corrected for the relative humidity, which averages ~93% for the July – September period (Brower et al., 1988). We also used the mean monthly cloud cover fractions at Barrow as determined by ARM for the 1999 – 2006 period and assumed that they were valid for the 2008 – 2010 period. These are 75%, 90%, 92%, and 95% for July, August, September, and October, respectively.

The latent and sensible heat flux values are based on the 6-hourly estimates of NCEP. The errors in the net longwave and latent and sensible heat terms are probably ~20%. The largest single source of error in the net shortwave measurements is associated with the assumption that the incoming measurements at Barrow are representative of those over the survey area. While variations in cloud cover between Barrow and the survey sites could lead to large day-to-day differences in the net shortwave estimates, when averaged over many days, as done here, these differences are expected to be small and negligible. The shortwave radiation values were corrected for the albedo of open water, α = 0.07.

Heat loss or gain by oceanic processes (horizontal transport by currents and/or horizontal mixing) was not measured and is thus the residual after summing and differencing all other terms in the equation, e.g.,

$$\underbrace{\frac{\Delta Q}{\Delta t}}_{\text{heat gain or lost per unit time}} - \underbrace{\left(1-\alpha\right)Q_{solar}}_{\text{albedo corrected solar radiation}} - \underbrace{Q_{net\ longwave}}_{\text{incoming+outgoing longwaveradiation}} - \underbrace{\left(Q_{latent} + Q_{sensible}\right)}_{\text{heat loss or gain by the ocean due to evaporative cooling/heating (latent) and sensible heat exchange with the atmosphere}} = \underbrace{Q_{oceanic}}_{\text{heat added or lost due to transport by ocean currents or horizontal mixing}}$$

We assumed that horizontal mixing is negligible then we can partition the oceanic heat flux into a cross-shelf (east-west) wind-forced Ekman heat flux and other advective components, e.g.,

$$Q_{oceanic} = Q_{Ekman} + Q_{other\ advection}$$

where $Q_{Ekman} = \rho_w C_p h_E u_{Ekman}\, \partial T/\partial x$. The cross-shelf temperature gradient ($\partial T/\partial x$) was estimated from satellite-derived data obtained from NOAA's National Environmental Satellite, Data, and Information Service (NESDIS; http://nomads.ncdc.noaa.gov/). We evaluated these along 71°N and between 161°W and 163°W for Burger and 161°W and 165°W for Klondike. These gradients are not well-known given the paucity of satellite imagery for the region but are generally on the order of 0.5 - 2°C between the coast and Burger or Klondike. The Ekman transport is assumed confined to a surface Ekman depth, h_E, of 15 m so that the vertically-averaged cross-shelf flow over this depth is:

$$u_{Ekman} = \frac{\rho_{air} C_D V_W \left(W_w\right)}{\rho_w f h_E}$$

71°N (=1.379x10^{-4} s^{-1}). Errors in this estimate may be as large as 100%.

Results

Winds and Sea Ice 2008 - 2010

In summarizing the results for 2008 and 2009 we used winds derived from the scatterometer aboard the QuikScat satellite. That instrument failed in November 2009. In order to use a consistent data set upon which to make comparisons across years, we used forecast (model) winds obtained from the National Center for Environmental Prediction (NCEP). These are spatially smoothed and available 4 times per day and output on a 2.5 x 2.5 degree grid. We averaged the NCEP winds at latitudes 70 and 72.5°N (hence at 71.4°N) and between longitudes 165 and 162.5°W longitude. The averaged position is shown as the yellow triangle in **Figure 4**. (We also examined winds to the north and south of these positions, but they are similar and are not presented.) We present these as vector sticks, smoothed with a 5-day running mean and resolved according to their principal axes of variance (**Figure 7**) and also as weekly means of the vector components along the major (V-component; **Figure 8**) and minor axes of variance (U-component; **Figure 9**) of variance.

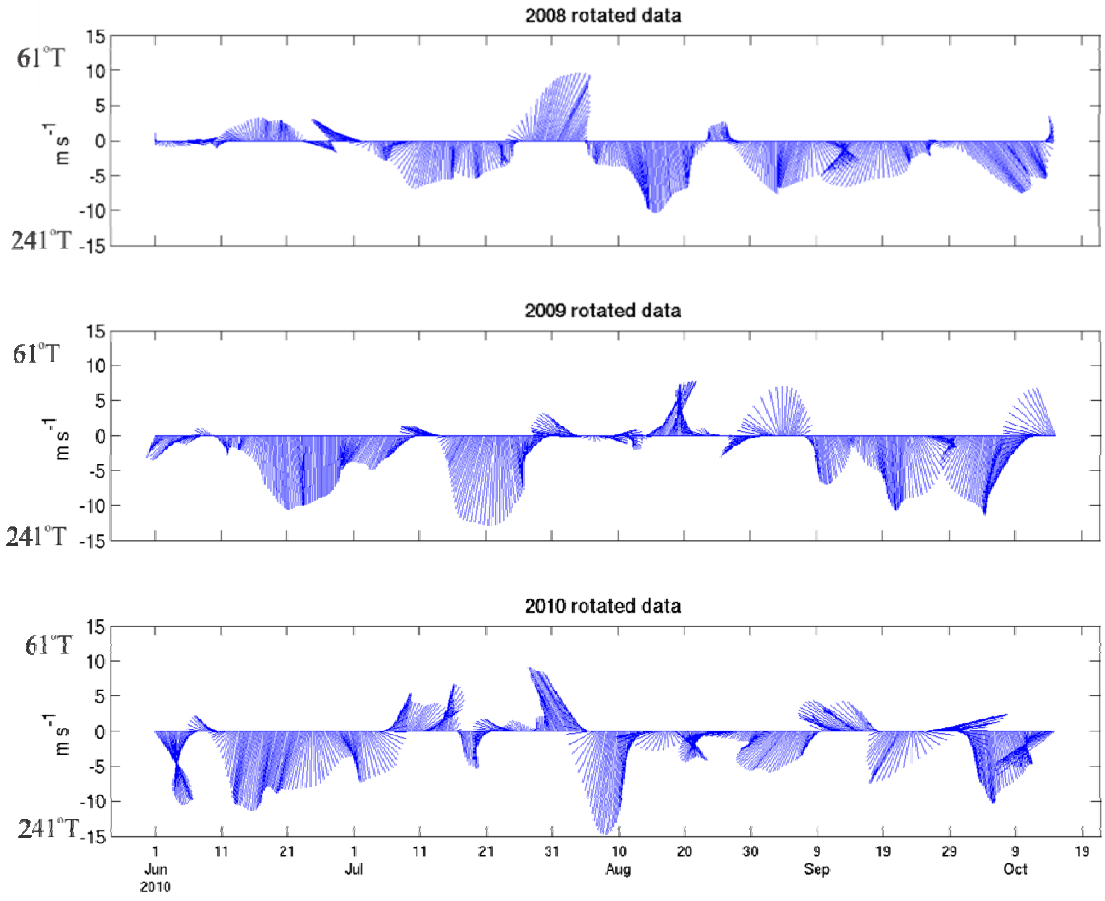

Figure 7. Vector "sticks" of winds rotated along their principal axis of variance and smoothed with a 5-day running mean for 2008 (top), 2009 (middle) and 2010 (bottom). The axis of

principal variance is aligned along 61°T – 241°T so that vectors oriented toward the top of the page are winds *to* 61°T while vectors oriented toward the bottom of the page are winds *to* 241°T.

In this representation, the major axis is aligned along the 61°T (northeast) - 241°T (southwest) direction and the minor axis is aligned in the 151°T (southeast) - 331°T (northwest) direction. Negative values along the major axis indicate winds blowing from the northeast to the southwest and positive values indicate winds blowing from the southwest to the northeast. A common axis of rotation was applied to all years, since differences in axes orientations among years were <2 degrees. The principal axis direction is approximately parallel to the coast and we will refer to this component of the wind as the along-shore wind component.

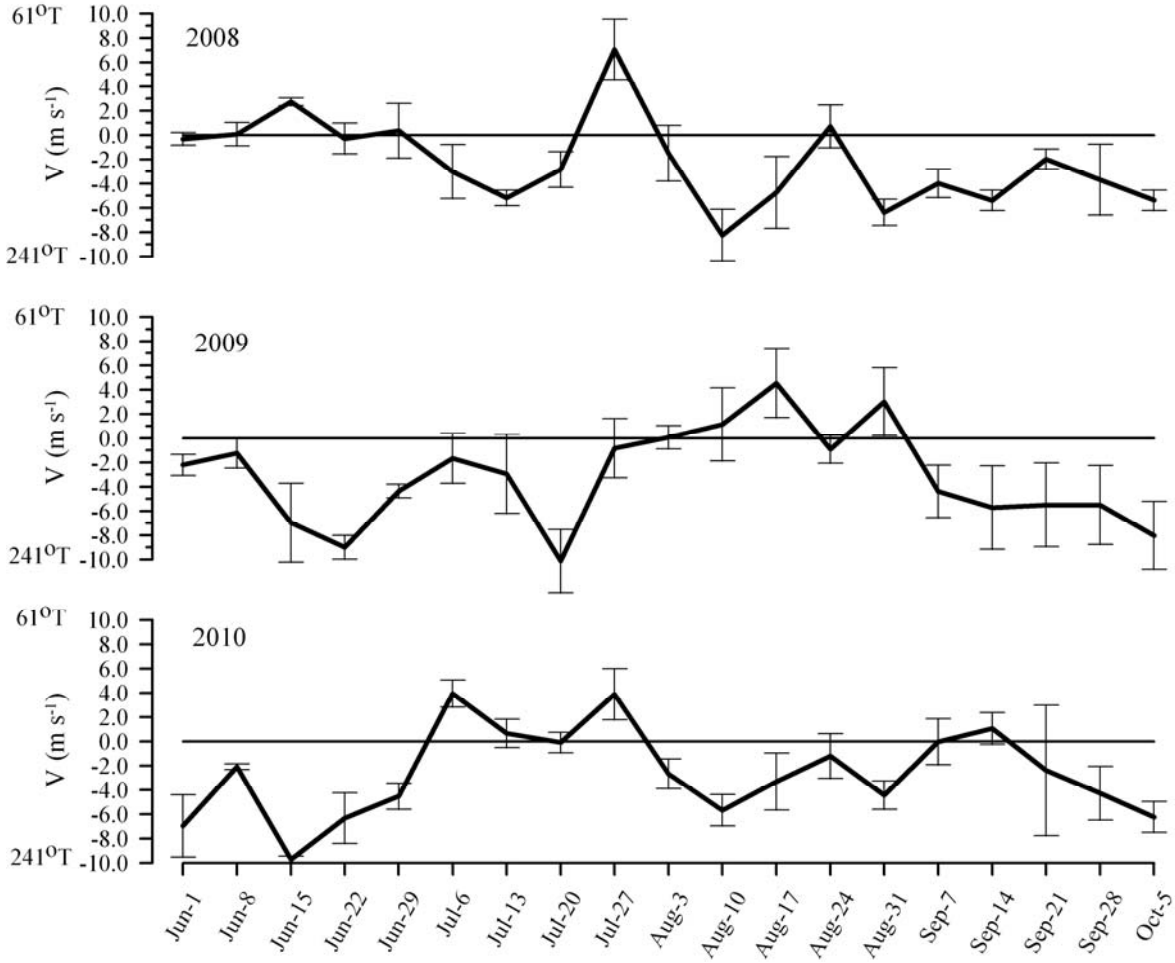

Figure 8. Weekly mean winds along the principal (major) axis of variance for from June 1 through October 5, 2008 - 2010. The averages are taken over the week following the given date. Standard deviation of the means are given by the error bars. The direction of the vector components are given on the y-axis.

The winds, while variable, were primarily from the northeast in all years. The patterns of variability among years are of interest, however, and may be of some importance in the seasonal evolution of the sea ice and water properties. In 2008 winds were from the northeast at 5 - 10 m s^{-1} (10 – 20 kts) from early July through early October except for a brief period of southwest

winds in late July. In 2009, winds were from the northeast through July and then generally mild or from the southwest through early September. Strong northeasterlies then developed by the second week of September and remained so until mid-October. In 2010, strong northeasterlies prevailed in June, while in comparison to the other years, winds from July through September were variable and relatively weak.

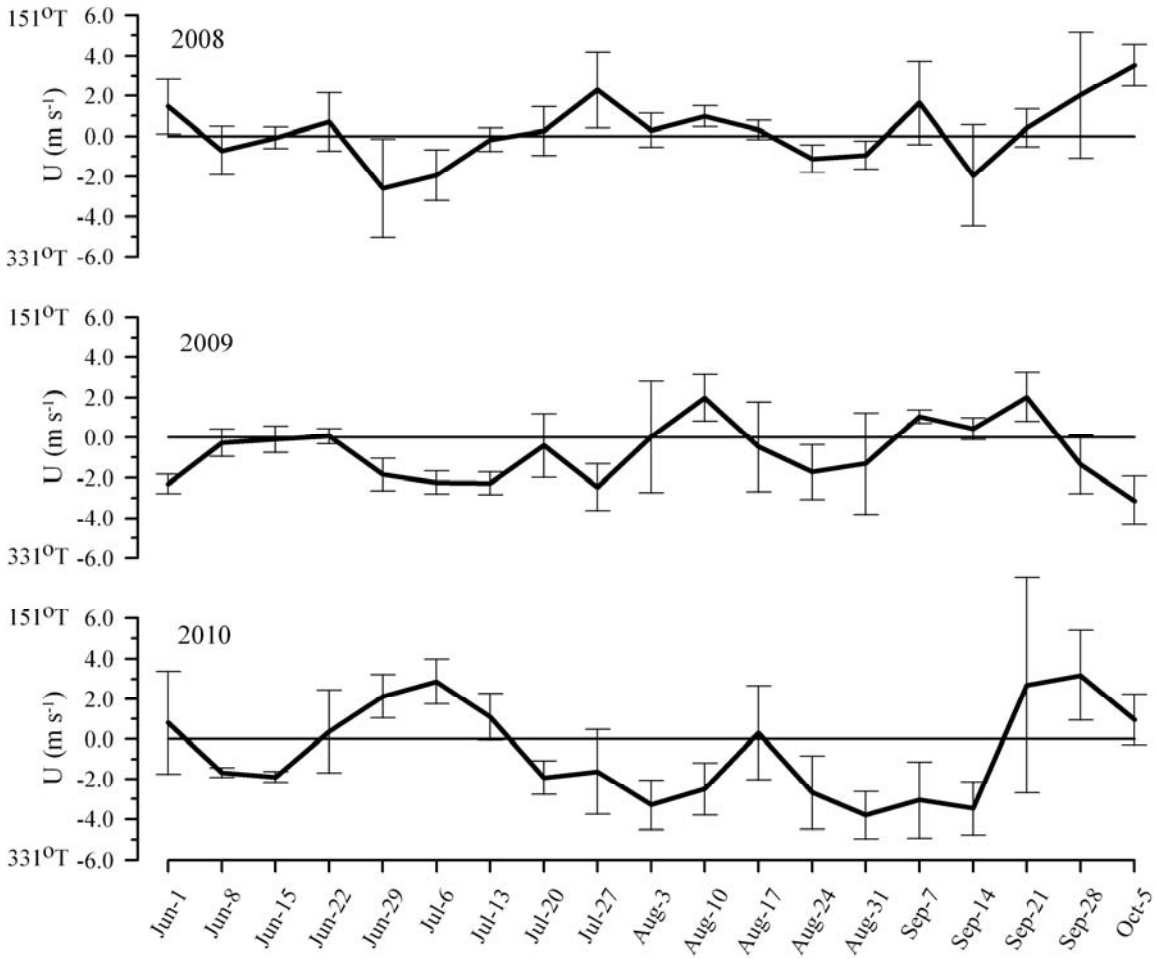

Figure 9. Weekly mean winds along the minor axis of variance for from June 1 through October 5, 2008 - 2010. The averages are taken over the week following the given date. Standard deviation of the means are given by the error bars. The direction of the vector components are given on the y-axis.

Sea ice concentrations

The seasonal distribution and retreat of sea ice varied among the years. We illustrate this based on ice concentration data from the Advanced Microwave Scanning Radiometer - Earth Observing System (*AMSR-E*) satellite sensor and processed according to Spreen et al., (2008). We show ice concentration maps for each year for May, June, and July in **Figures 10 – 12** to provide a broader perspective of the seasonal evolution in sea ice retreat over the Chukchi shelf prior to the vessel surveys

These provide a broader perspective of the seasonal evolution in sea ice retreat over the Chukchi shelf prior to the vessel surveys. In early May (**Figure 10**) of 2008 and 2010 relatively large expanses of open water extended westward (offshore) of the NW coast of Alaska even though the southern Chukchi Sea, including Bering Strait, was still covered by ice. By contrast, in early May 2009 (**Figure 10**, middle panel) the Chukchi shelf was ice-covered except for Bering Strait and a narrow opening along the southeastern portion of the Chukotka Peninsula. Similar conditions prevailed throughout the rest of May, although ice retreat began to spread northward in all years from Bering Strait and across the southern Chukchi shelf.

By the end of the first week of June 2008 (**Figure 11**) open water area had decreased in the northeast Chukchi Sea implying southward transport of ice onto the shelf, although ice conditions in the southern Chukchi Sea had not changed appreciably. Ice continued to erode in the southern Chukchi Sea in both 2009 with little change over the northeast shelf. In 2010, there was considerable ice retreat over the southern shelf and perhaps some additional retreat on the northeast shelf. Although there was little change in ice conditions by June 20, 2008, ice had continued to retreat rapidly northward by this date in both 2009 and 2010. In fact, in 2010 the shelf was ice-free from Bering Strait nearly to Barrow. By the end of June 2008, heavy ice concentrations remained over the northeast shelf with the northern limit of the ice edge near Icy Cape. By late June 2009, ice-free conditions extended nearly to Barrow along the Alaskan coast, while in 2010 open water extended westward to ~169^{o}W in the central Chukchi Sea.

Very likely the difference in timing in ice retreat along the NW coast of Alaska (Cape Lisburne to Barrow) is associated with the seasonal evolution of the east-west (zonal) component of the winds. Winds toward the west tend to force ice offshore and open water along the coast, whereas winds to the east tend to trap ice along the coast. **Figure 12** shows April through mid-July time series of the zonal component of the NCEP winds over the NE Chukchi Sea for each year. In all years this wind component was variable throughout April and no open water appeared. In 2008 and 2010, relatively strong westward winds developed in late April and early May and led to the development of an ~100 km wide band of open water along the coast between Cape Lisburne and Barrow Canyon. (The approximate date of this occurrence is indicated by the blue circles in **Figure 12**.) By contrast, in 2009 the zonal wind component was variable throughout May until the mid-June. At that time relatively strong west winds developed and the coastal band of open water formed by June 23.

Ice conditions did not change very much by the end of the first week of July (**Figure 13**). Little additional retreat occurred along the Alaskan coast in 2008 and heavy ice concentrations remained over Herald Shoal on the central shelf. By contrast relatively little ice covered Herald Shoal in 2009, although there were heavy concentrations extending to the south of Hanna Shoal. In 2010, heavy ice occurred over Herald Shoal, while relative low concentrations occurred over Hanna Shoal.

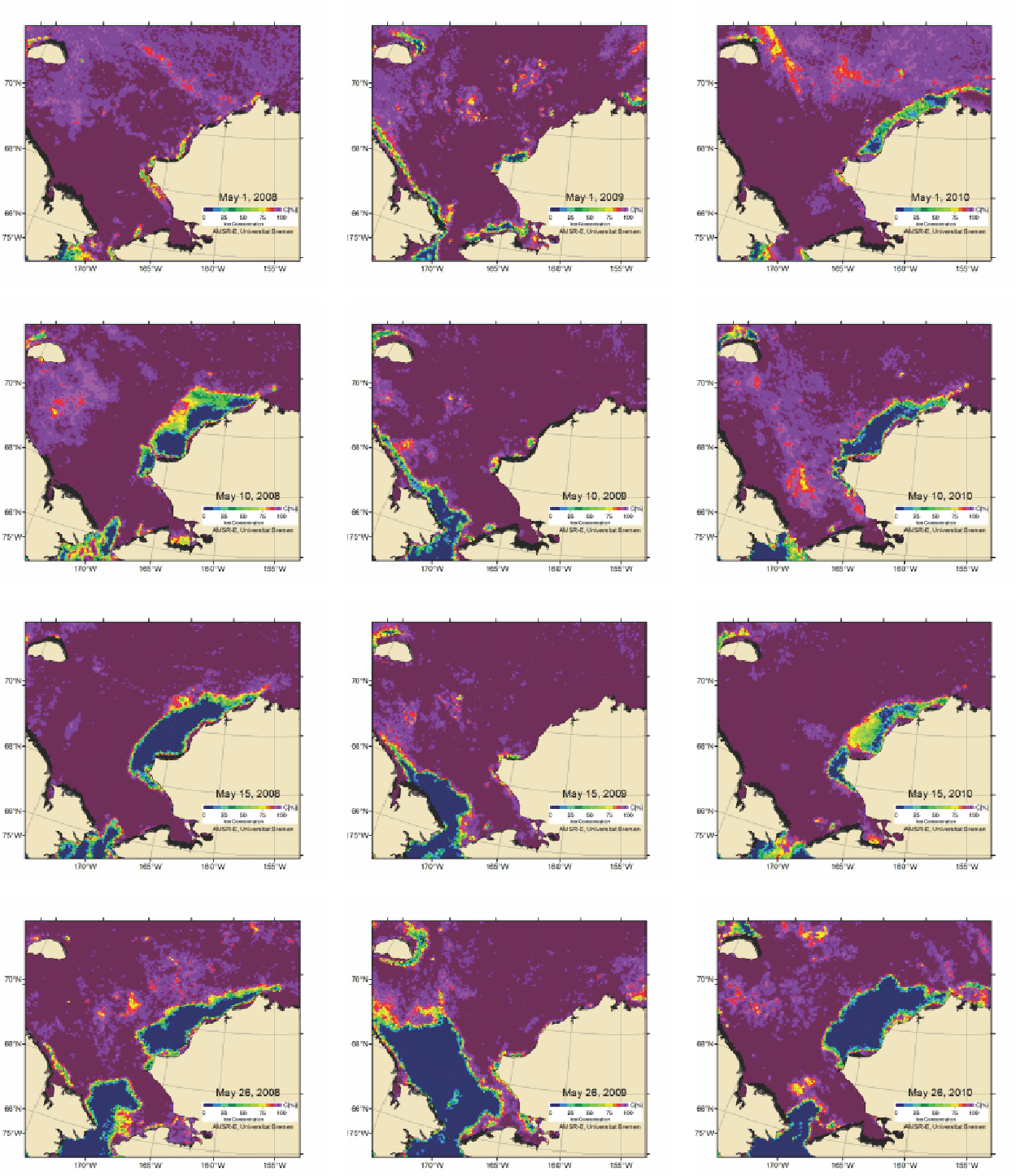

Figure 10. AMSRE-E sea ice concentration maps for the Chukchi shelf throughout May 2008 (left column), 2009 (middle column) and 2010 (right column).

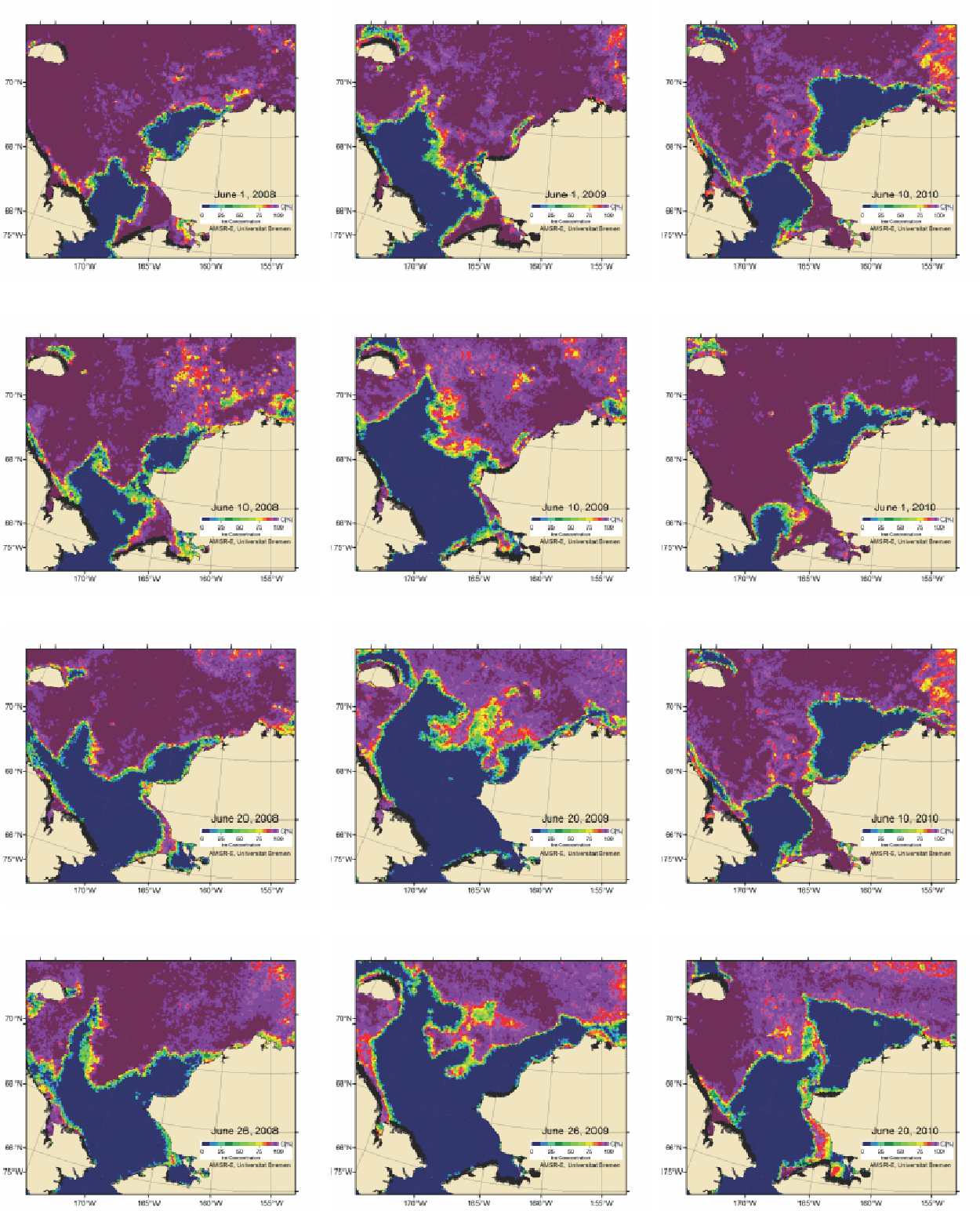

Figure 11. AMSRE-E sea ice concentration maps for the Chukchi shelf throughout June 2008 (left column), 2009 (middle column) and 2010 (right column).

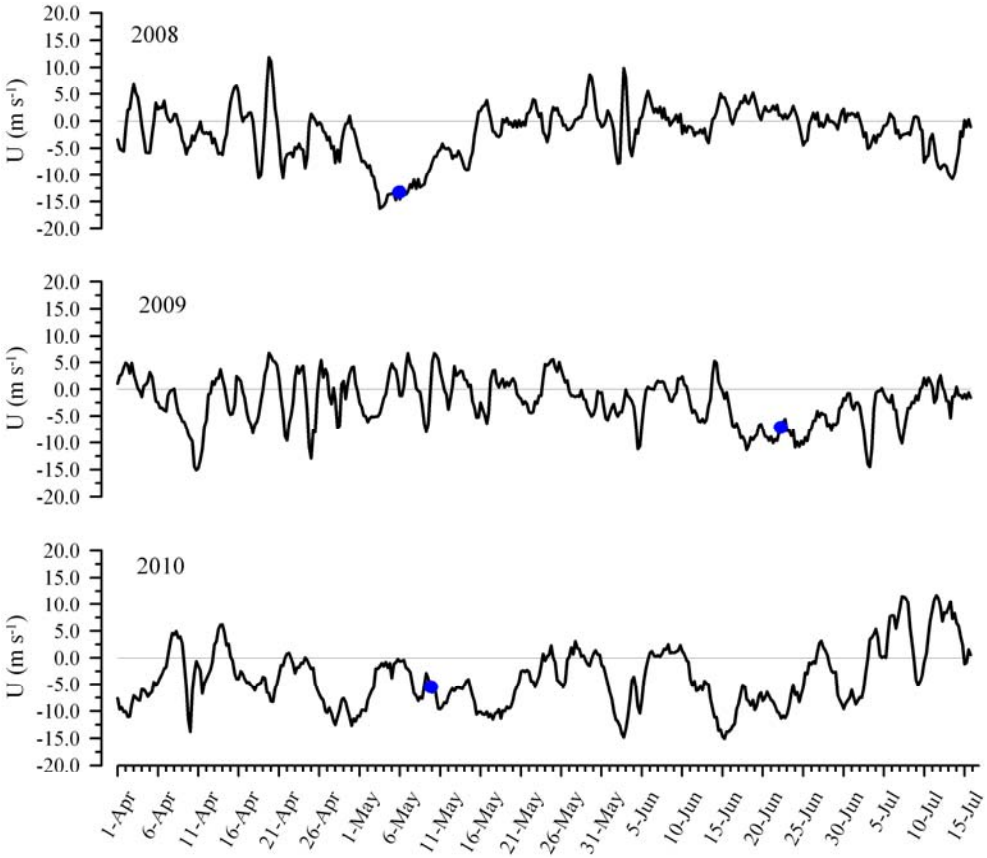

Figure 12. Time series of the eastward (positive) and westward (negative) component of winds along the northwest coast of Alaska between April 1 and July 15, 2008 – 2010. The blue circles mark the date when an ~100km wide band of open water extended continuously along the coast between Cape Lisburne and Barrow Canyon.

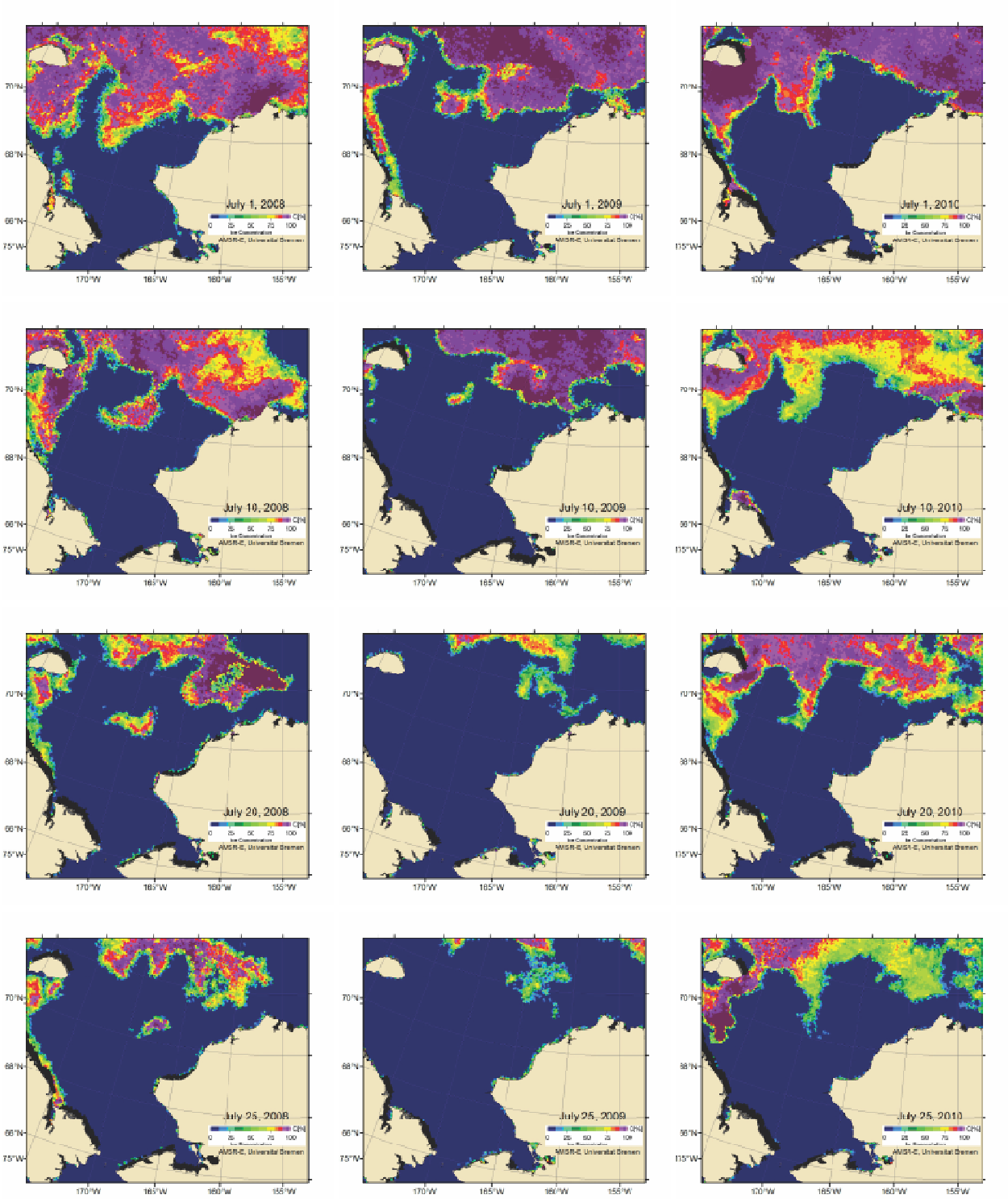

Figure 13. AMSRE-E sea ice concentration maps for the Chukchi shelf throughout July 2008 (left column), 2009 (middle column) and 2010 (right column).

Differences in the seasonal evolution of sea ice may have biological consequences. The large expanses of open water over the northeast Chukchi Sea seen in May 2008 and 2010 suggest that conditions were conducive to the early establishment of an open water phytoplankton bloom (as suggested by **Figure 14**) and warming of the surface waters. In contrast the extensive ice cover in early summer 2009, implies that ice algal production and ice-edge production may have been more important contributors to primary production then.

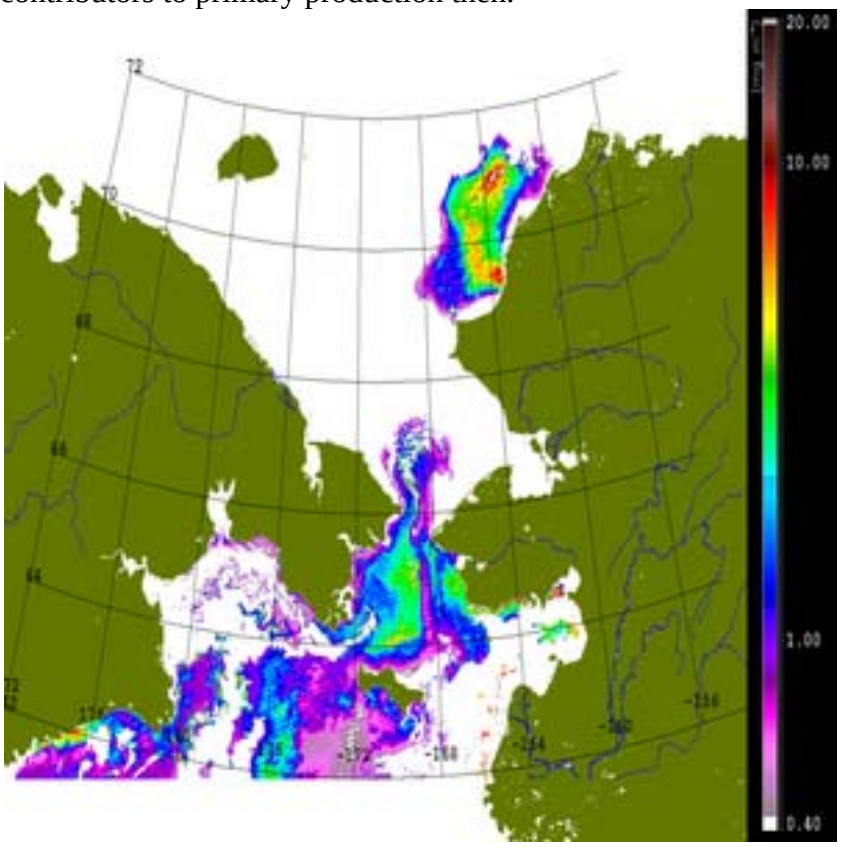

Figure 14. MODIS/Aqua image and estimated chlorophyll a concentrations (mg m^3) over the northern Bering and northeast Chukchi Sea on May 29, 2010 (courtesy of G. M. Schmidt; MODIS/Aqua data obtained from Ocean Color Data Processing Archive NASA / Goddard Space Flight Center Greenbelt, MD – USA).

A more detailed perspective on ice concentrations over the northeast shelf is afforded by the ice concentration maps derived from Synthetic Aperture Radar (SAR) imagery shown in (**Figures 15 – 21**). These show that by the end of July, Hanna Shoal was covered by heavy to moderate ice concentrations. For example, in both 2008 and 2010 ice concentrations over the Shoal were ~9 – 10 tenths (**Figures 15** and **17**), while in 2009 (**Figure 16**) ice concentrations over the Shoal were much lower and more variable as they ranged from 3 – 7 tenths. There was also an extensive region of low ice concentrations (<1 tenth) to the northeast and east of Hanna Shoal in 2009. In contrast moderately heavy ice covered this area in 2008, while very high concentrations occurred here in 2010.

Ice concentrations diminished through August in all years. However, in 2008, 3 – 7 tenths ice cover remained over Hanna Shoal through the end of August (**Figures 18** and **19**) and early September (not shown). In contrast, by mid-August 2009 the northeast shelf was largely ice-free

with only small diffuse patches remaining over the Shoal (**Figure 20**) and in 2010, the northeast shelf was completely ice-free by mid-August (**Figure 21**). Although the reasons for these differences are not entirely understood, it seems probable that the relatively steady southward winds in August 2008 played a role in delaying the northward retreat (and perhaps ablation) of ice over the northeastern shelf. We shall show that these various in ice concentration are reflected in some of the regional water properties. It is also apparent from this brief overview that the seasonal evolution of ice retreat is quite variable from year-to-year and it is clear that August ice concentrations are not readily predictable from May – July ice concentrations.

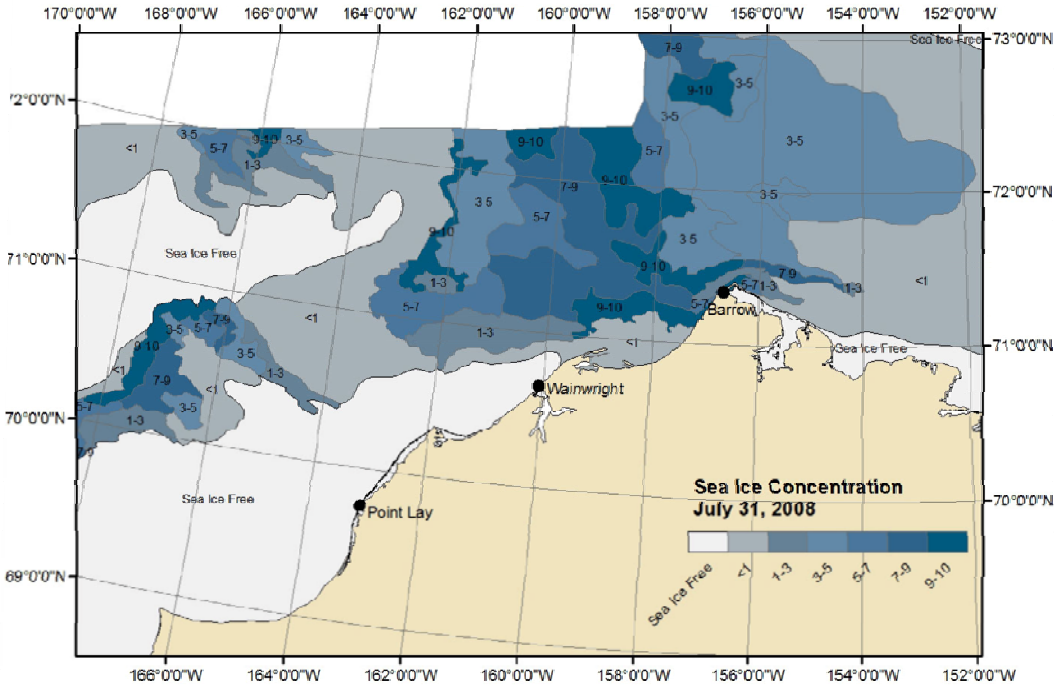

Figure 15. July 31, 2008 sea ice concentration from SAR imagery. Concentrations are in tenths (e.g., 3 implies an ice concentration of 30%) and the white region was not analyzed.

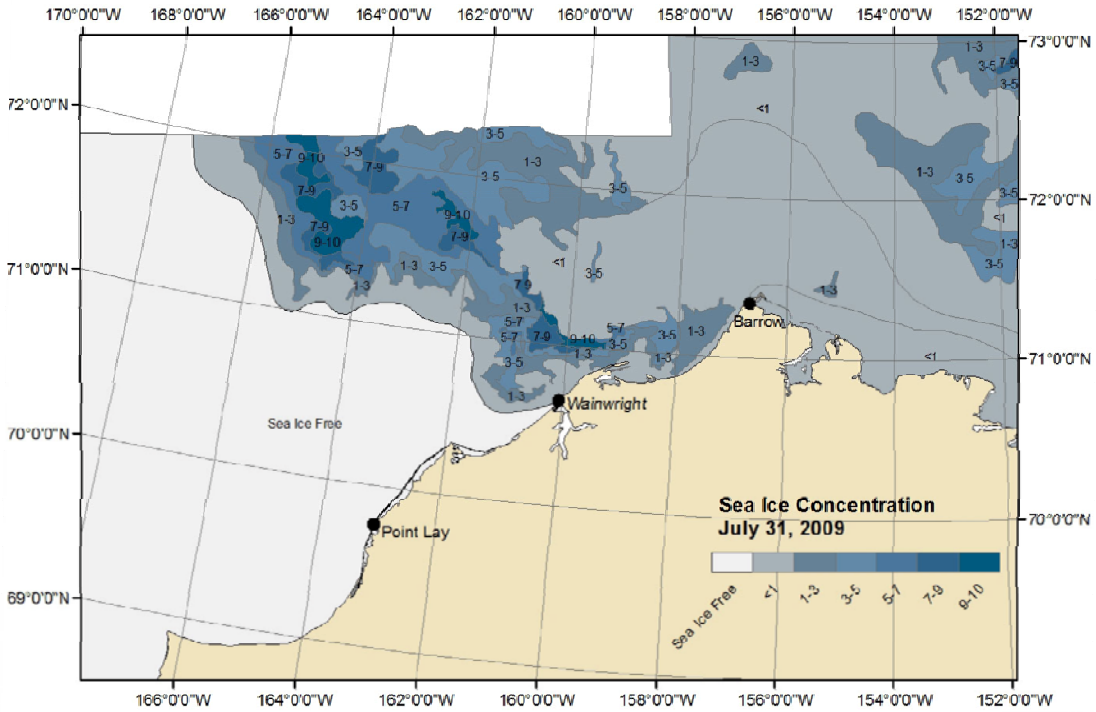

Figure 16. July 31, 2009 sea ice concentration from SAR imagery. Concentrations in tenths (e.g., 3 implies an ice concentration of 30%) and the white region was not analyzed.

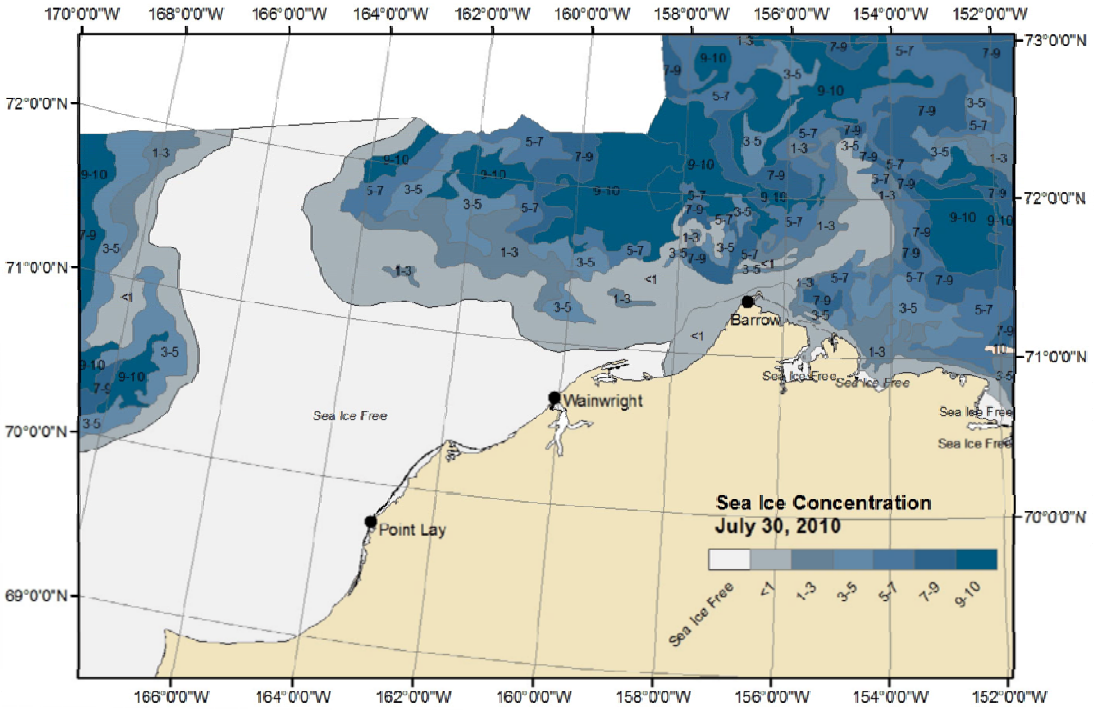

Figure 17. July 31, 2010 sea ice concentration from Synthetic Aperture Radar imagery. Concentrations are in tenths (e.g., 3 implies an ice concentration of 30%). The white area was not analyzed.

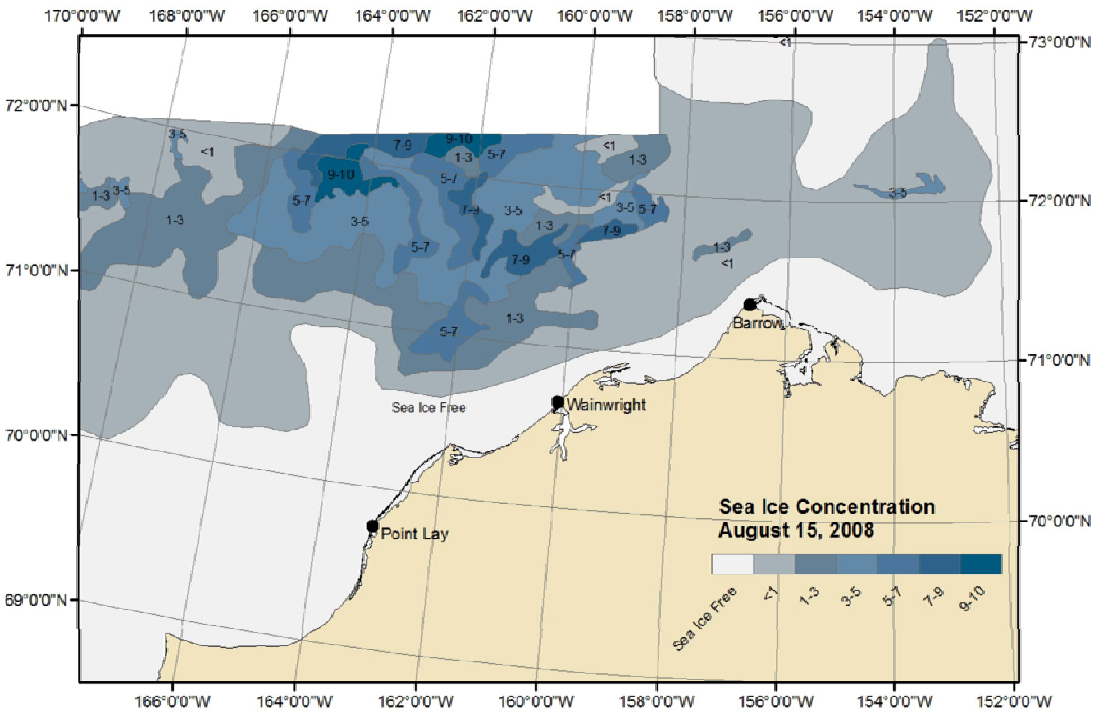

Figure 18. August 15, 2008 sea ice concentration from Synthetic Aperture Radar imagery. Concentrations are in tenths (e.g., 3 implies an ice concentration of 30%). The white area was not analyzed.

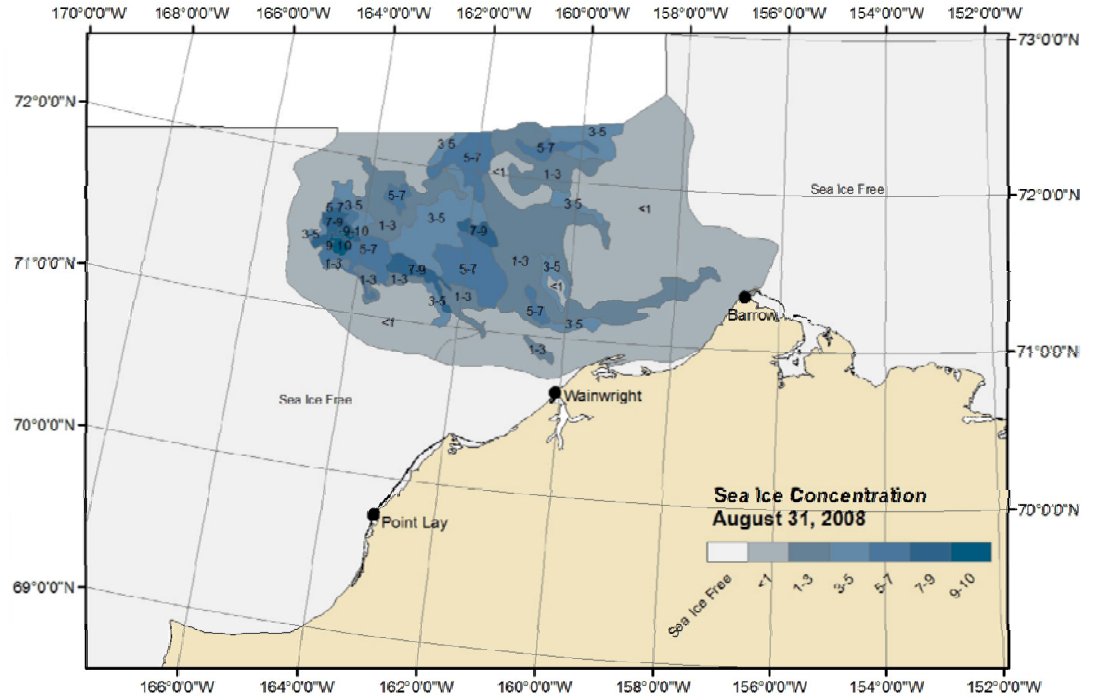

Figure 19. August 31, 2008 sea ice concentration from Synthetic Aperture Radar imagery. Concentrations are in tenths (e.g., 3 implies an ice concentration of 30%). The white area was not analyzed.

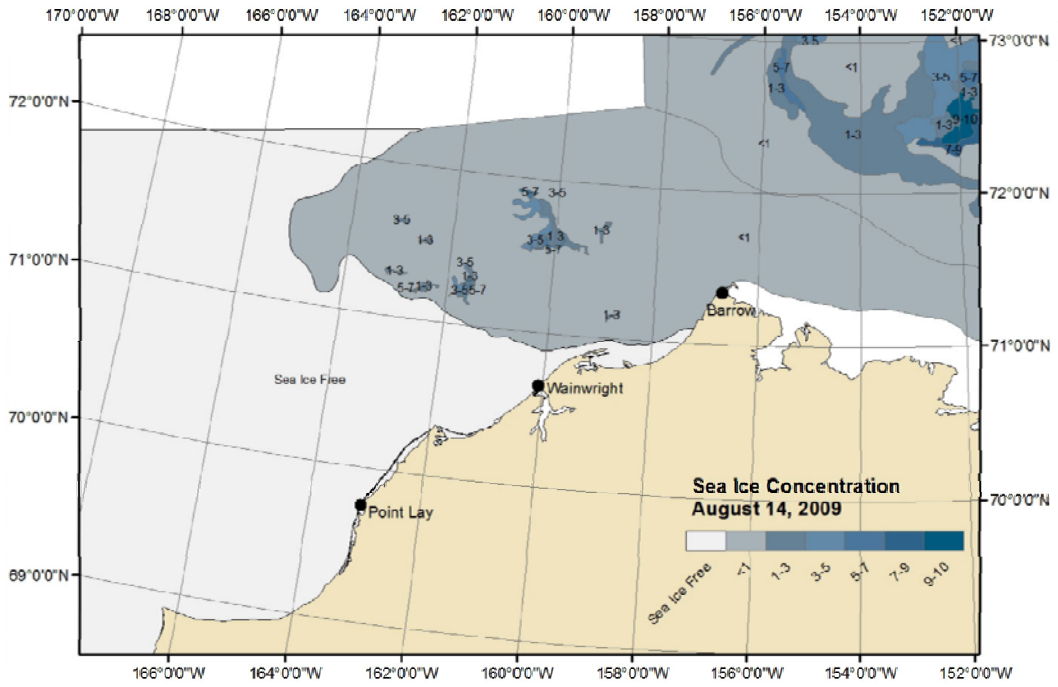

Figure 20. August 14, 2009 sea ice concentration from Synthetic Aperture Radar imagery. Concentrations are in tenths (e.g., 3 implies an ice concentration of 30%). The white area was not analyzed.

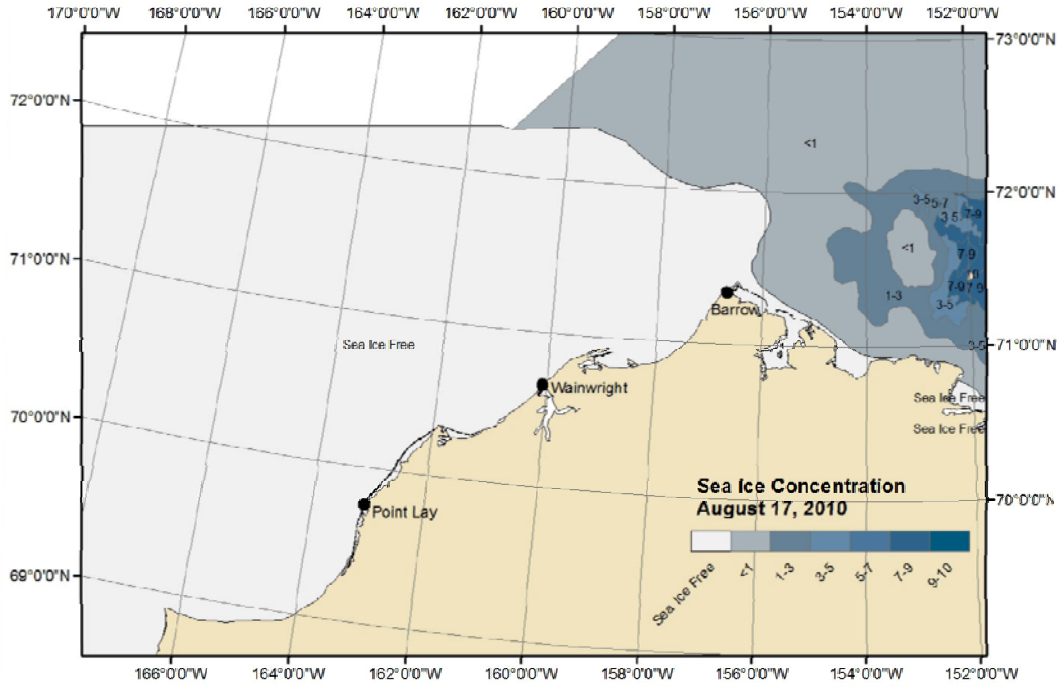

Figure 21. August 17, 2010 sea ice concentration from Synthetic Aperture Radar imagery. Concentrations are in tenths (e.g., 3 implies an ice concentration of 30%). The white area was not analyzed.

Results: 2008 Survey

Temperature and salinity

Before presenting the spatial distribution of temperature and salinity along the CTD transects we first describe the various water masses observed in both survey areas with the aid of **Figure 22.** The figure is a T/S diagram (scatterplot) depicting the temperature (T) and salinity (S) characteristics at each 1-meter averaged CTD sample from all casts. The data are color-coded red for Burger and blue for Klondike. Separate plots are presented for each cruise, which allows us to examine the seasonal evolution of water properties at each site. The data distribution shows that temperatures ranged from ~5.8^{o}C to –1.7^{o}C and that salinities varied from <28 to ~33 in 2008. The temperature range is greater at Klondike than Burger while the salinity range is greater at Burger than Klondike. The water types in Burger and Klondike tend to differ from one another for each cruise, with the greatest overlap of water properties occurring on the 8/18 – 9/20 cruise. In general, Klondike waters are saltier and warmer than Burger waters for all water types with salinities <32.5. At higher salinities, the temperatures are at or near the freezing point so that the water properties at each station merge. The coldest and saltiest waters were formed the previous winter during freezing and the extrusion of salt during ice formation. These water types are only slowly removed from this portion of the NE Chukchi shelf in summer) by the flow (*Weingartner et a*l., 2005. As shown later, these waters are all found near the bottom in both Burger and in the northeast portion of Klondike. The winter-formed waters were absent from Klondike during the 20 September- 9 October cruise, although still present at Burger. Relatively cold (<2^{o}C) and fresh (e.g., salinity ~ <30) waters likely reflect ice melt and primarily occurred at Burger. The warmer and saltier waters were probably recently advected northward onto the Chukchi shelf from Bering Strait and were chiefly found at Klondike.

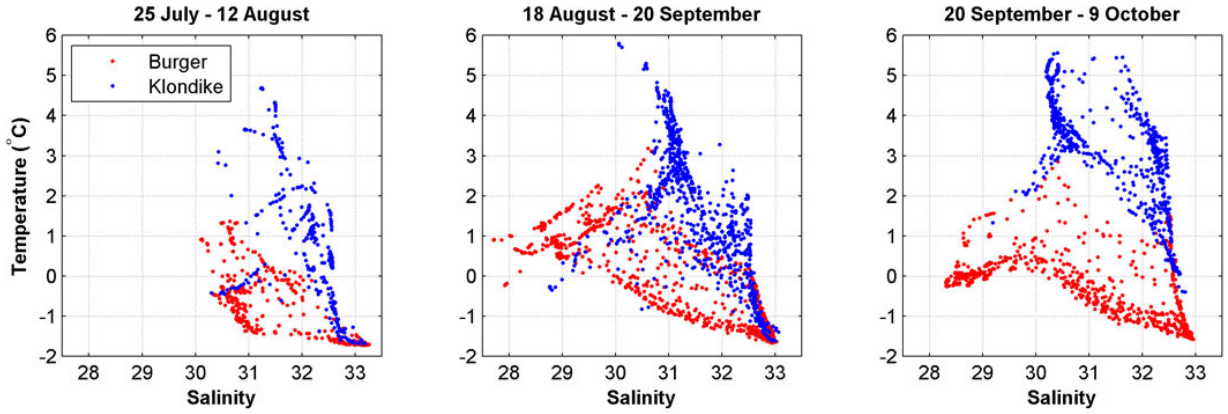

Figure 22. Temperature-salinity diagrams for each survey conducted in 2008.

We next investigate the temperature, salinity, density, and fluorescence distributions as a function of distance and depth (pressure) along a number of transects across both the Klondike and Burger survey areas. For each survey, we constructed transects that extend from west-east, south-north and from southwest-northeast and across both survey areas. **Figure 23** shows the transect locations used in these constructions. These transects were selected because they comprise the broadest possible coverage from the survey cruises. Note that the diagonal and south-north transects each include a dogleg.

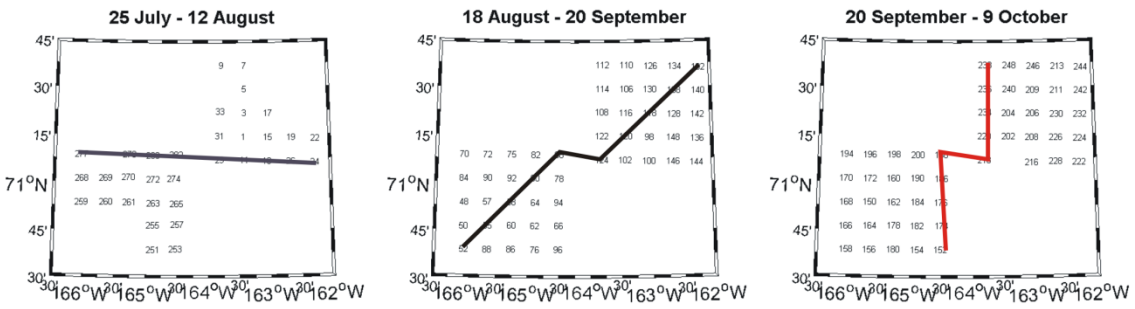

Figure 23. The distribution of stations during each survey in 2008. The black line in the 25 July – 12 August survey shows the stations that were used in constructing the east-west transects. The black line in the 18 August- 20 September survey shows the stations used in constructing the southwest-northeast transects. The red line in the 20 September – 9 October survey shows the stations used in constructing the south-north transect. The west-east, southwest-northeast, and south-north transects were contoured for each survey.

August 3 – 12 2008 Survey

The spatial distributions of water mass properties are shown in **Figures 24 – 26** along the west-east, south-north, and southwest-northeast transects, respectively. Each transect is represented by four panels that show temperature (^{o}C), salinity (unitless), sigma-t (a scaled variable for water density), and fluorescence (volts); the latter being a relative measure of chlorophyll biomass.

The section from the 3-12 August survey (**Figure 24**) indicates a west-east division in water masses. The two westernmost stations are relatively warm (1 to 1.5^{o}C), moderately saline (~32 to 32.5) and weakly stratified in the lower 10 m of the water column. These stations are separated from those to the east by a weak surface temperature and salinity front across which temperatures (salinities) decrease by 1^{o}C (1). We suspect that this front lies along the eastern flank of the Central Channel that carries Bering shelf water northward onto the outer Chukchi shelf. East of the front, the stations have a nearly 20 m thick bottom layer of cold (~-1.5^{o}C), salty (33) water remnant from the previous winter. The bottom layer is separated by a strong halocline (across which salinities increase by about 2 over 10 m), from a relatively fresh (<31) and cold (0 – 1.0^{o}C) 15 m thick surface layer. The southwest to northeast section across Klondike and Burger is shown in **Figure 25** and has many of the same features seen in the west-east section.

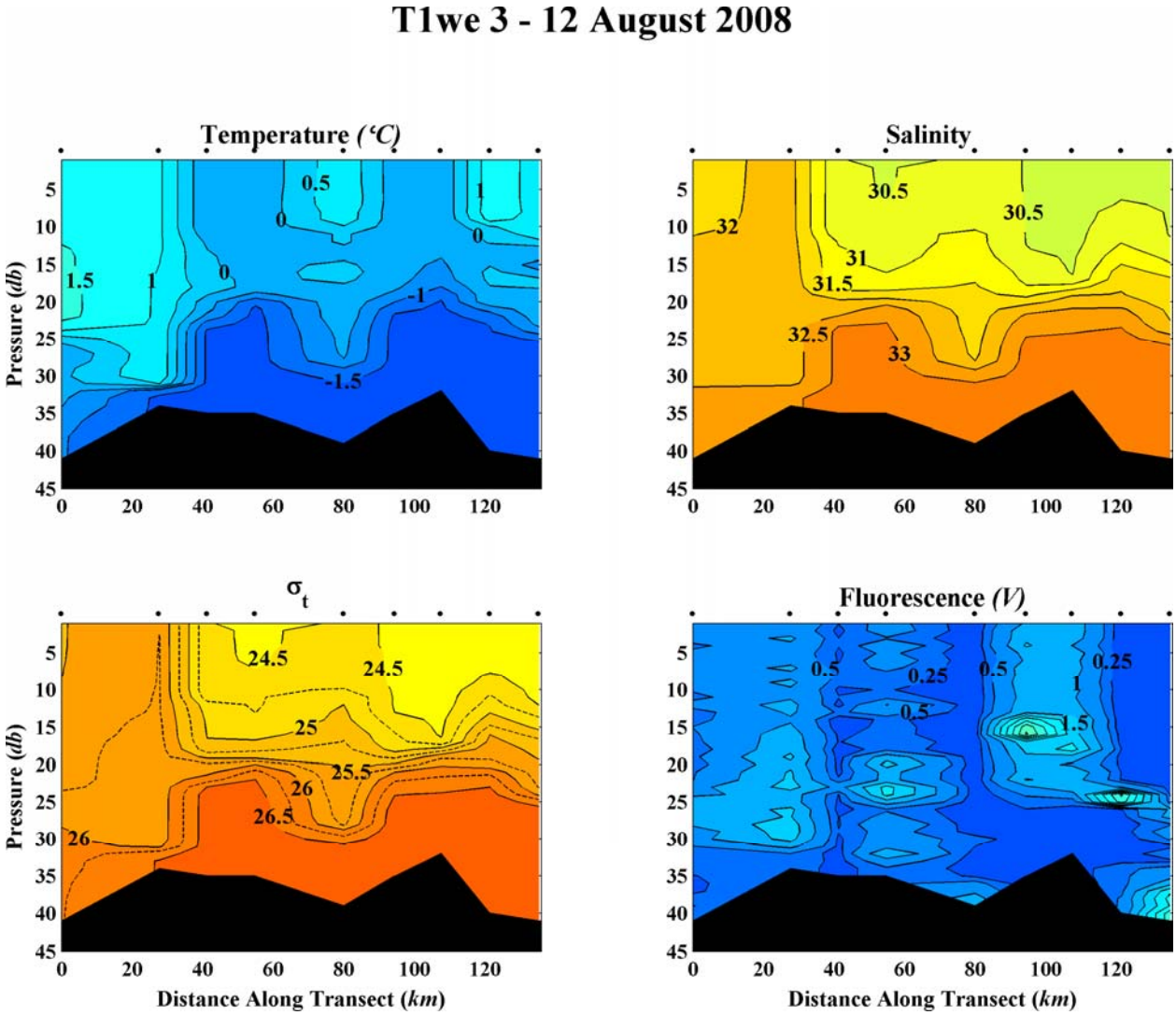

Figure 24. West-east section of temperature (upper left), salinity (upper right), sigma-t (lower left), and fluorescence (lower right) from the 3-12 August survey.

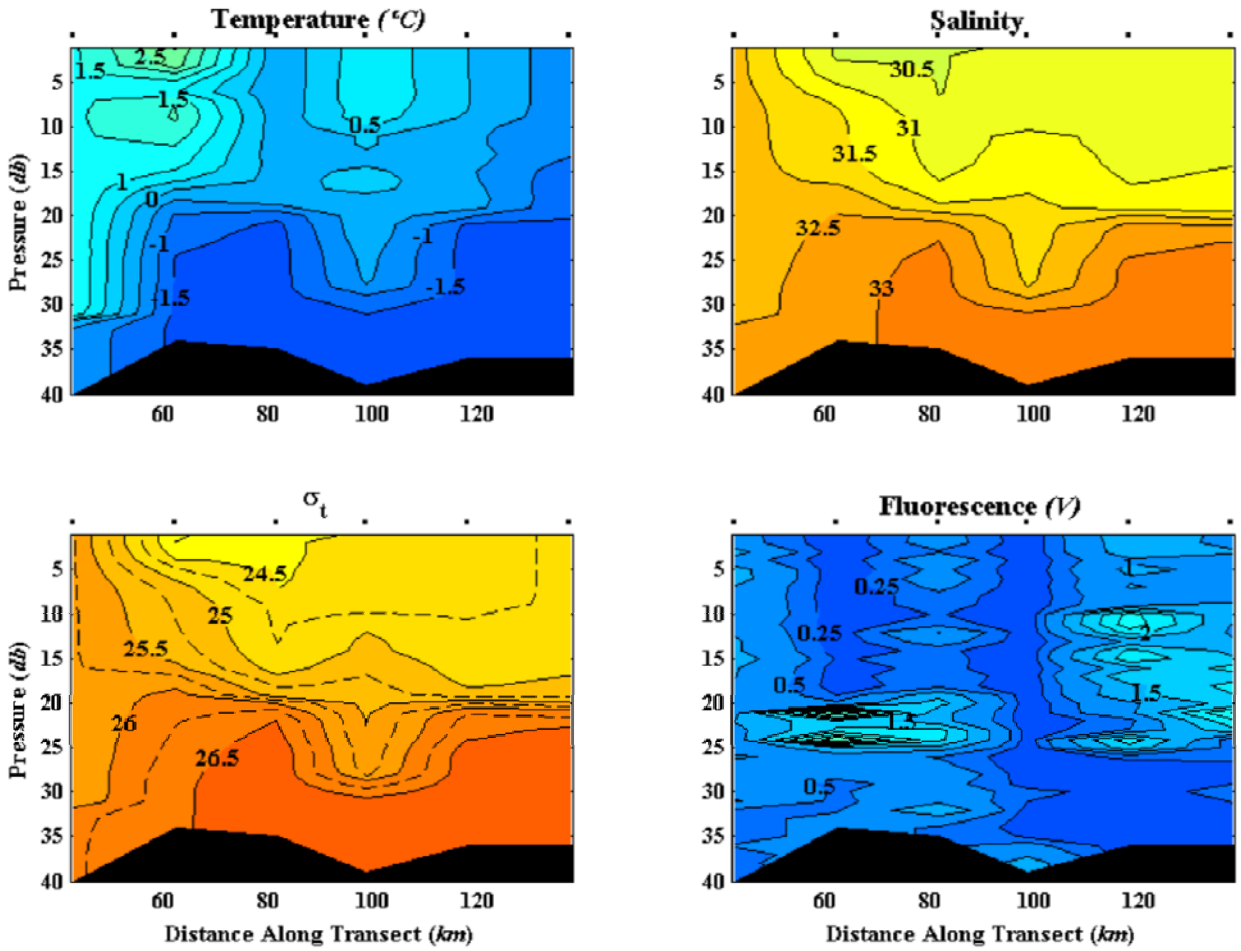

Figure 25. The southwest-northeast section of temperature (upper left), salinity (upper right), sigma-t (lower left), and fluorescence (lower right) from the 3-12 August survey.

The south-north sections (**Figure 26**) from the August 2008 survey further illustrate the spatial variations in water properties. Warm (>4°C) waters are found at the southern end of the transect and are confined to the upper 10 m of the water column. Surface temperatures decrease rapidly north of this warm water (e.g., they decrease by 3°C across a temperature front that spans a distance of 40 km), before more gradually decreasing to about 0°C at the northern end of the transect. Temperatures are, however, relatively cold beneath the surface layer and range from 0°C at the southern end of the section to -1.5°C at the northern end. The surface temperature front slopes downward to the south, indicating that relatively warm surface waters are moving over the colder subsurface water. The salinity structure along this section includes relatively dilute surface waters at the northern end of the section and moderately saline surface waters at the southern end and at mid-depth over the middle of the section. At depths greater than 20 m the entire section is filled with high salinity water, with the highest salinities at the northern end of the section. Note also that the 31 and 31.5 isohalines bow upward toward the south. The inclination of these isohalines is opposite to that of the isotherms. However, there is no strong

frontal structure evident in the isopycnals (sigma-t isopleths), which implies that the density of the fresh, cold waters along the northern end of the transect is similar to the density of the warm, salty waters penetrating from the south. Hence, neither the thermal or haline front along this section is a dynamic front that inhibits frontal exchange; thus the water masses can easily mix laterally with one another here.

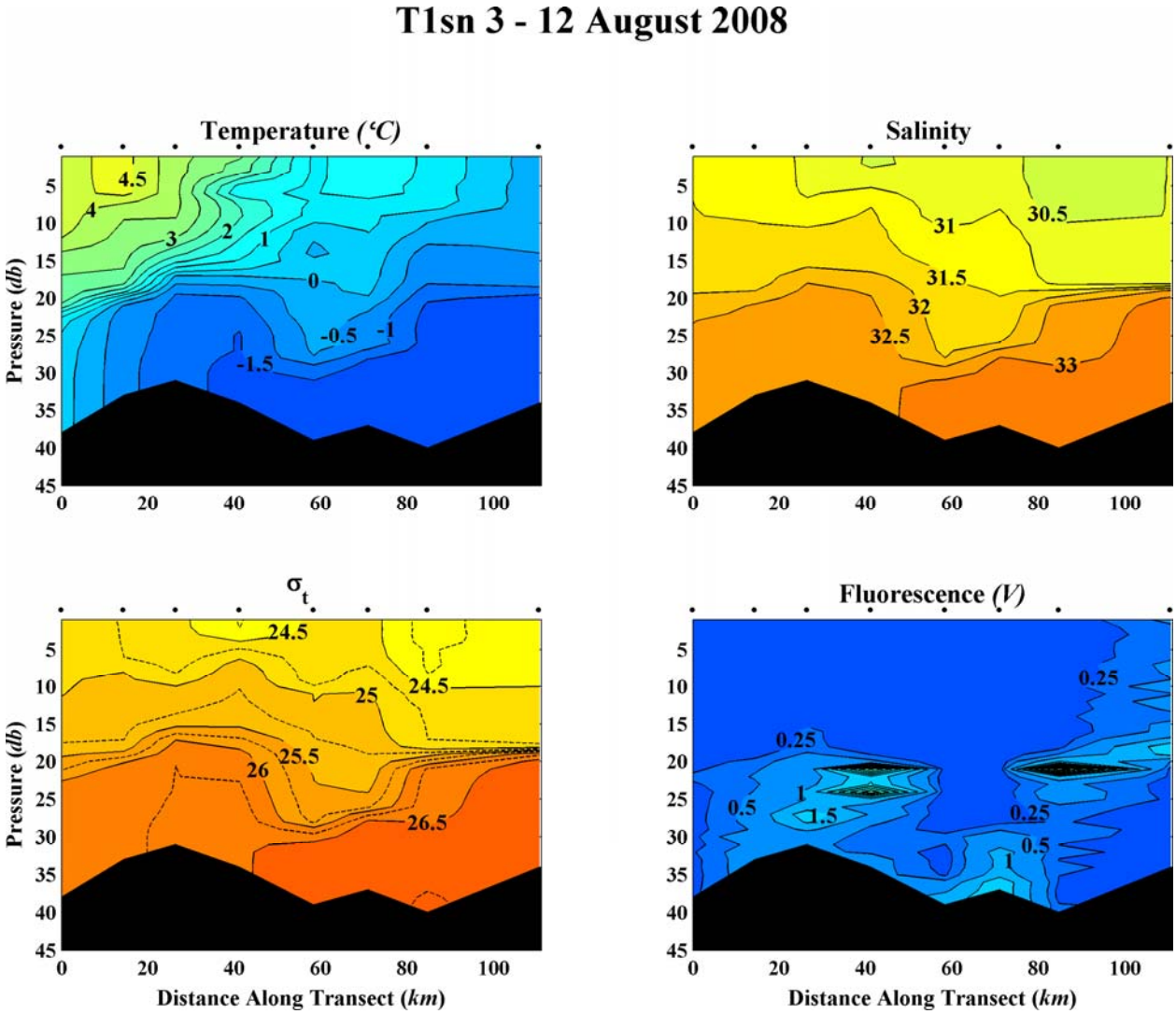

Figure 26. The south-north section of temperature (upper left), salinity (upper right), sigma-t (lower left), and fluorescence (lower right) from the 3-12 August survey.

August 18 – September 20 2008 Survey

The corresponding figures for this survey are shown in **Figure 27** (west-east), **Figure 28** (southwest-northeast) and **Figure 29** (south-north). At this time bottom waters with salinities $\geq$ 33 are absent and bottom temperatures had warmed slightly since only a few stations had bottom temperatures <-1.5°C. Instead the lower half of the water column, in both Klondike and Burger, has salinities of 32.5 or more and temperatures <0°C. The surface layer, however, has a more complicated temperature and salinity structure. Along the western end of the section, relatively

warm and moderately saline waters are found adjacent to the Central Channel, and the water column here was relatively unstratified compared to the other stations. Elsewhere, and primarily in the northeastern corner of Klondike and within Burger, the surface layer contained bands of cool (~0^{o}C), low salinity (29) water, very likely associated with ice meltwater, separated by warmer and saltier filaments. These bands are shallow, ~20 m or less, and were most likely associated with shallow eddies and meanders emanating from dynamic instabilities associated with ice edge fronts and/or meltwater presumably trapped over Hanna Shoal. Ice-melt pools are also suggested in both the southwest-northeast (**Figure 28**) and south-north (**Figure 29**) transects, as indicated by the cold (<2^{o}C), low-salinity (<30) water in the upper right hand panel of each figure.

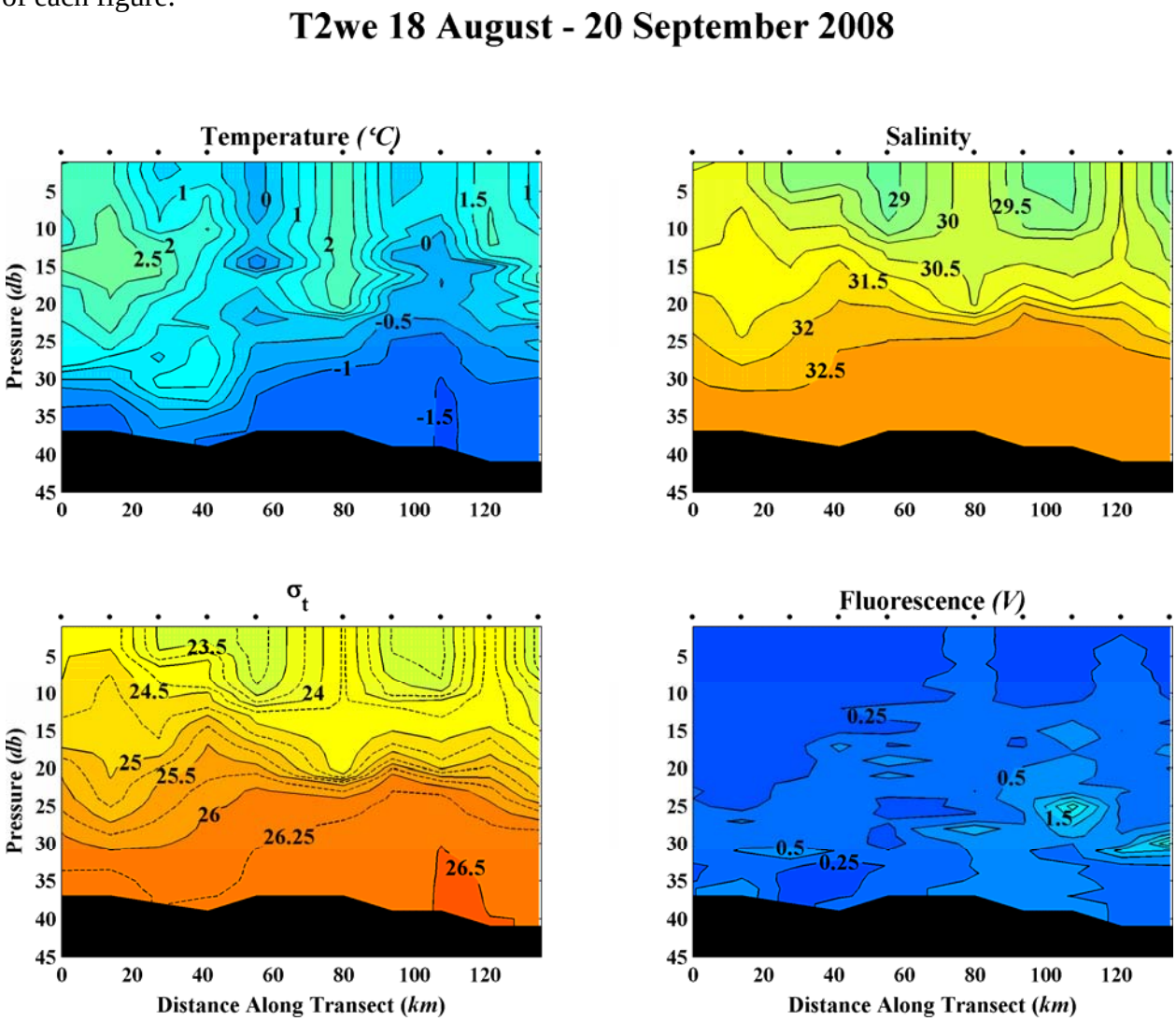

Figure 27. The west-east section of temperature (upper left), salinity (upper right), sigma-t (lower left), and fluorescence (lower right) from the 18 August – 20 September survey.

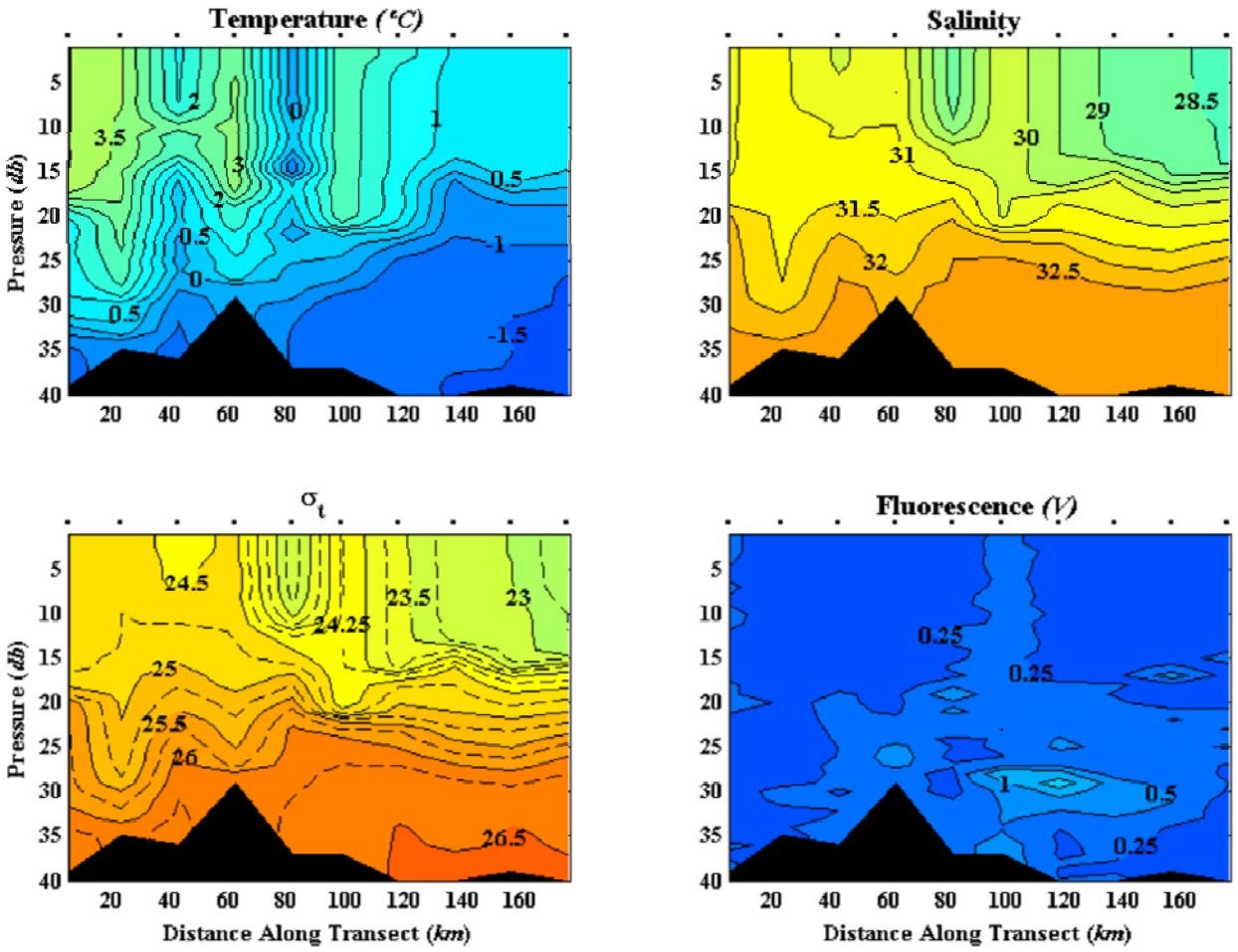

Figure 28. The southwest-northeast section of temperature (upper left), salinity (upper right), sigma-t (lower left), and fluorescence (lower right) from the 18 August – 20 September survey.

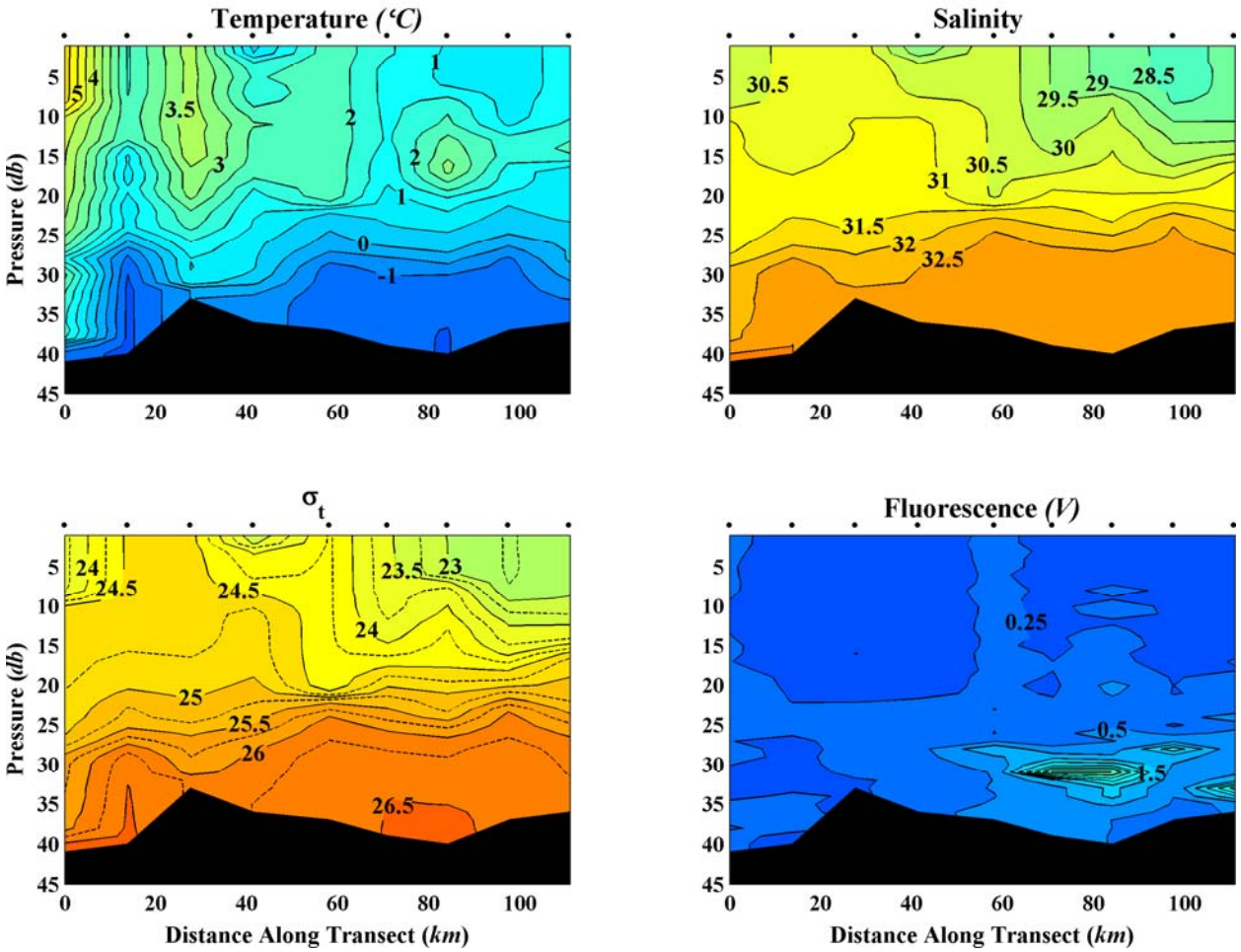

Figure 29. The south-north section of temperature (upper left), salinity (upper right), sigma-t (lower left), and fluorescence (lower right) from the 18 Aug. – 20 Sept. survey.

September 20 – October 9 2008 Survey

Many of the basic features of the hydrography evident during the first two surveys were present by the time of the third and final 2008 survey. For example, relatively warm and moderately saline water is still found in the westernmost stations along the west-east line (**Figure 30**), and cold, saline water occupies the bottom 15 m or so of the water column, while cool, dilute water occupies most of the upper water column. There is a noticeable decrease in the amount of water with salinity of 32.5 found in all sections compared with the second survey. In addition, the bands and filaments inferred on the second survey have largely disappeared. These have been replaced with broad pools of cool, dilute water. Conceivably the filaments inferred from the second survey mixed (both laterally and vertically) through time and thus formed a rather thick upper layer water mass with salinities <30 and temperatures of from 0.0 to 2°C. There was still a considerable amount of warm water entering the southwestern, southern and western flank of the Klondike prospect (**Figures 30** and **31**), although that water has not penetrated much farther

north than in the other surveys. This is consistent with the notion that the waters south of Hanna Shoal are only replenished slowly throughout the summer and fall.

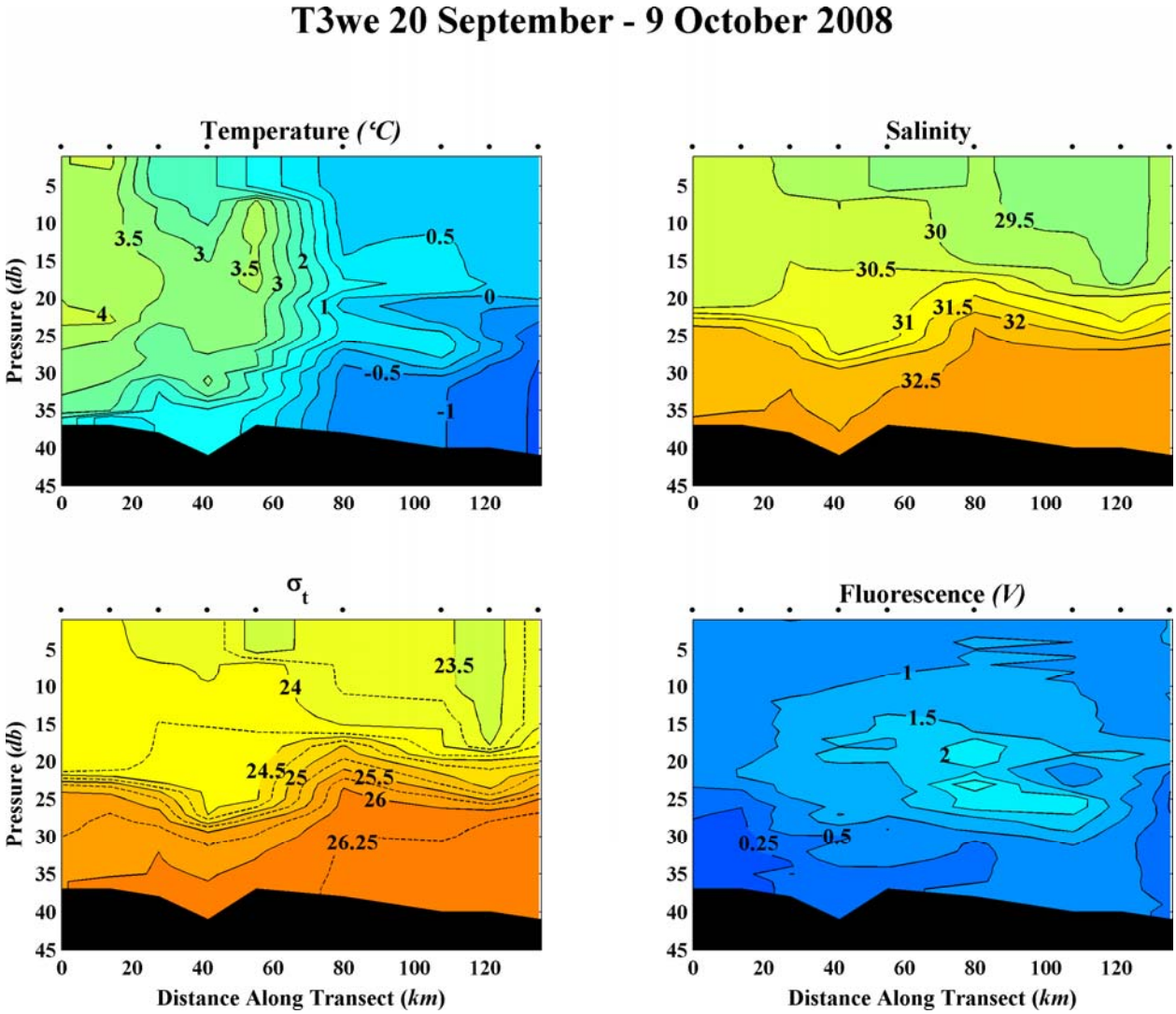

Figure 30. The west-east section of temperature (upper left), salinity (upper right), sigma-t (lower left), and fluorescence (lower right) from the 20 September – 9 October survey.

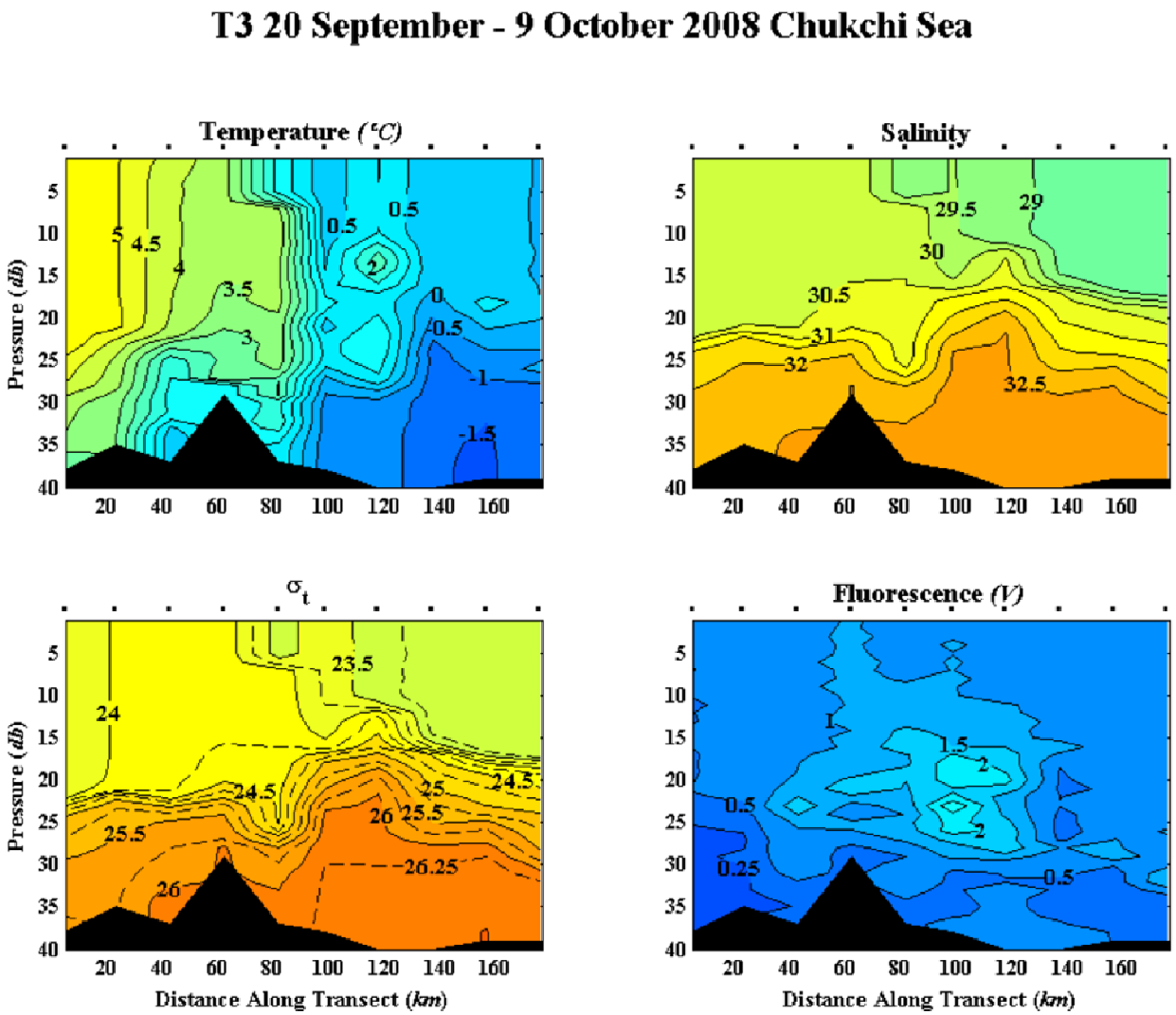

Figure 31. The southwest-northeast section of temperature (upper left), salinity (upper right), sigma-t (lower left), and fluorescence (lower right) from the 20 September – 9 October survey.

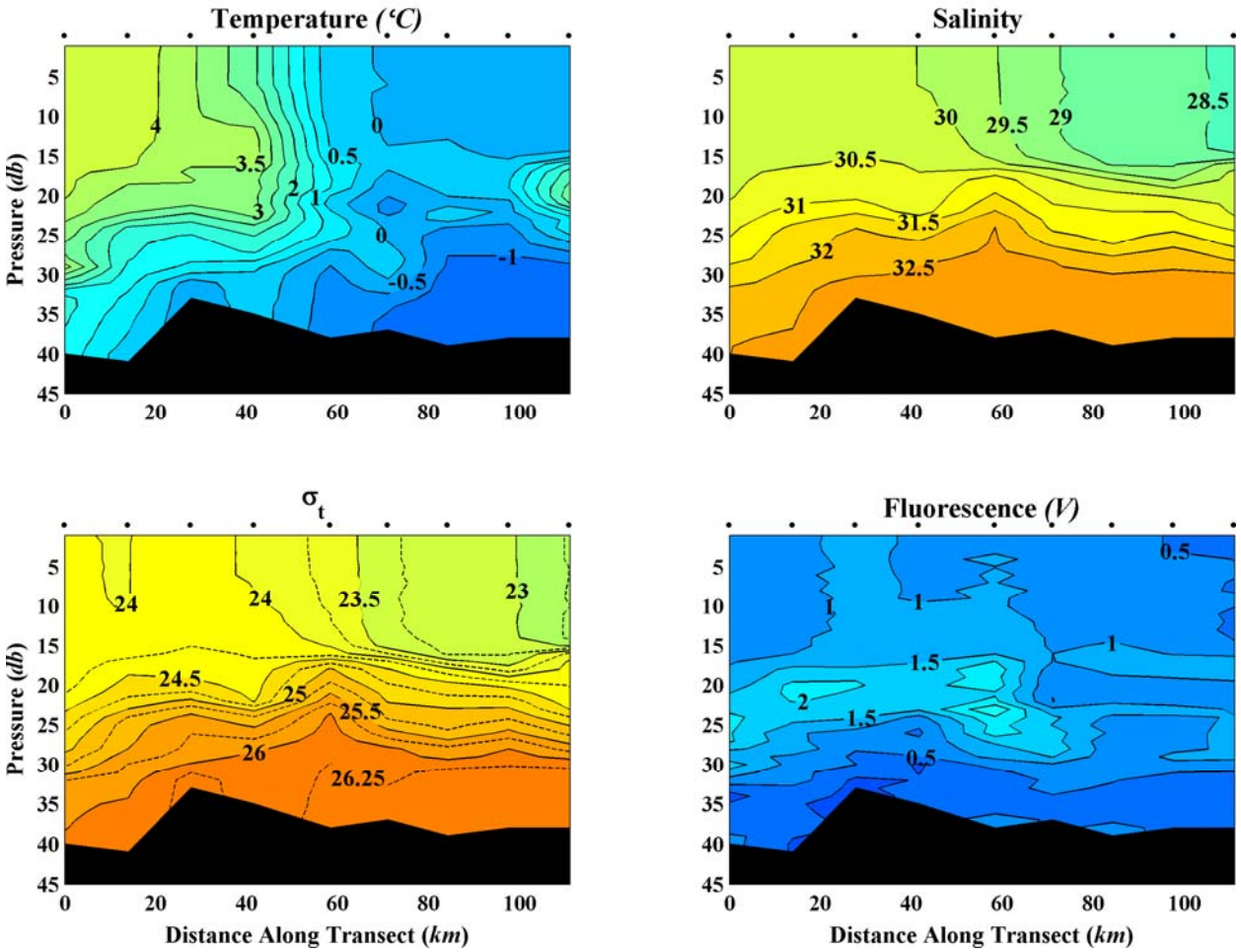

Figure 32. The south-north section of temperature (upper left), salinity (upper right), sigma-t (lower left), and fluorescence (lower right) from the 20 September – 9 October survey.

We close by noting that in all the sections the maximum fluorescence is not found at the surface, but at mid-depth and within the halocline that separates the surface mixed layer from the deeper waters. This suggests that the upper layers were depleted in nutrients by the time of the first survey, but that sufficient light and nutrients were available at mid-depth to maintain some level of primary production throughout the summer and early fall.

Many of the features alluded to above are also evident in vertically-averaged temperature and salinity properties. For example, **Figures 33** and **34** show these variables for each survey averaged over the upper 10 m and contoured in plan view. **Figure 33** shows that upper ocean temperatures in the Burger prospect changed only slowly through time, whereas, Klondike surface temperatures warmed appreciably between early August and late September. Moreover, the temperature and salinity (**Figure 34**) pattern also suggest the northward penetration of warmer salty water on the west side of Klondike and the presence of a moderately strong thermal front in Klondike. That front appears to have migrated within Klondike through time, so that by

the late September it developed in the northeast corner of Klondike and separated Klondike waters from the cooler waters within Burger.

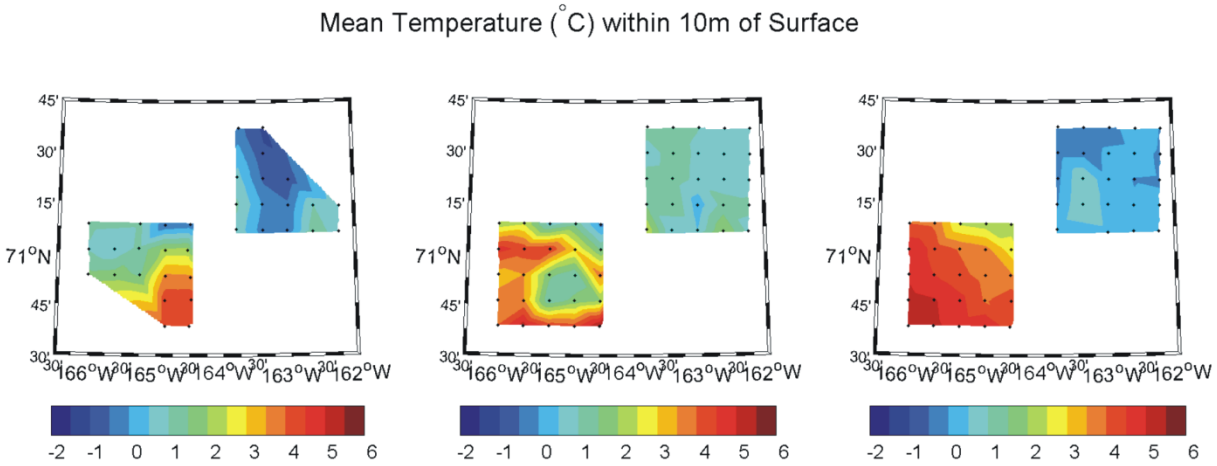

Figure 33. Plan view of mean temperature over the upper 10 m of the water column for the 27 July - 12 August survey (left), the 19 August -20 September survey (middle) and the 20 September – 9 October survey (right).

The front is also evident in satellite imagery, which affords a broader scale perspective (**Figure 35**). The image shows warm water spreading northward from Bering Strait, with a tongue protruding northward through the Central Channel (indicated by an arrow in the figure), while to the north and northeast surface temperatures are cooler. Note that the sharp color (and thermal) contrast between the warm water from the south and the cold water to the north defines the approximate location of the front. In addition the warm water does not extend along the

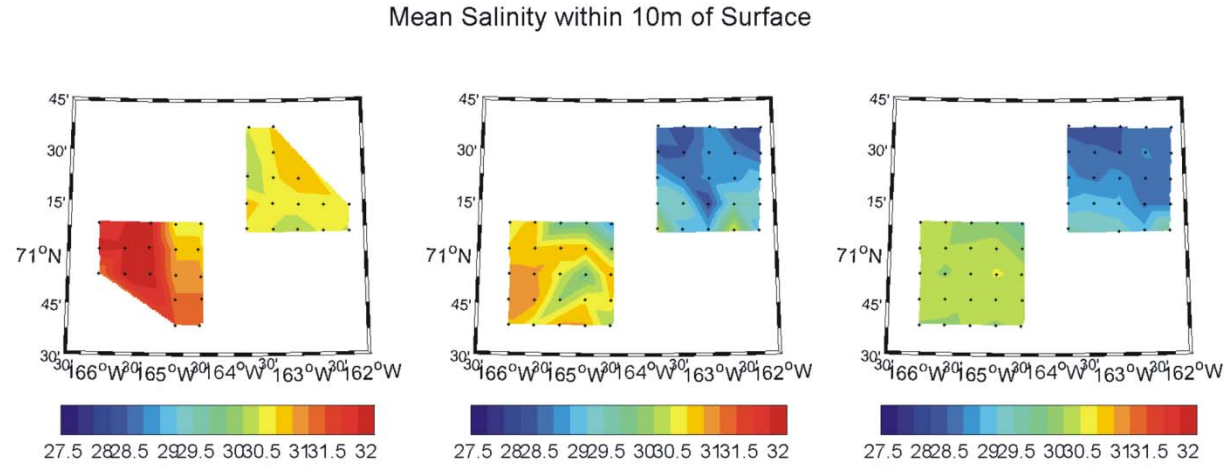

Figure 34. Plan view of mean salinity over the upper 10 m of the water column for the 27 July - 12 August survey (left), the 19 August -29 September survey (middle) and the 20 September – 9 October survey (right).

northwest coast of Alaska (as is often the case at this time of the year) in this image. Most likely this reflects the effect of the winds from the northeast that prevailed through much of August

2008. These winds would have promoted upwelling of cold water along the coast and southwestward transport of cooler water along the Alaskan coast.

By contrast, in 2007 winds were more frequently from the south in summer. Hence the comparable image from August 24, 2007 (**Figure 36**), shows that warm waters pervaded the entire northeast Chukchi shelf, with the warmest waters appearing along the Alaskan coast and extending to the northeast of Barrow onto the Beaufort Sea slope.

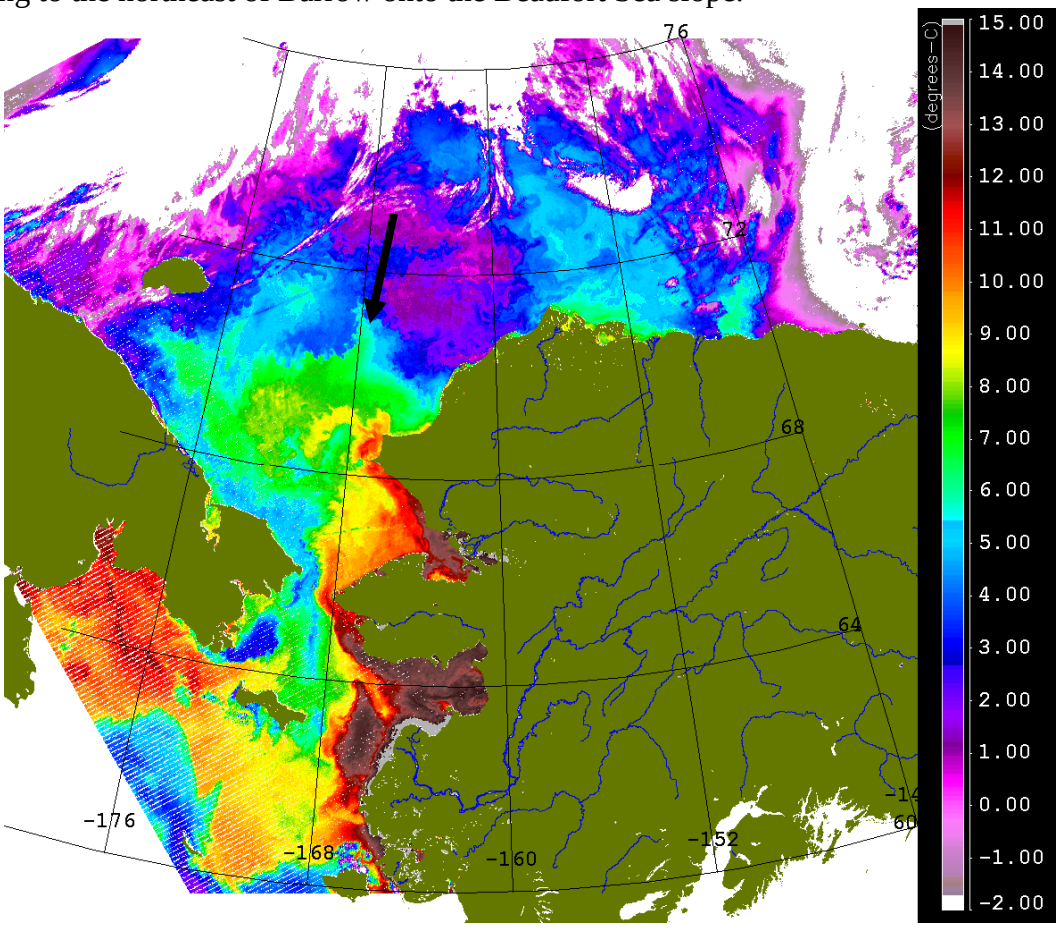

Figure 35 August 22, 2008 MODIS sea surface temperature image of the Chukchi Sea and Bering Strait. (MODIS/Aqua data obtained from Ocean Color Data Processing Archive NASA/Goddard Space Flight Center Greenbelt, MD – USA and available at: http://mather.sfos.uaf.edu/~mschmidt/ims_chukchi_sea_summary.html. The black arrow indicates the tongue of relatively warm water in the Central Channel.

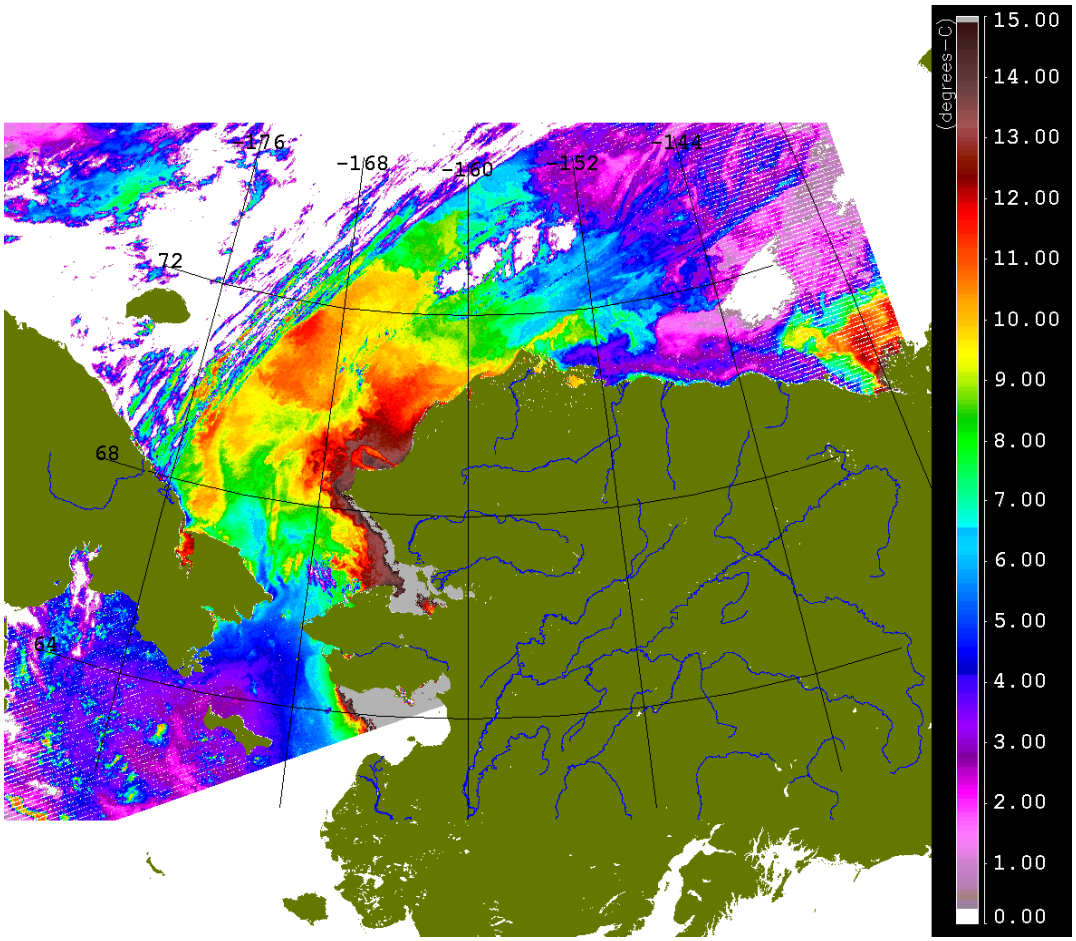

Figure 36. August 24, 2007 MODIS sea surface temperature image of the Chukchi Sea and Bering Strait. (MODIS/Aqua data obtained from Ocean Color Data Processing Archive NASA/Goddard Space Flight Center Greenbelt, MD – USA and available at: http://mather.sfos.uaf.edu/~mschmidt/ims_chukchi_sea_summary.html.

We conclude this section with **Figures 37 and 38**, which show the temperature and salinity averaged over the bottom 10-m of the water column for each survey. Once again these figures underscore that relatively rapid changes in temperature and salinity occur in Klondike over the season, while nearly constant temperature and salinity conditions occurred at Burger.

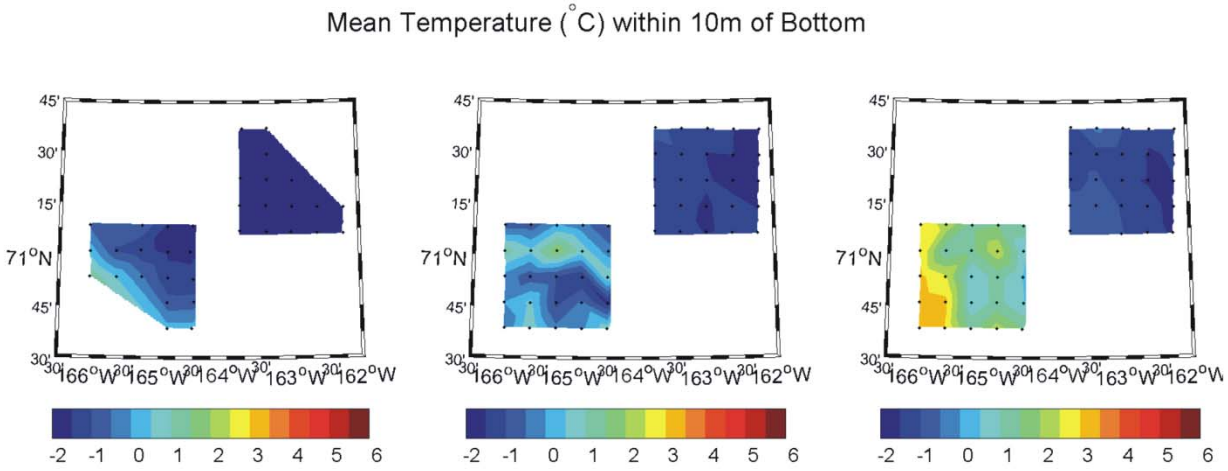

Figure 37. Plan view of mean temperature over the bottom 10 m of the water column for the 27 July - 12 August survey (left), the 19 August -29 September survey (middle) and the 20 September – 9 October survey (right).

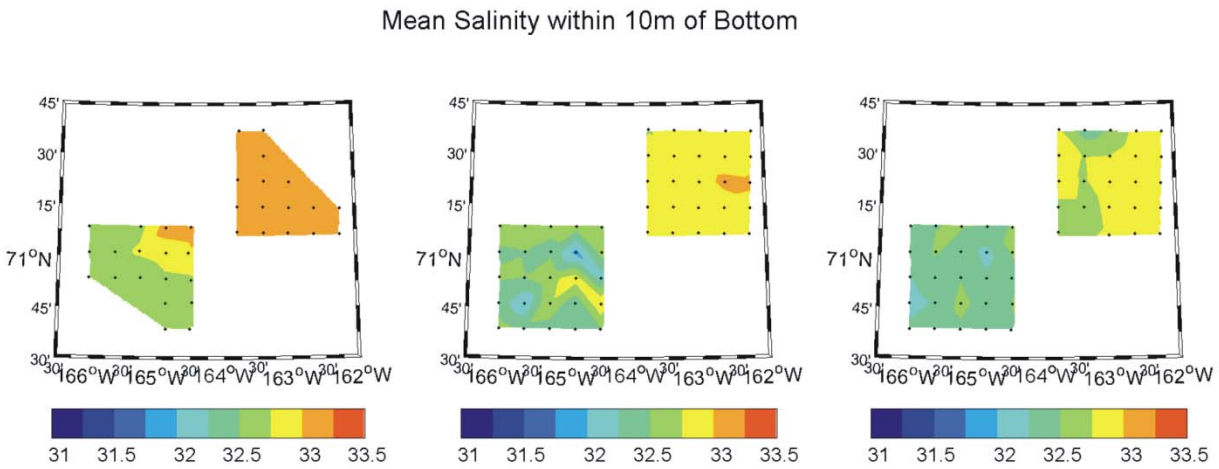

Figure 38. Plan view of mean salinity over the bottom 10 m of the water column for the 27 July - 12 August survey (left), the 19 August -29 September survey (middle) and the 20 September – 9 October survey (right).

Results: 2009 Survey

As with the 2008 survey, we begin by reviewing the temperature-salinity (T/S) diagrams for each cruise (**Figure 39**), with red dots signifying data from Burger and blue dots indicating data from Klondike. Separate plots are presented for each cruise and these may be directly compared with their 2008 counterparts. The data distribution indicates considerable variability with temperatures ranging from nearly 8°C to –1.7°C and salinities ranging from ~28 to ~32.8. As in 2008, the temperature range is greater at Klondike than Burger while the range in salinity is greater at Burger than Klondike. However, for salinities >32, the water properties at each prospect are similar to one another. The broad range in T/S properties at Burger, especially for water types with salinities <~31, reflects warming of ice-melt waters and mixing with adjacent

water masses. In general, Klondike waters are saltier and warmer than Burger waters for all water types with a salinity <32.5.

The T/S diagrams for each site and cruise reflect the seasonal transition in water masses. For example, at Klondike the salinity distribution varies very little between cruises, although the systematic decrease through time in temperatures at the high temperature end of the Klondike distribution reflects seasonal cooling of the upper ocean. This seasonal temperature decrease is also evident at Burger, particularly between the second and third surveys. There is also a systematic change in the properties of the cold, salty winter-formed waters at each site between summer and fall. The coldest and saltiest waters were present on the 14 – 29 August cruise and gradually replaced by warmer and fresher waters through time, with these changes reflecting the gradual replacement of the winter-formed by warmer and less saline water flowing northward from the Bering Sea.

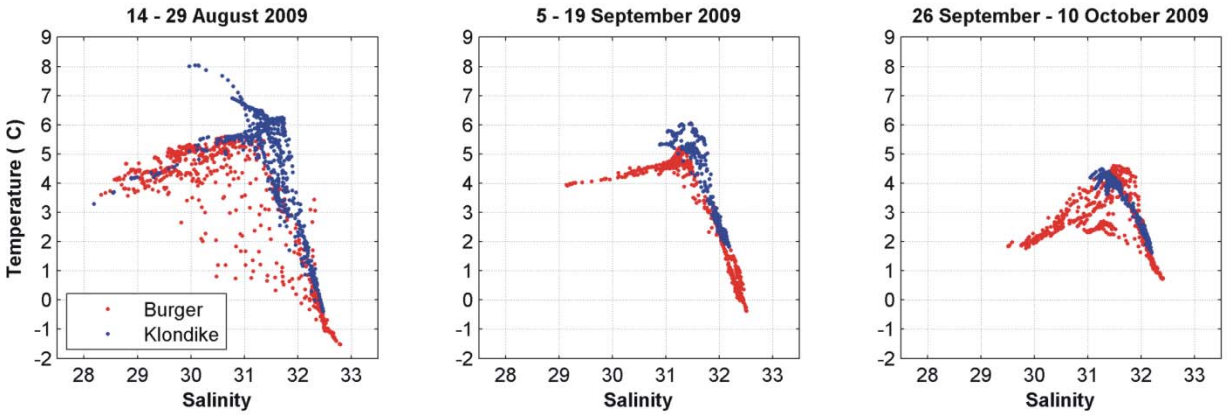

Figure 39. Temperature-salinity diagrams for each of the three surveys conducted in 2009.

Figure 40 shows the distribution of stations and sections occupied in 2009 for the three surveys. As with the 2008 data we constructed vertical cross-sections of temperature, salinity, density and fluorescence. For each survey we constructed west-east, south-north and southwest-northeast transects that cross both survey areas.

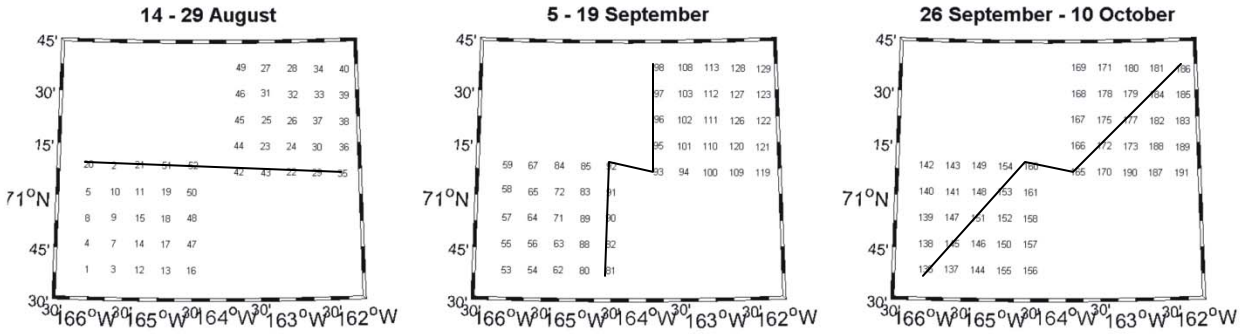

Figure 40. The distribution of stations during each survey. The black line in the 25 July – 12 August survey shows the stations that were used in constructing the west-east transects. The black line in the 18 August- 20 September survey shows the stations used in constructing the southwest-northeast transects. The red line in the 20 September – 9 October survey shows the stations used in constructing the south-north transect. The west-east, southwest-northeast, and south-north transects were contoured for each survey.

August 14 – 29 2009 Survey

Figures 41 - 43 are the west-east, southwest-northeast, and south-north transects formed from stations occupied in both survey areas. The west-east sections from this survey (**Figure 41**) indicate an essentially 2-layer system with temperatures exceeding 4°C and salinities <31.5 in the upper 25 m and colder and saltier waters below. Note that the pycnocline separating the two layers is only ~5 m thick, so that the waters in each layer are nearly uniform in the vertical. Temperatures decrease by ~4°C and salinities increase by about 0.5 across the pycnocline. There are however important differences across this section. At the two westernmost stations (near the Central Channel), the upper layer is warmer and saltier than elsewhere suggesting that these waters have recently arrived from the Bering Sea. In contrast the surface waters in the easternmost part of the transect are relatively fresh and may either be vestiges of ice melt waters that have warmed or are filaments of Alaskan Coastal Water extending westward from the coast. The coldest (~-1 C) and saltiest (>32.5) waters, formed during winter, were also found in the east and along the bottom. Consequently the stratification is stronger in the east than in the west. Fluorescence varies but little throughout the section, although there is a suggestion of a small sub-surface maximum within the pycnocline at some of the stations. The southwest to northeast (**Figure 42**) and the south-north (**Figure 43**) sections across Klondike and Burger have many of the same features seen in the west-east section. Note again that the warmest (>7°C) water occurs at the surface at the southwestern stations.

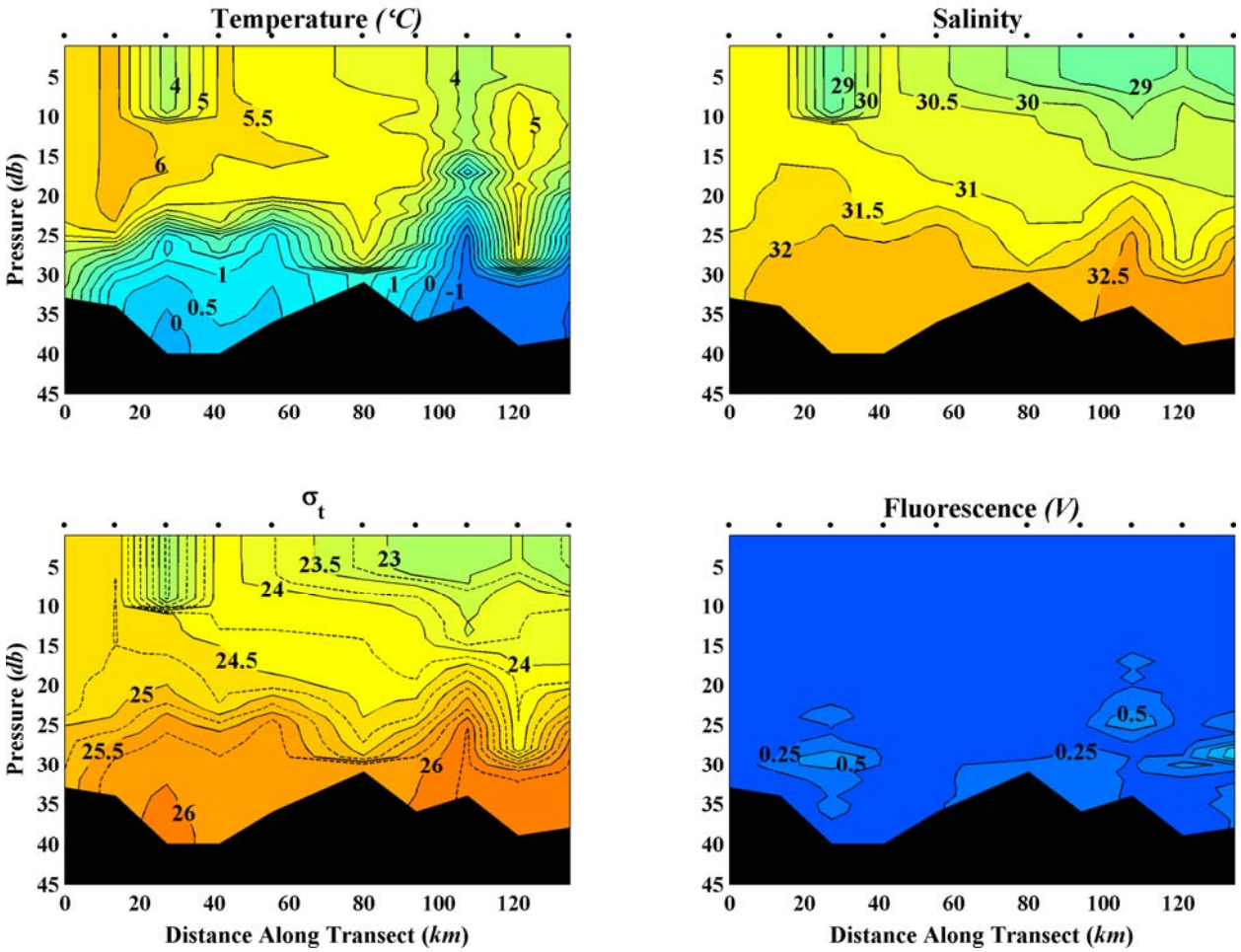

Figure 41. West-east section of temperature (upper left), salinity (upper right), sigma-t (lower left), and fluorescence (lower right) from the 14-29 August survey.

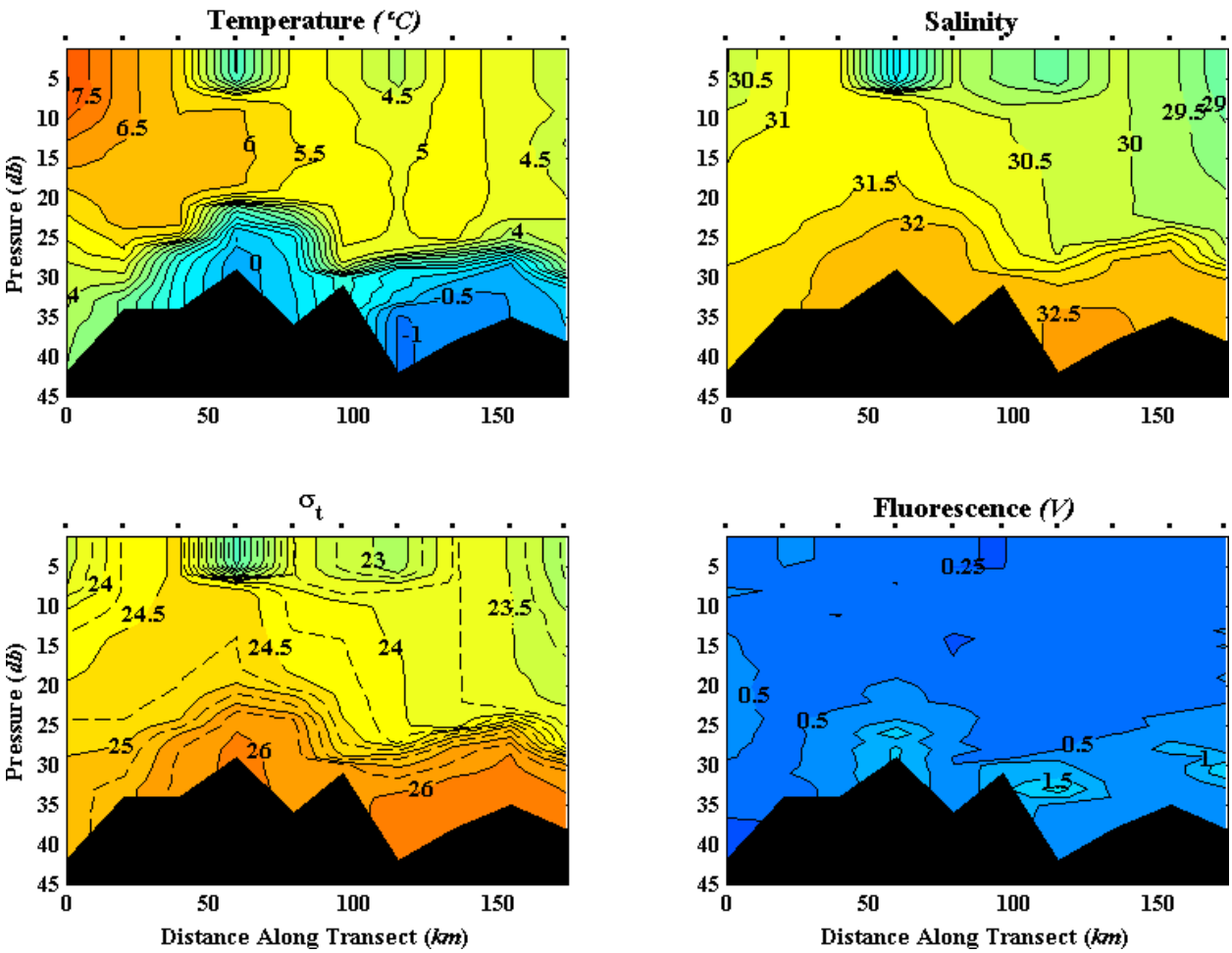

Figure 42. Southwest-northeast section of temperature (upper left), salinity (upper right), sigma-t (lower left), and fluorescence (lower right) from the 14-29 August survey.

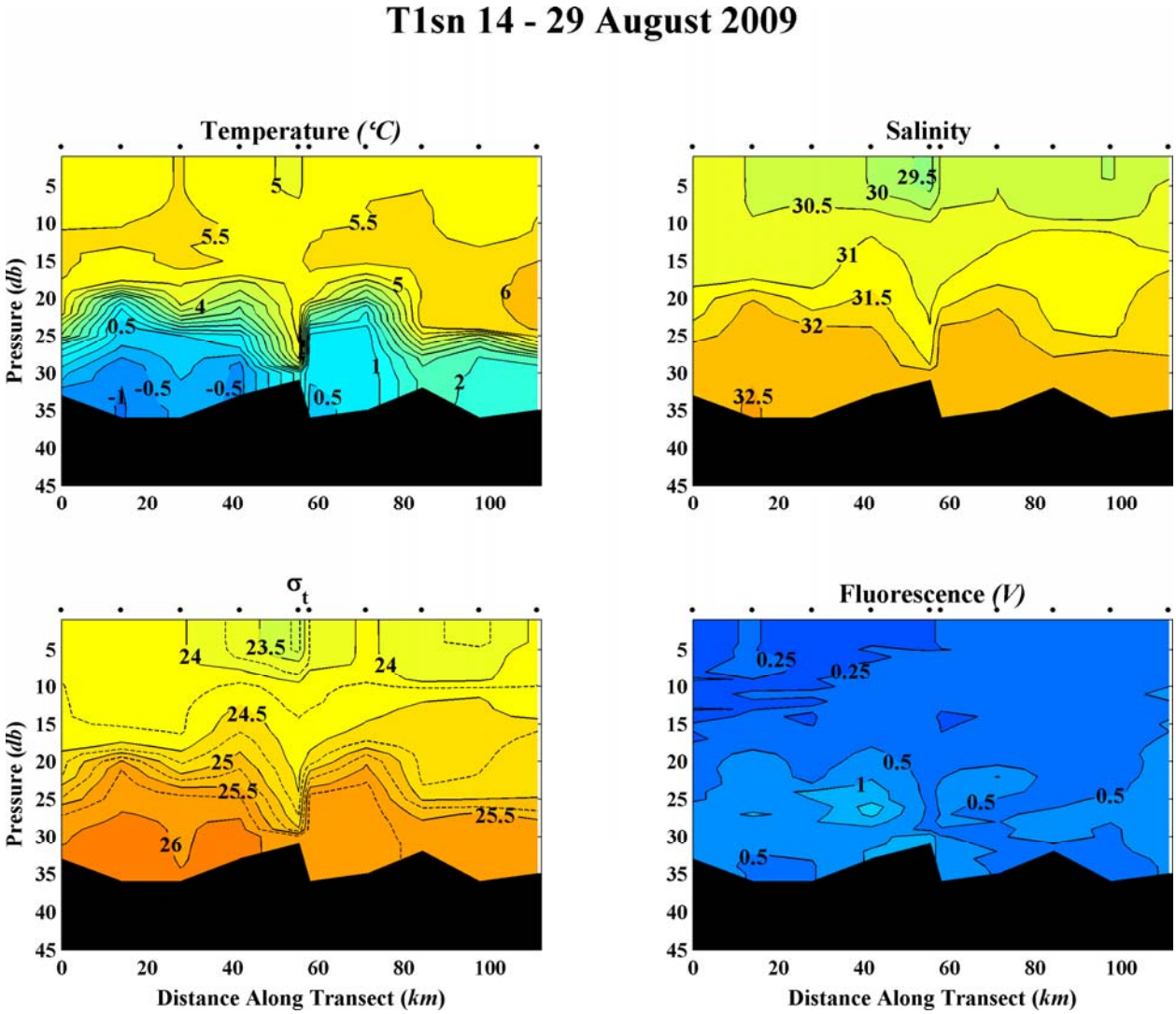

Figure 43. South-north section of temperature (upper left), salinity (upper right), sigma-t (lower left), and fluorescence (lower right) from the 14-29 August survey.

September 5 – 19 2009 Survey

The west-east, southwest-northeast, and south-north transects for this survey are shown in **Figures 44 - 46**. Conditions at this time were remarkably uniform in that both surface and bottom properties show little horizontal variability. Upper ocean salinities vary between 30 and 31.4 and temperatures range from 5.5 to 4.25°C. In comparison to the previous survey the upper layer has deepened so that the pycnocline is thinner and at 30 m depth. Deep water properties have also changed; deep temperatures had warmed to >0°C and salinities decreased to between 32 and 32.4. These changes reflect the seasonal evolution of shelf properties due to cooling and wind mixing in the upper ocean and the replacement, presumably by the currents, of the very cold, saline winter-formed bottom water by warmer and moderately saline water from the Bering Sea. Not surprisingly, fluorescence is low on all these transects.

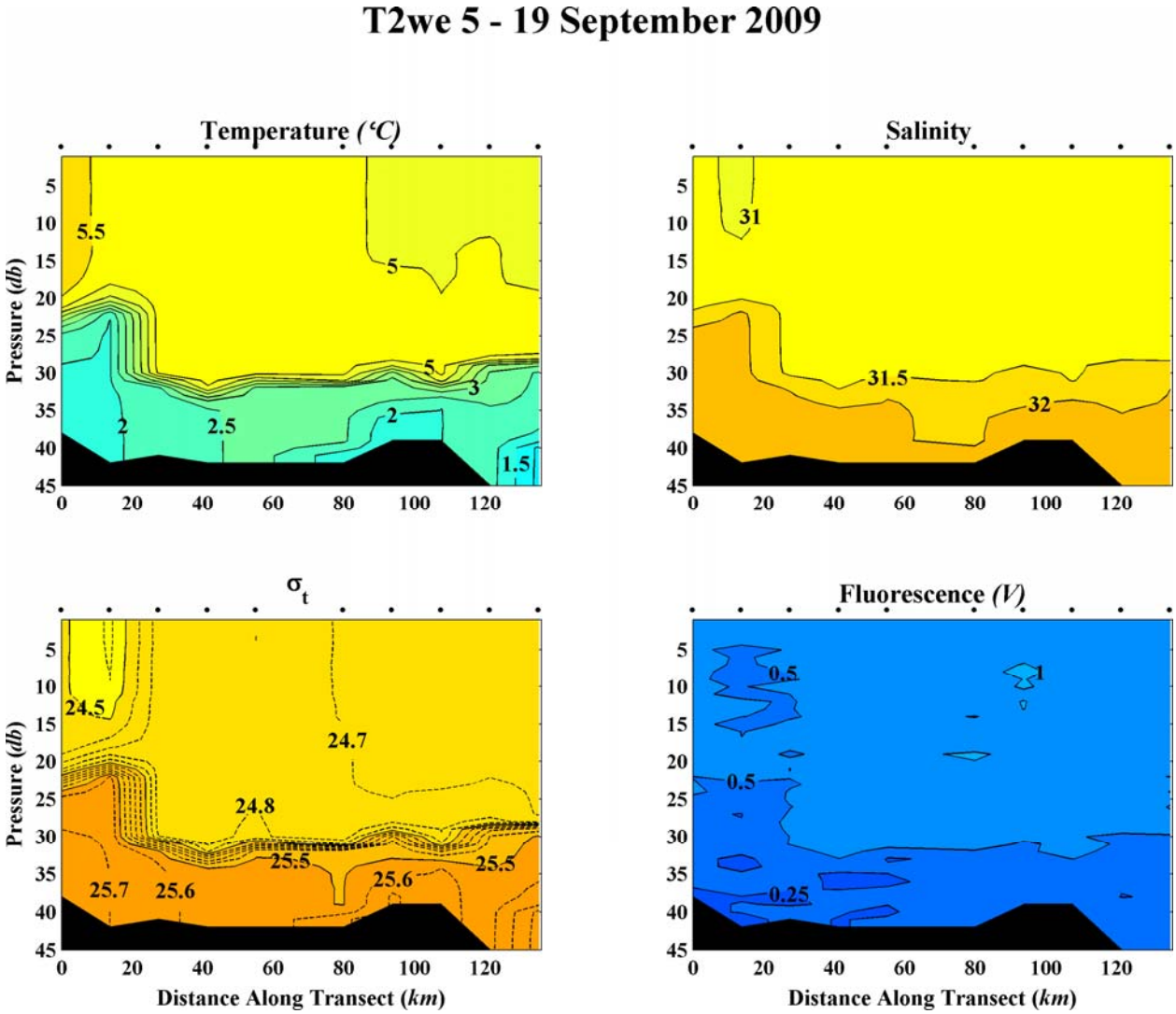

Figure 44. West-east section of temperature (upper left), salinity (upper right), sigma-t (lower left), and fluorescence (lower right) from the 5-19 September survey.

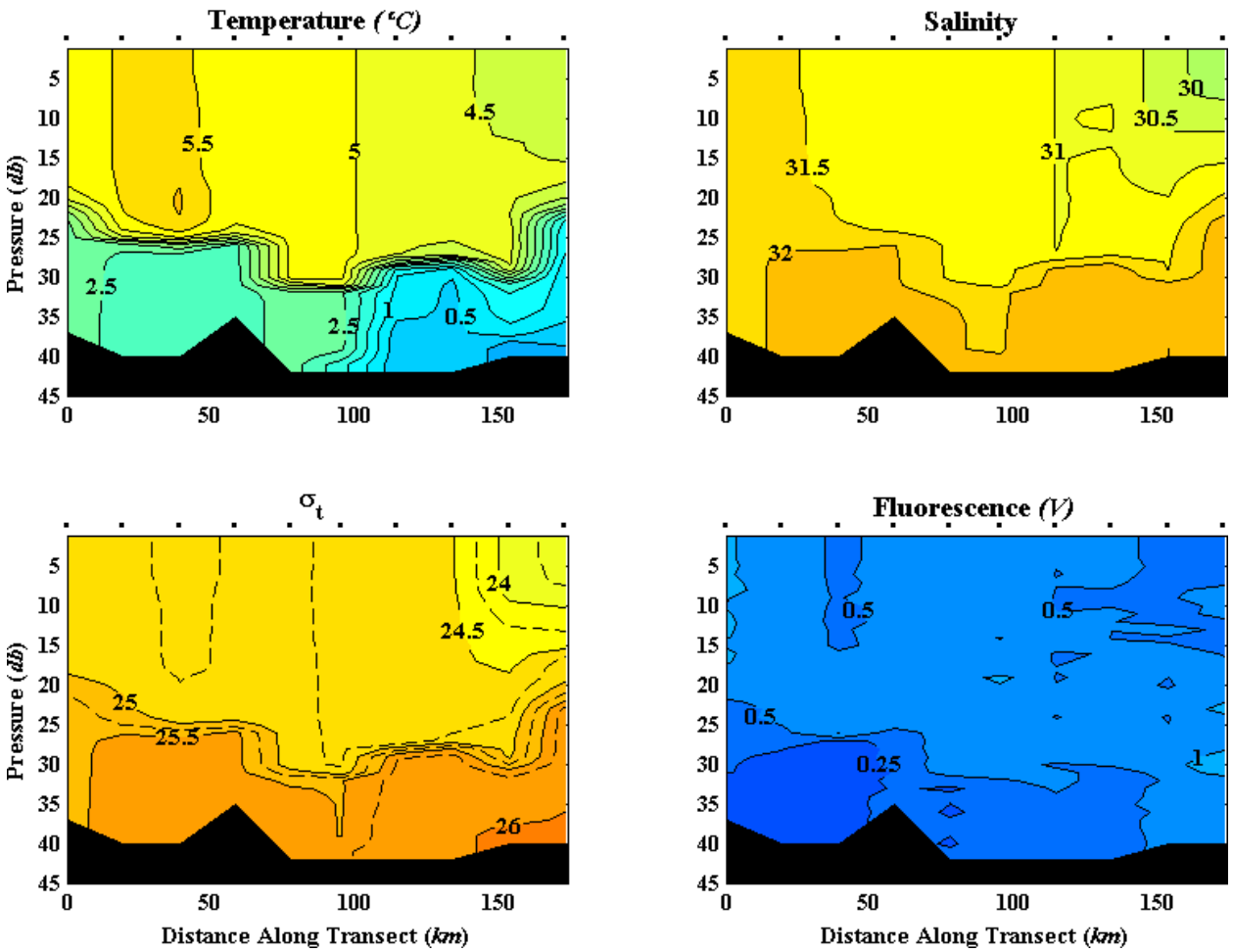

Figure 45. Southwest-northeast section of temperature (upper left), salinity (upper right), sigma-t (lower left), and fluorescence (lower right) from the 5-19 September survey.

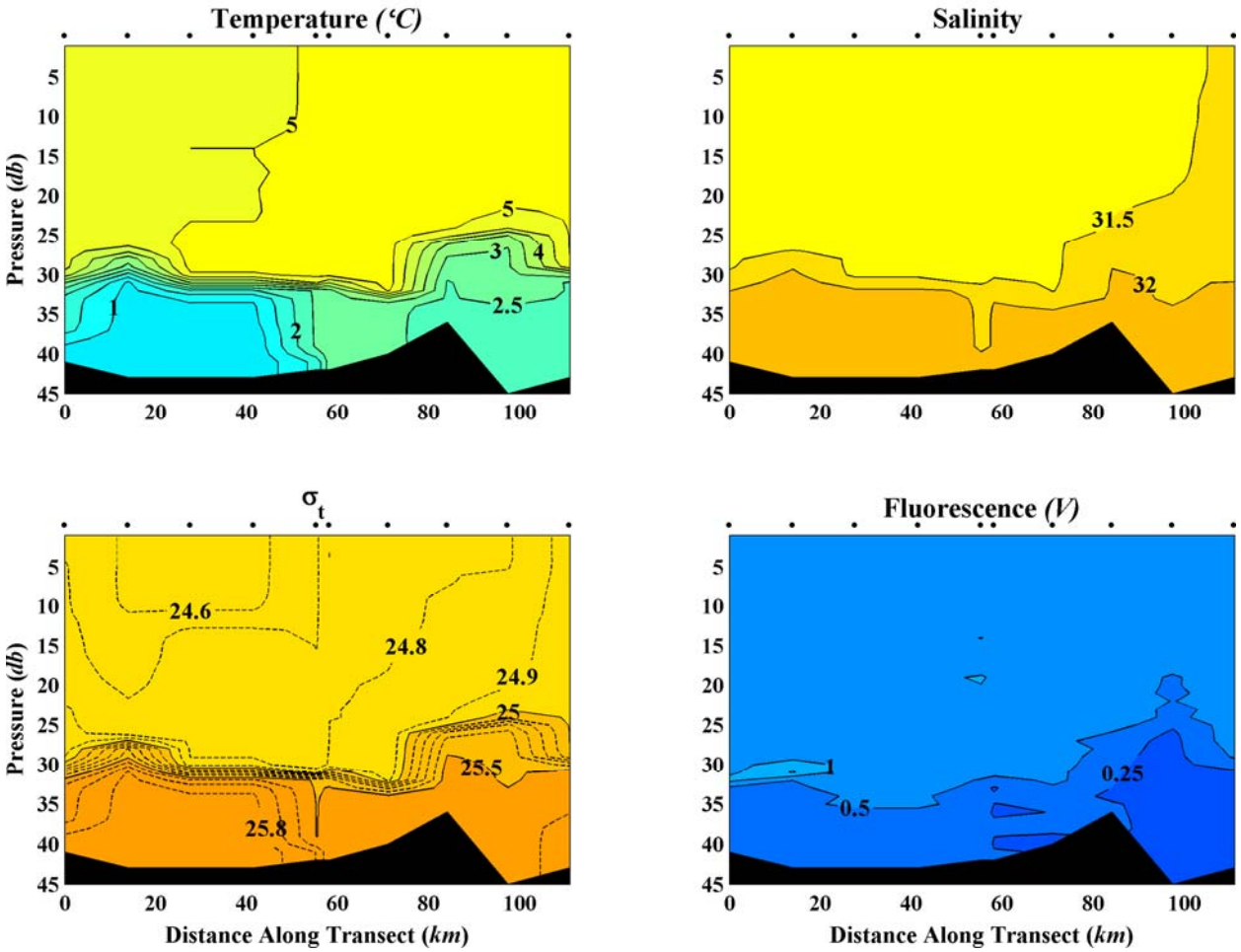

Figure 46. South-north section of temperature (upper left), salinity (upper right), sigma-t (lower left), and fluorescence (lower right) from the 5-19 September survey.

September 26 – October 10 2009 Survey

The west-east, southwest-northeast, and south-north transects for the final 2009 survey are shown in **Figures 47 - 49**. Temperatures above the pycnocline have cooled to ~4^{o}C or less over the upper ocean and the pycnocline has deepened to ~35 m and further eroded over most of both survey areas. The warmest waters are found at the westernmost stations (**Figures 47** and **48**) again reflecting the influence of Bering Sea waters entering into the Central Channel. The stations at the northeast corner of Burger (**Figure 48**) are cooler and fresher than in the previous survey as are the southernmost stations in the Klondike prospect (**Figure 49**).

Surface current mapping, shore-based radars recorded southwesterly flow in the northeast Chukchi Sea between Barrow and Wainwright and also over Hanna Shoal prior to and through the period of this survey (**Figures 50 -52**). For example, from Sept 17 – 24 (**Figure 50**) winds at Barrow were from the northeast at ~9 m s^{-1} and forced southwestward flow along the coast and

westward flow toward Burger. The winds temporarily relaxed between Sept. 25 and Oct 2 (**Figure 51**), at which time the coastal flow reversed to the northeast and the offshore flow was weak and variable. From October 3 – 10 winds were generally westward at ~7 m s^{-1} resulting in westward movement of surface waters (**Figure 56**) toward Burger.

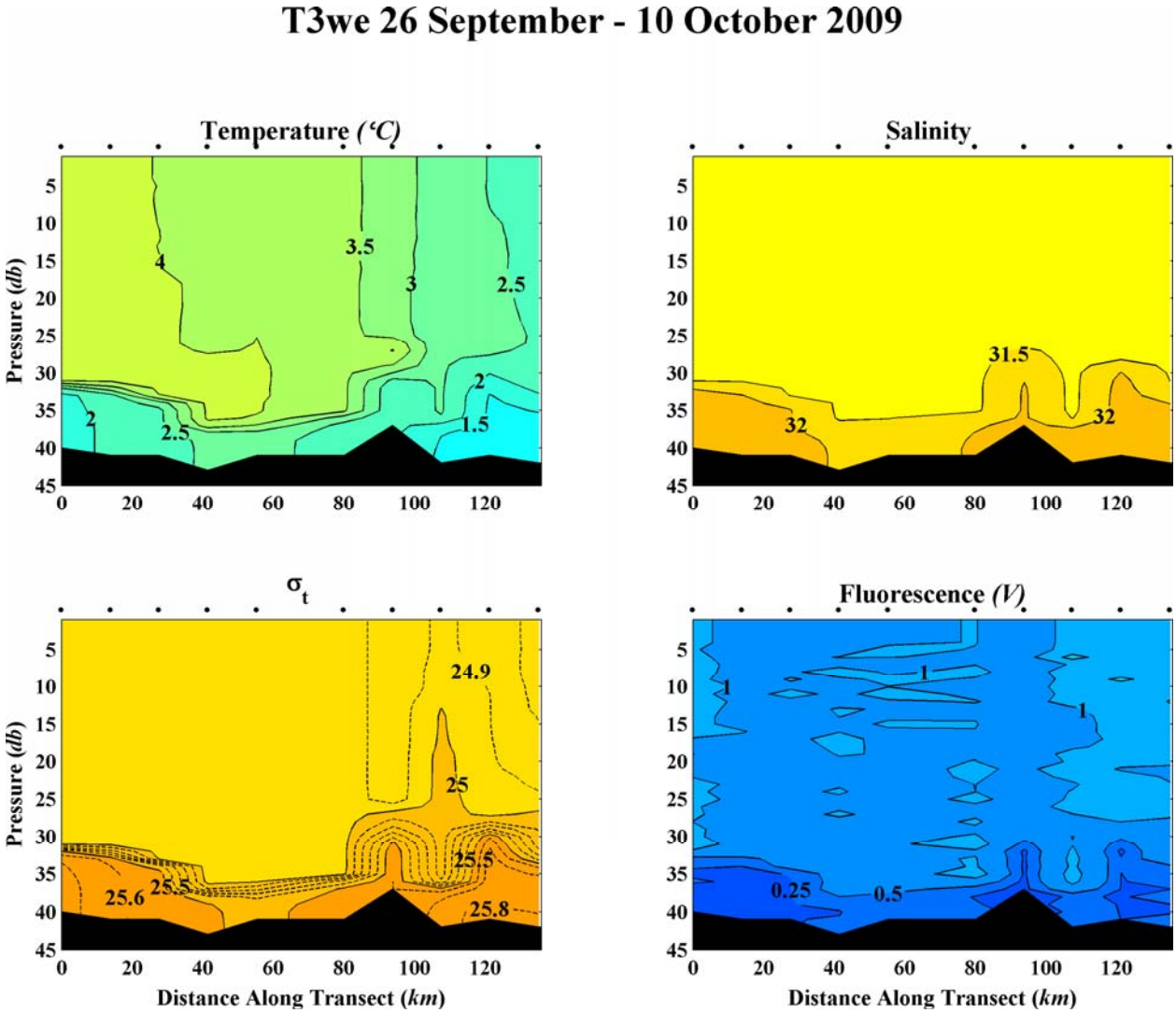

Figure 47. West-east section of temperature (upper left), salinity (upper right), sigma-t (lower left), and fluorescence (lower right) from the 26 September-10 October survey.

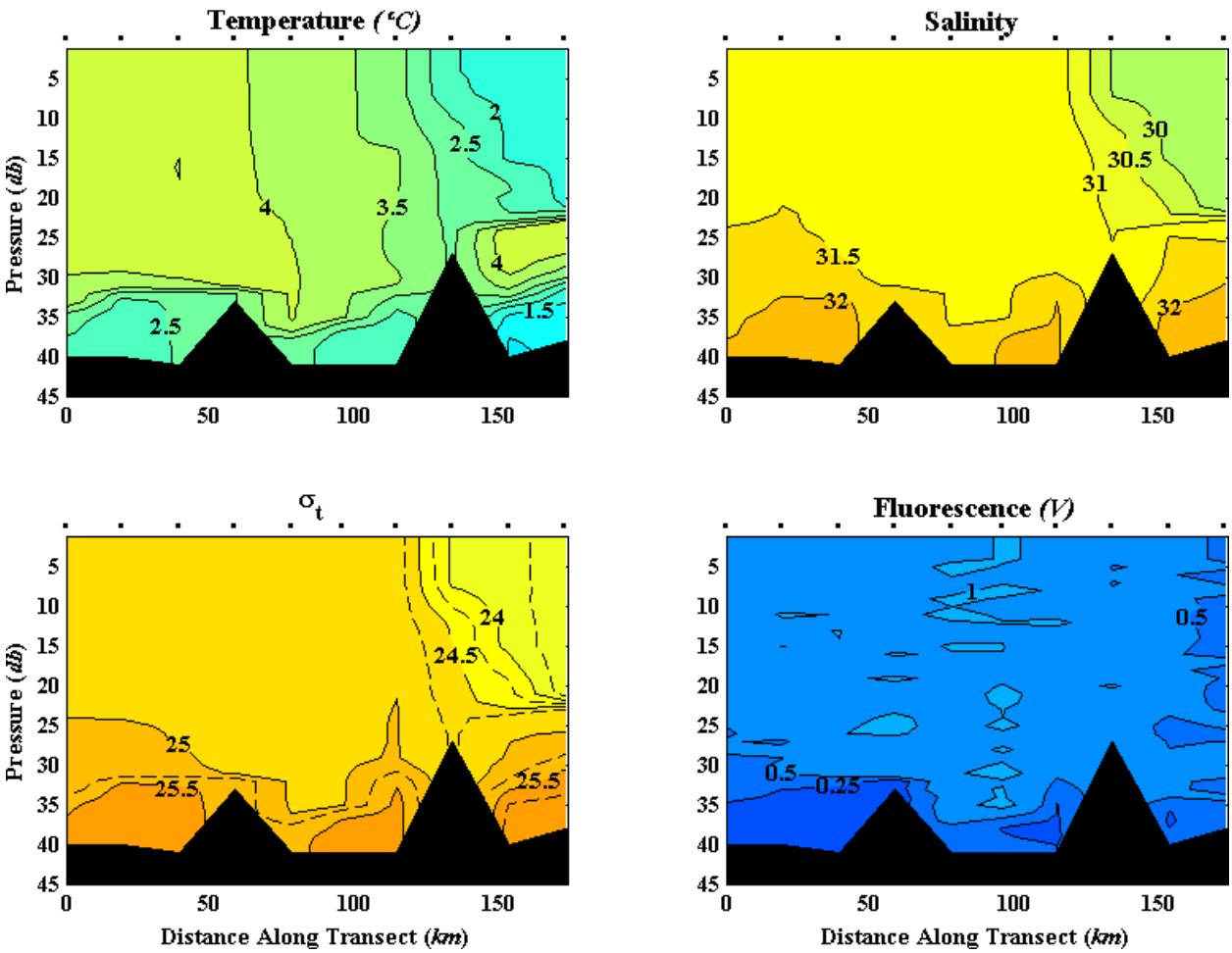

Figure 48. Southwest-northeast section of temperature (upper left), salinity (upper right), sigma-t (lower left), and fluorescence (lower right) from the 26 September-10 October survey.

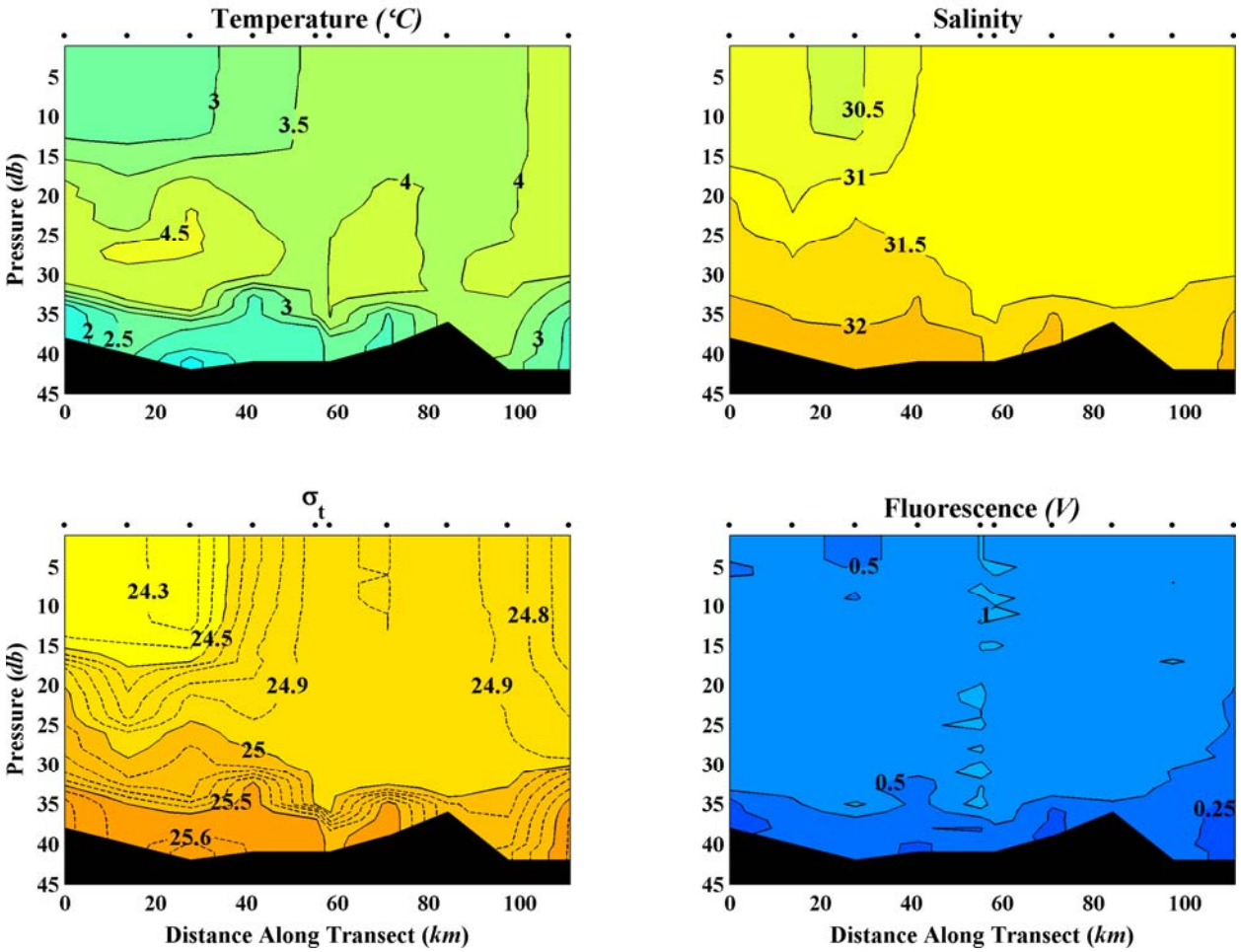

Figure 49. South-north section of temperature (upper left), salinity (upper right), sigma-t (lower left), and fluorescence (lower right) from the 26 September-10 October survey.

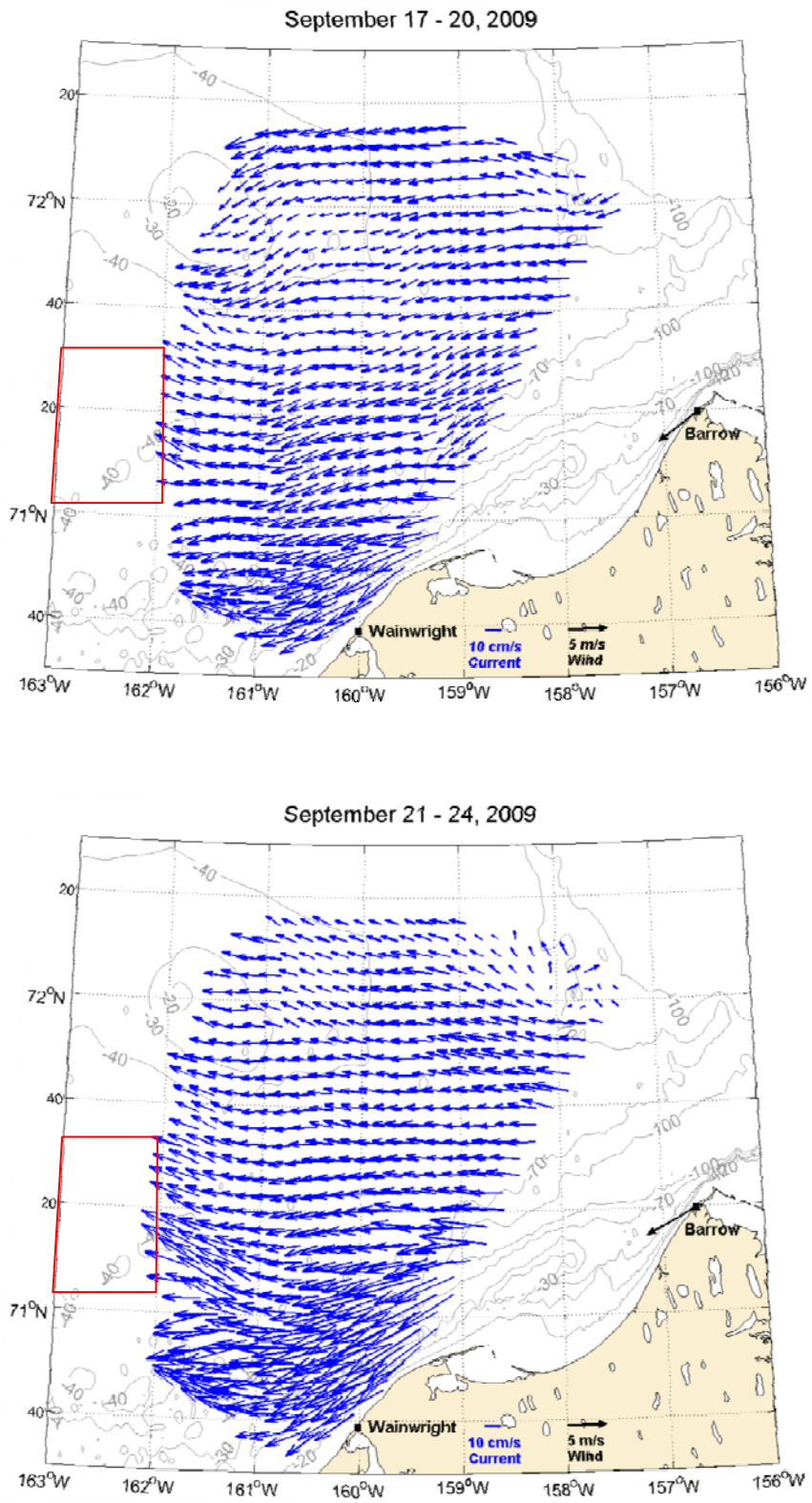

Figure 50. Four-day mean surface currents for Sept 17 -20 (top) and Sept. 21 – 24, 2009 (bottom). The vector at Barrow is the 4-day mean wind velocity measured at Barrow. The red box shows the approximate location of the Burger survey area.

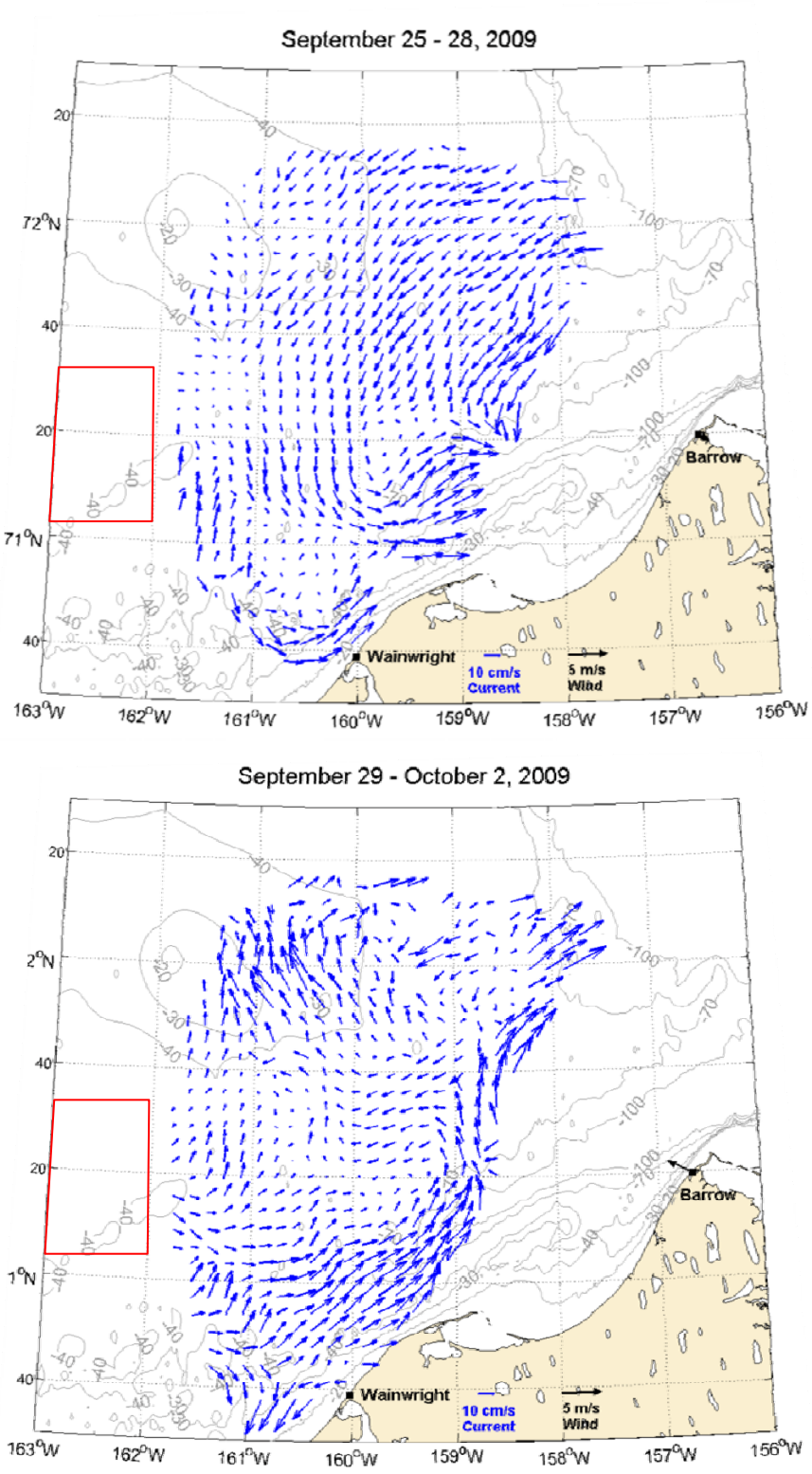

Figure 51. Four-day mean surface currents for Sept 17 -20 (top) and Sept. 21 – 24, 2009 (bottom). The vector at Barrow is the 4-day mean wind velocity measured at Barrow. The red box shows the approximate location of the Burger survey area.

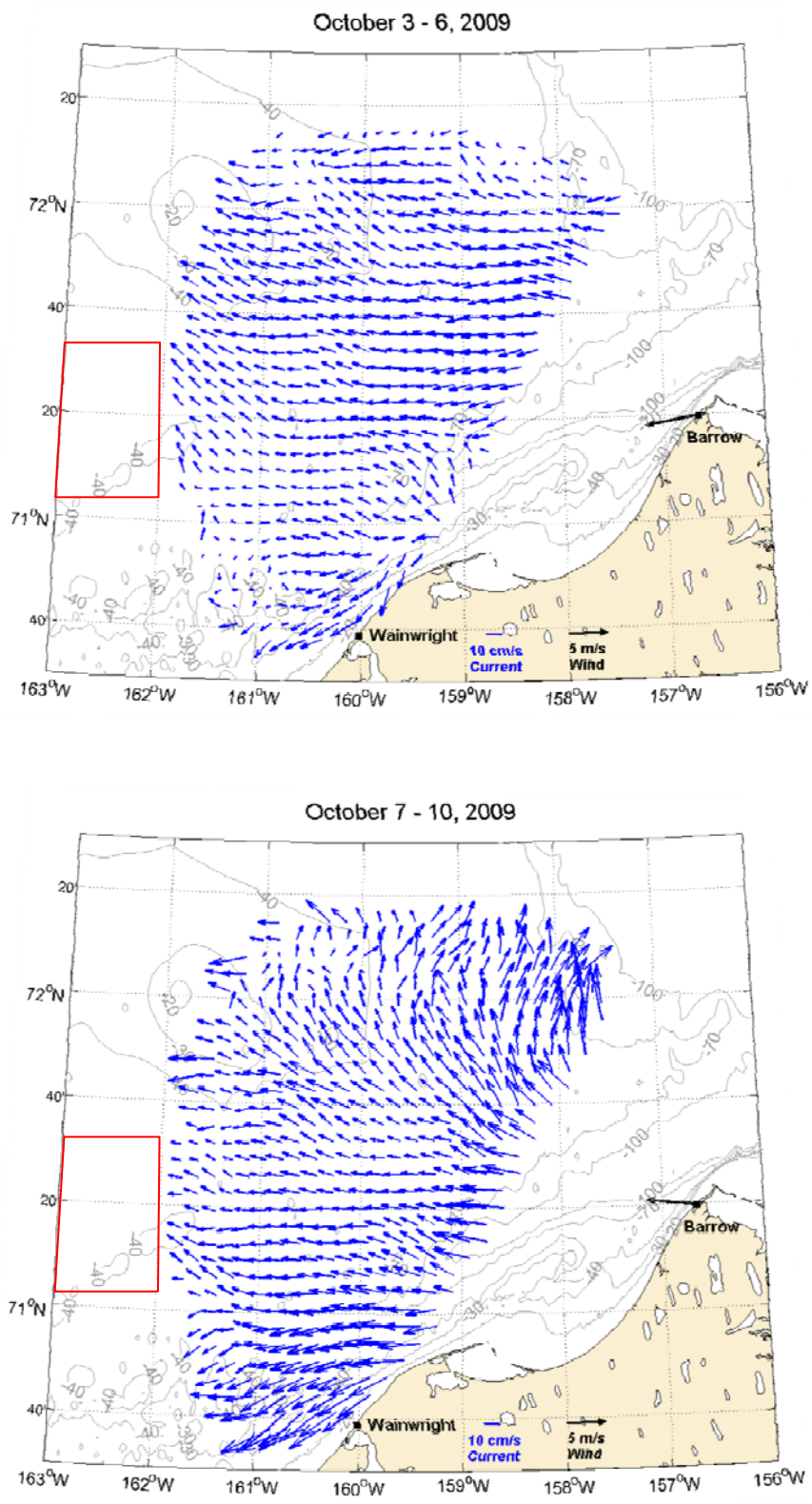

Figure 52. Four-day mean surface currents for Sept 17 -20 (top) and Sept. 21 – 24, 2009 (bottom). The vector at Barrow is the 4-day mean wind velocity measured at Barrow. The red box shows the approximate location of the Burger survey area.

Figures 53 and **54** are maps of the 0 – 10 m averaged temperatures and salinities for each survey in 2009. Upper ocean horizontal temperature and salinity gradients were much weaker in 2009 compared to 2008. For example, upper ocean temperatures differed by only 1 to 2°C across the survey sites in 2009 whereas in 2008 these differences were as large as 4 to 5.5°C. Similarly, horizontal salinity differences were also substantially smaller in 2009 than in 2008.

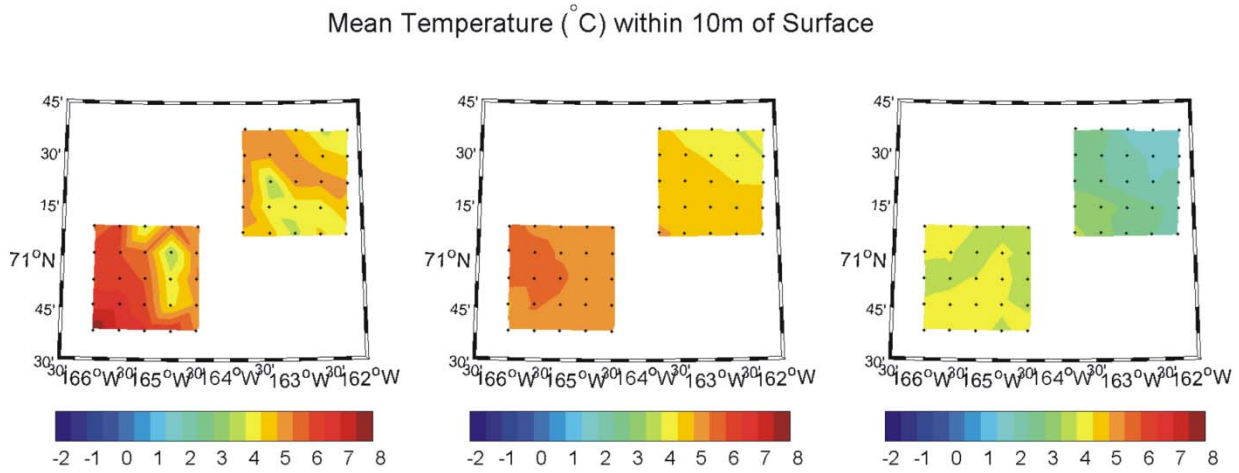

Figure 53. Plan view of the mean temperature over the upper 10 m of the water column for the 14-29 August survey (left), the 5-19 September survey (middle) and the 26 September – 10 October survey (right).

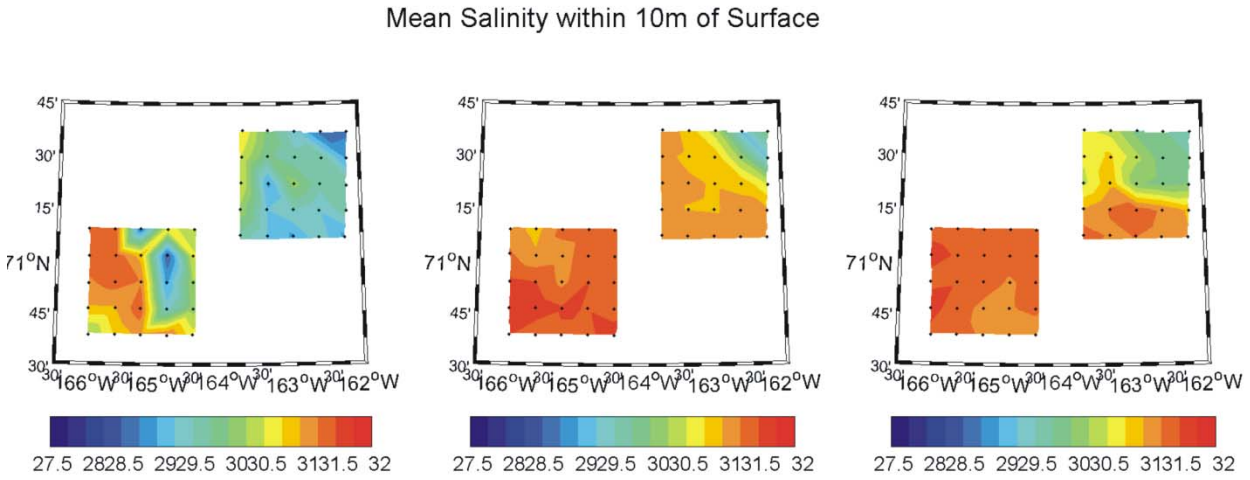

Figure 54. Plan view of the mean salinity over the upper 10 m of the water column for the 14-29 August survey (left), the 5-19 September survey (middle) and the 26 September – 10 October survey (right).

The corresponding maps for the bottom temperature and salinity averages are show in **Figures 55** and **56**. Bottom temperatures were 3 – 4°C in 2009 and generally increased from August through October 2009, especially in Burger. Bottom salinities were everywhere <32.5 in 2009

and only slightly decreased through time. The largest decreases occurred in Burger and amounted to about 0.5.

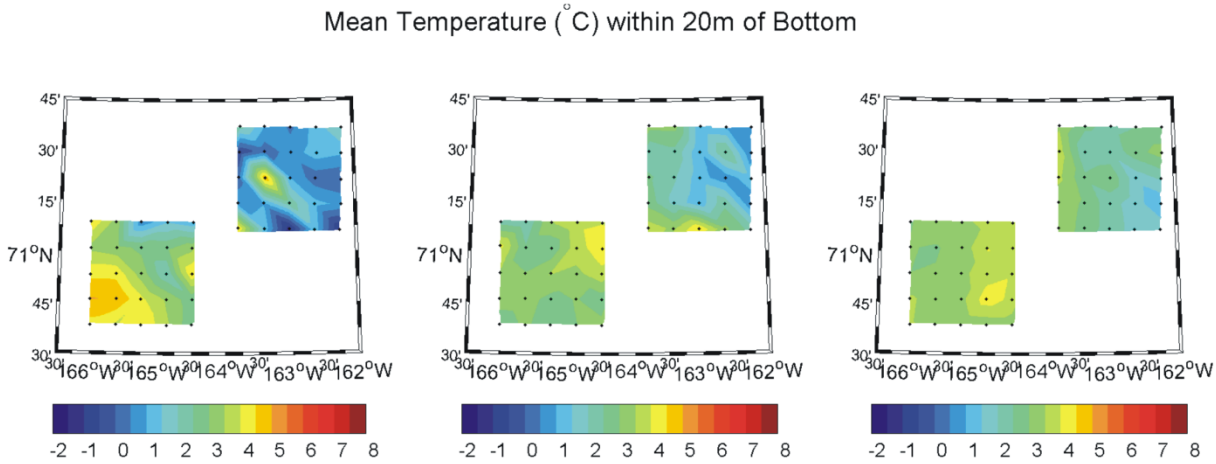

Figure 55. Plan view of the mean temperature over the bottommost 20 m of the water column for the 14-29 August survey (left), the 5-19 September survey (middle) and the 26 September – 10 October survey (right).

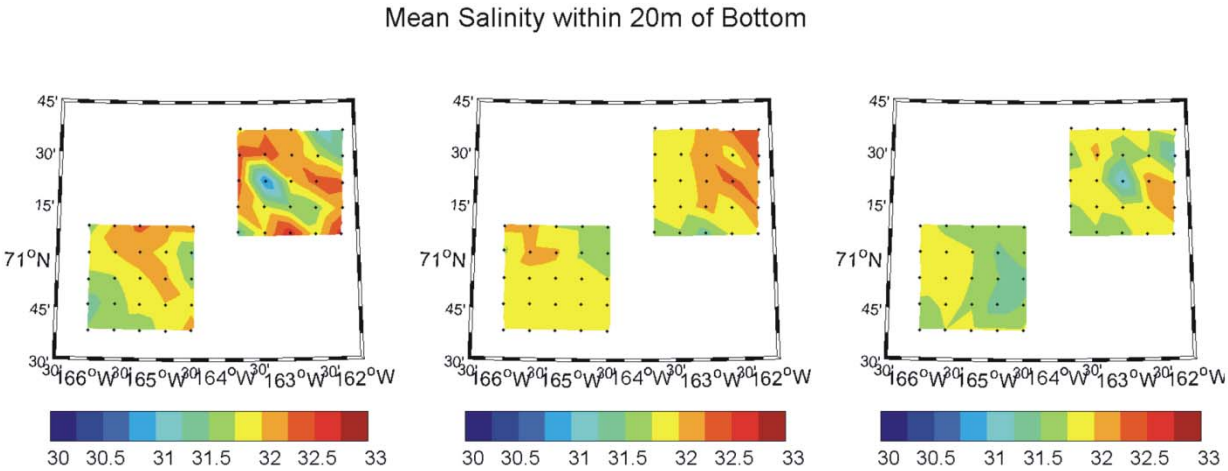

Figure 56. Plan view of the mean salinity over the bottommost 20 m of the water column for the 14-29 August survey (left), the 5-19 September survey (middle) and the 26 September – 10 October survey (right).

Results: 2010 Survey

Temperature-Salinity

The 2010 temperature-salinity diagrams for each survey are shown in **Figure 57**. These include data from within the Statoil survey area (green dots) and data from "transitional" stations between Klondike and Statoil (yellow dots). In general, the water property distributions are similar to the previous years. For example, the 6 – 29 August 2010 survey is similar to the August 14 – 29 2009 T/S diagram in having broad temperature (-1.7 C to 7 C) and salinity (28 – 33.2) ranges. The water types include ice-melt (fresh, cool) signatures, winter-formed waters

(cold, salty), summer waters (warm, salty) recently transported northward from Bering Strait and mixtures amongst these. Note that the Statoil site also has the same basic water mass properties as found in Klondike and Burger indicating that the regional waters share common water formation processes and sources.

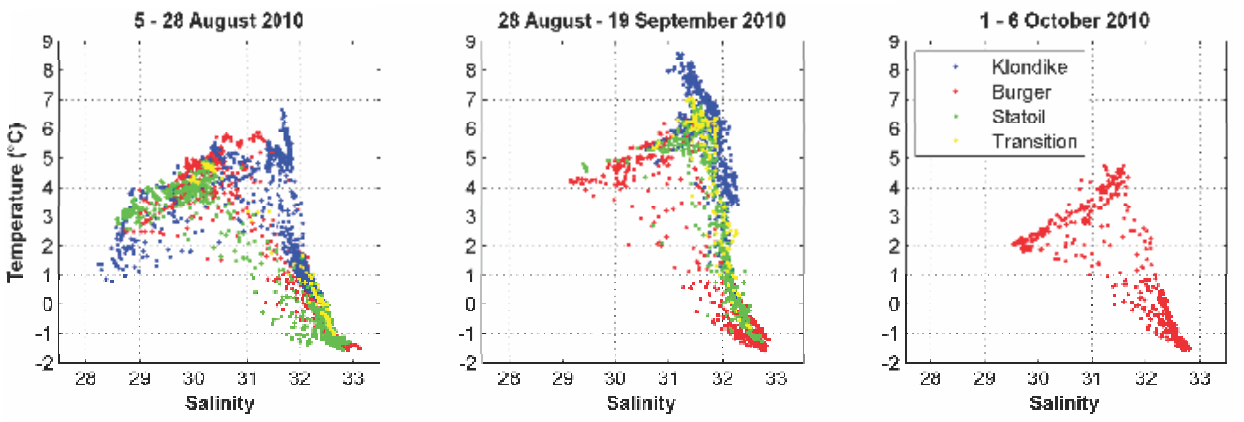

Figure 57. Temperature-salinity diagrams for each survey conducted in 2010.

The second survey (29 Aug – 20 Sept) differs from the previous years in two key respects. First, in 2010 there was more warm (>6°C) water present than in previous years. Maximum temperatures approached 9°C in 2010, whereas in 2008 and 2009 the maximum temperatures at approximately the same time were ~6°C. Second, in 2010 (and also 2008) the cold, salty winter-formed waters remained throughout the entire period in contrast to 2009 when these waters were steadily removed from August through early October. By October conditions in the Burger prospect were similar to previous years.

Since the Statoil survey area was added in 2010, the sampling grid was different from 2008 and 2009. **Figure 58** shows the distribution of stations occupied in 2010 for the first survey. The second survey was similar but did not include several of the stations in the northeast corner of the first survey. Only the Burger area was surveyed during the October 2 - 6 cruise.

As in prior years we constructed vertical cross-sections of temperature, salinity, density and fluorescence. In 2010 we used five separate sections to describe the horizontal and vertical distribution of water properties. These sections, sketched and labeled in **Figure 58,** were common to both the 6 – 28 August and the 29 August – 20 September surveys. Three of the sections (T2we, T2 and T2sn; **Figures 59 - 61**) consist of the same stations occupied in 2008 and 2009 and can be compared directly with those results. We have added two additional sections (T2snKTS and T2BS; **Figures 62 - 64**) to extend the description to include measurements from the Statoil area.

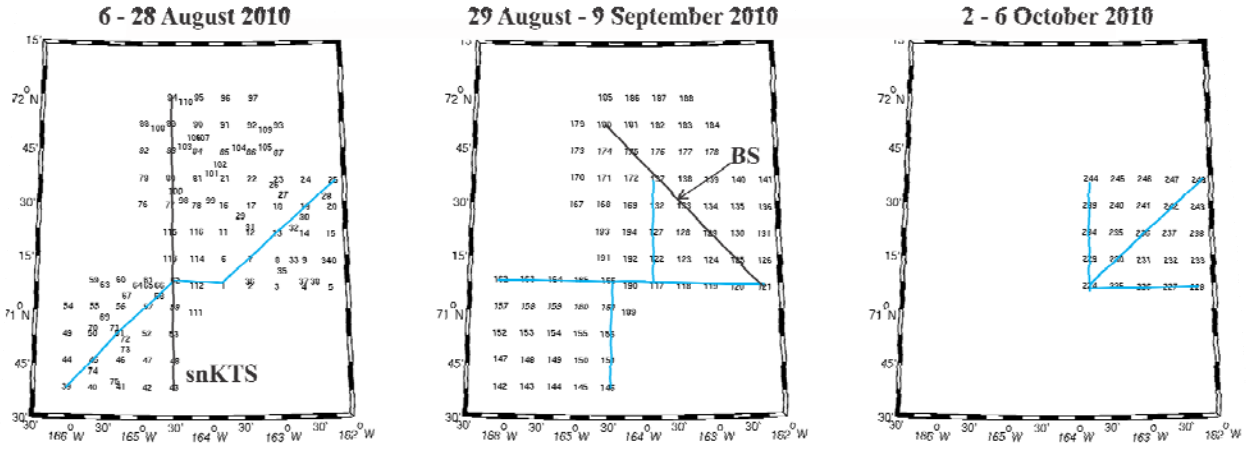

Figure 58. Station distributions during the 6-28, 2010 cruise. The blue solid lines correspond to the west-east, south-north, and southwest – northeast transects contoured in 2008 and 2009. Sections snKTS runs north-south between Klondike and Statoil, while section BS runs from the southeast corner of Burger to the northwest corner of Statoil. Both the BS and snKTS lines (black lines) were occupied in 2010 only.

Taken collectively the sections depict a relatively uniform horizontal distribution of water properties and vertical structure throughout the area. For example, the region contains a 15 – 20 m thick surface layer, over which temperatures and salinities are nearly constant in the vertical. Temperatures and salinities in the surface layer are 4 - 5^{o}C and 30 – 31, respectively. In general temperature and salinities decrease from south to north, although patches of cooler, fresher water were also observed intermittently. One such a patch is evident along the western edge of Klondike (**Figures 59** and **60)**. Most likely this is meltwater derived from the ice that was over the central shelf in late July (cf. **Figure 17**).

Throughout the region, surface waters were separated from the bottom waters by a strong ~5 m thick pycnocline, which begins at 15 – 20 m depth and across which density increases by 2 -3 kg m^{-3} over ~4 m. Beneath the pycnocline the waters tend to be vertically uniform with temperatures and salinities ranging from 0^{o}C to -1^{o}C and 32.0 – 32, respectively. Note that temperature-salinity relationships differ above and below the pycnocline. Above the pycnocline, warmer waters are saltier than cooler waters, while below it, colder waters are saltier than warmer waters.

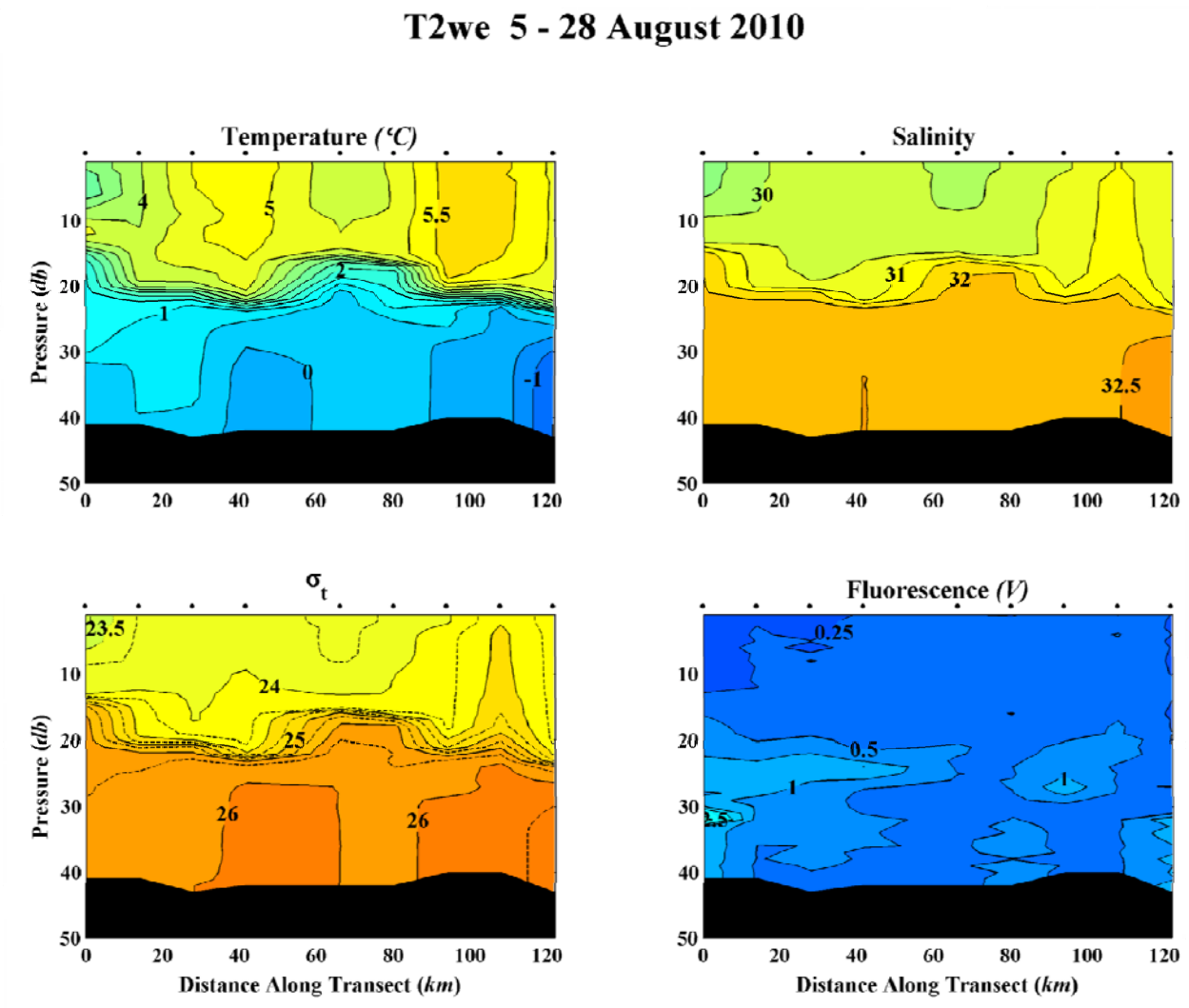

Figure 59. West – east section of temperature (upper left), salinity (upper right), sigma-t (lower left), and fluorescence (lower right) from the 6 – 28 August 2010 survey.

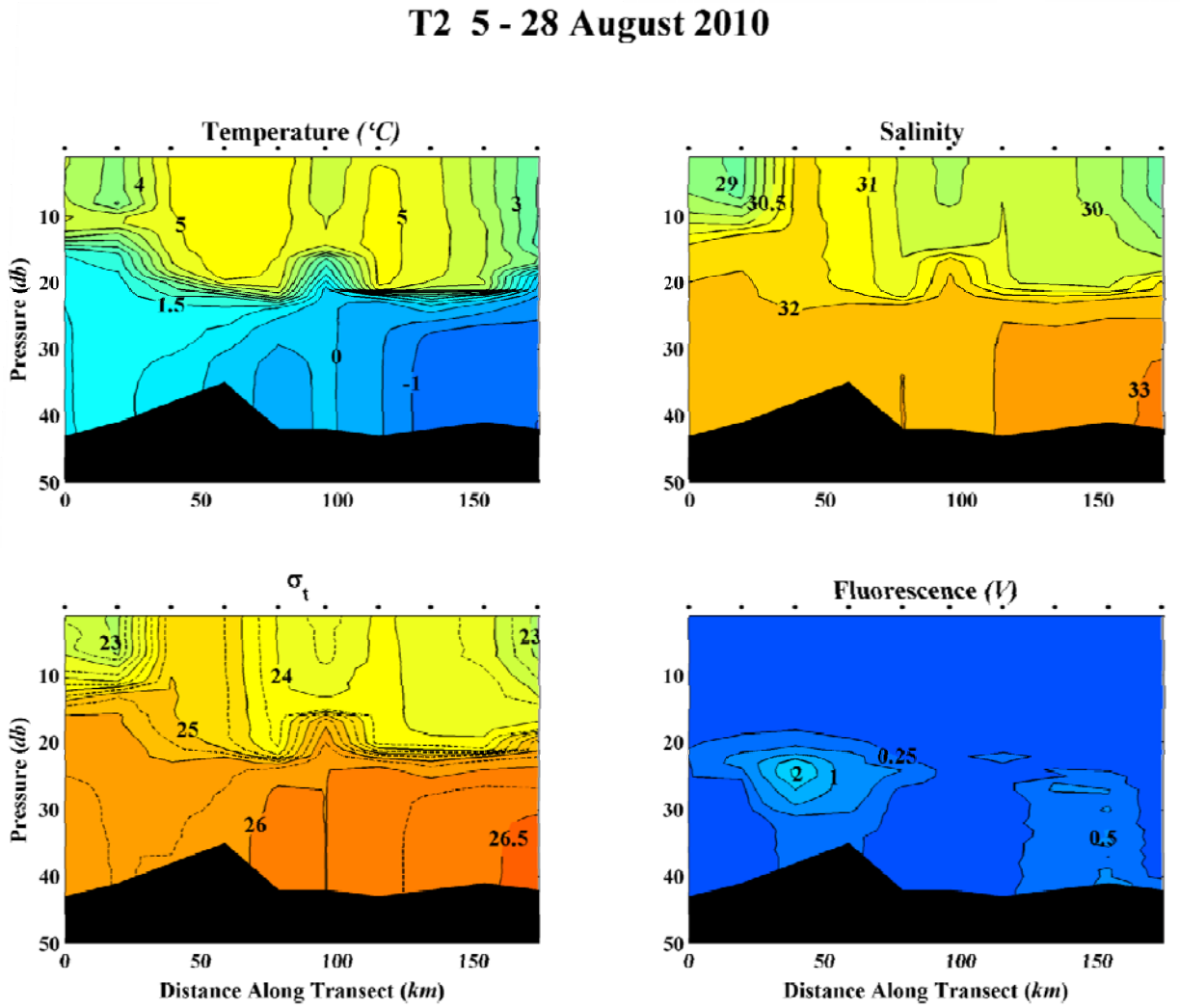

Figure 60. Southwest to northeast section of temperature (upper left), salinity (upper right), sigma-t (lower left), and fluorescence (lower right) from the 6 – 28 August 2010 survey.

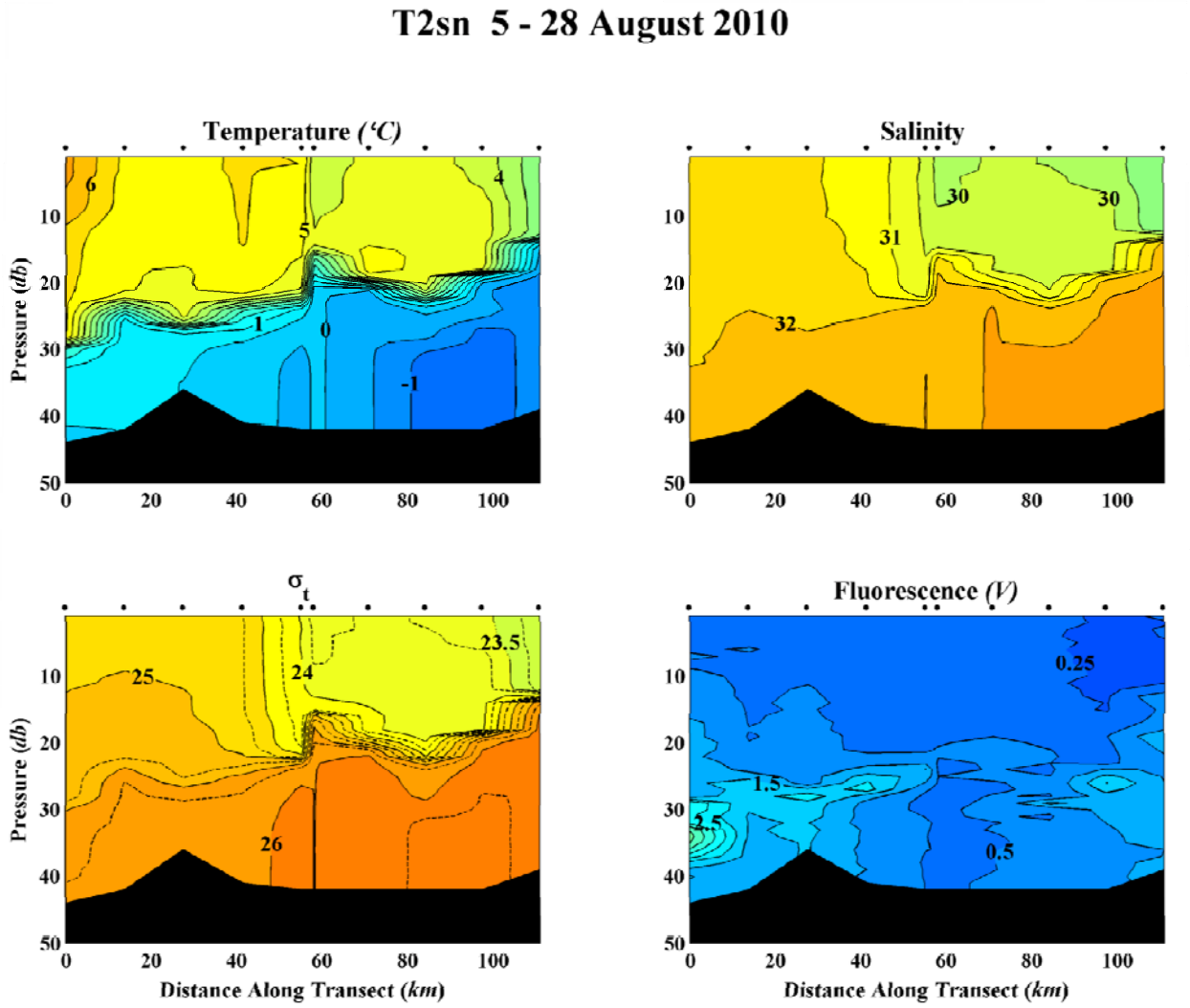

Figure 61. South-north section of temperature (upper left), salinity (upper right), sigma-t (lower left), and fluorescence (lower right) from the 6 – 28 August 2010 survey.

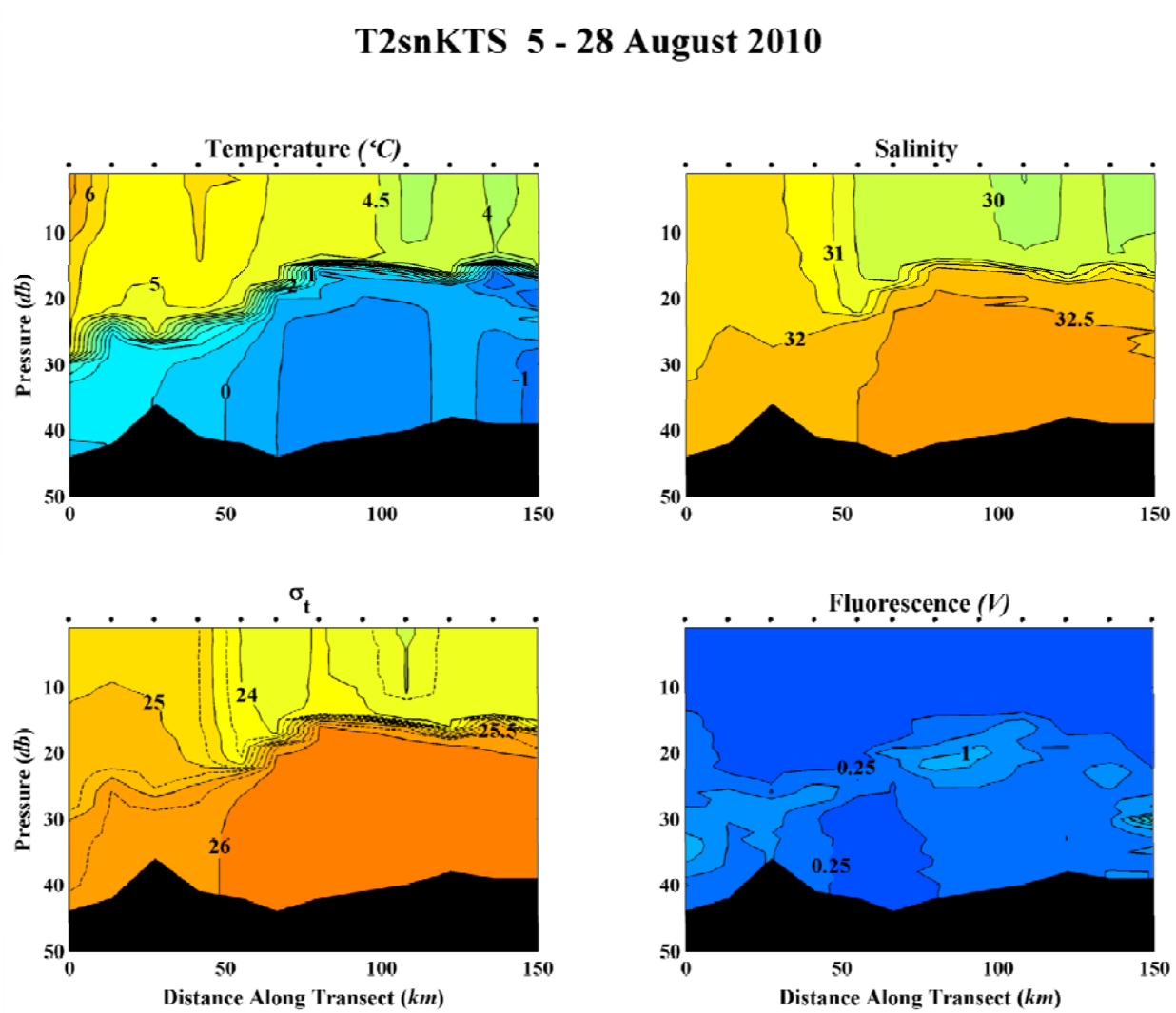

Figure 62. The south – north section connecting Klondike to the Statoil survey areas of temperature (upper left), salinity (upper right), sigma-t (lower left), and fluorescence (lower right) from the 6 – 28 August 2010 survey.

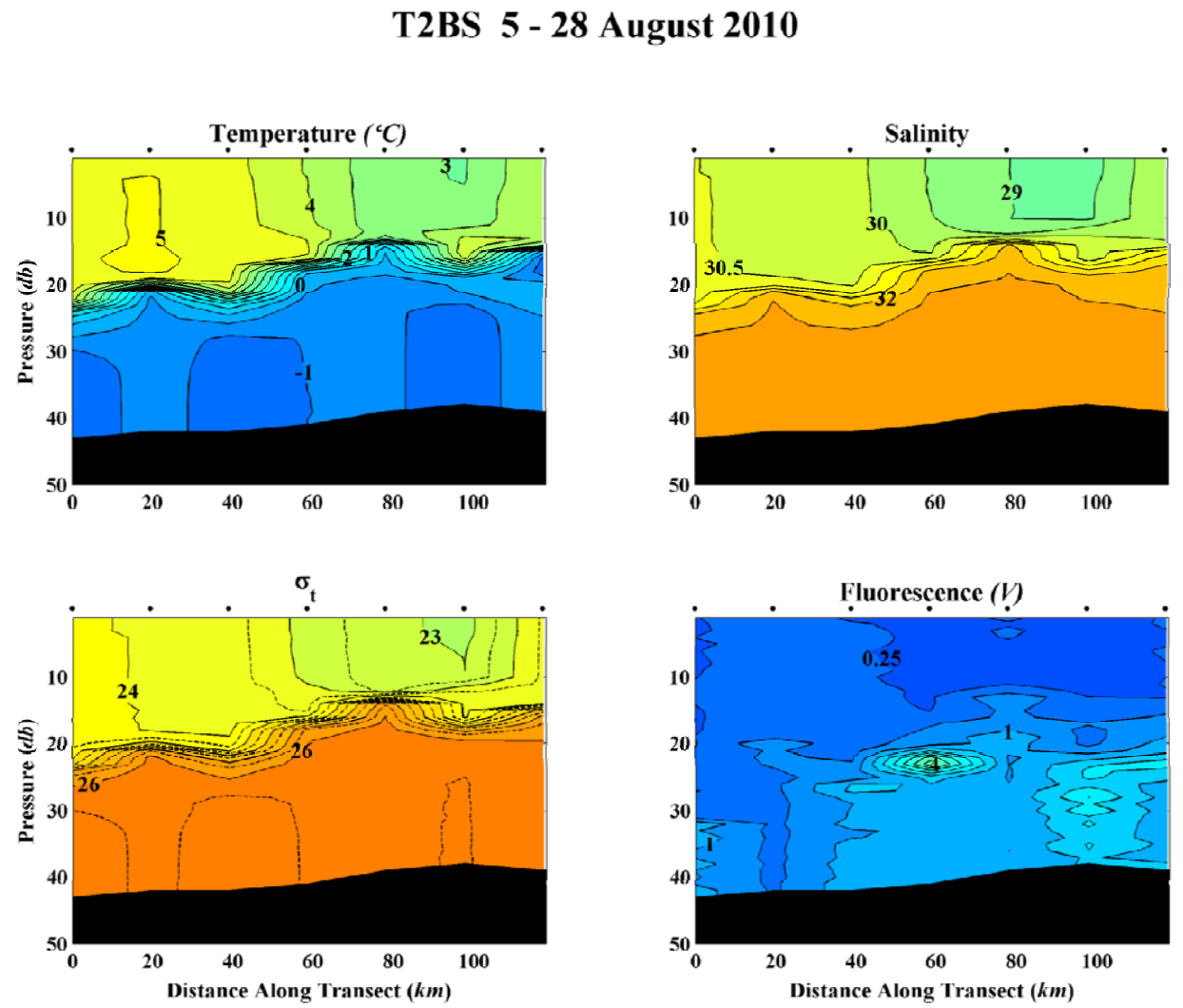

Figure 63. The southeast to northwest section connecting Burger and Statoil areas of temperature (upper left), salinity (upper right), sigma-t (lower left), and fluorescence (lower right) from the 6 – 28 August 2010 survey.

The corresponding transects for the 29 August – 19 September cruise are shown in **Figures 64 – 68**. In general, upper layer temperatures increased to between 5 and 7°C and salinities increased by about 1, while near-bottom waters have warmed and freshened slightly. The largest changes occurred along the southern (Klondike) and western (Klondike and Statoil) region. We will return to this point later, but note for the moment that the bottom waters in the Burger area showed the least amount of change.

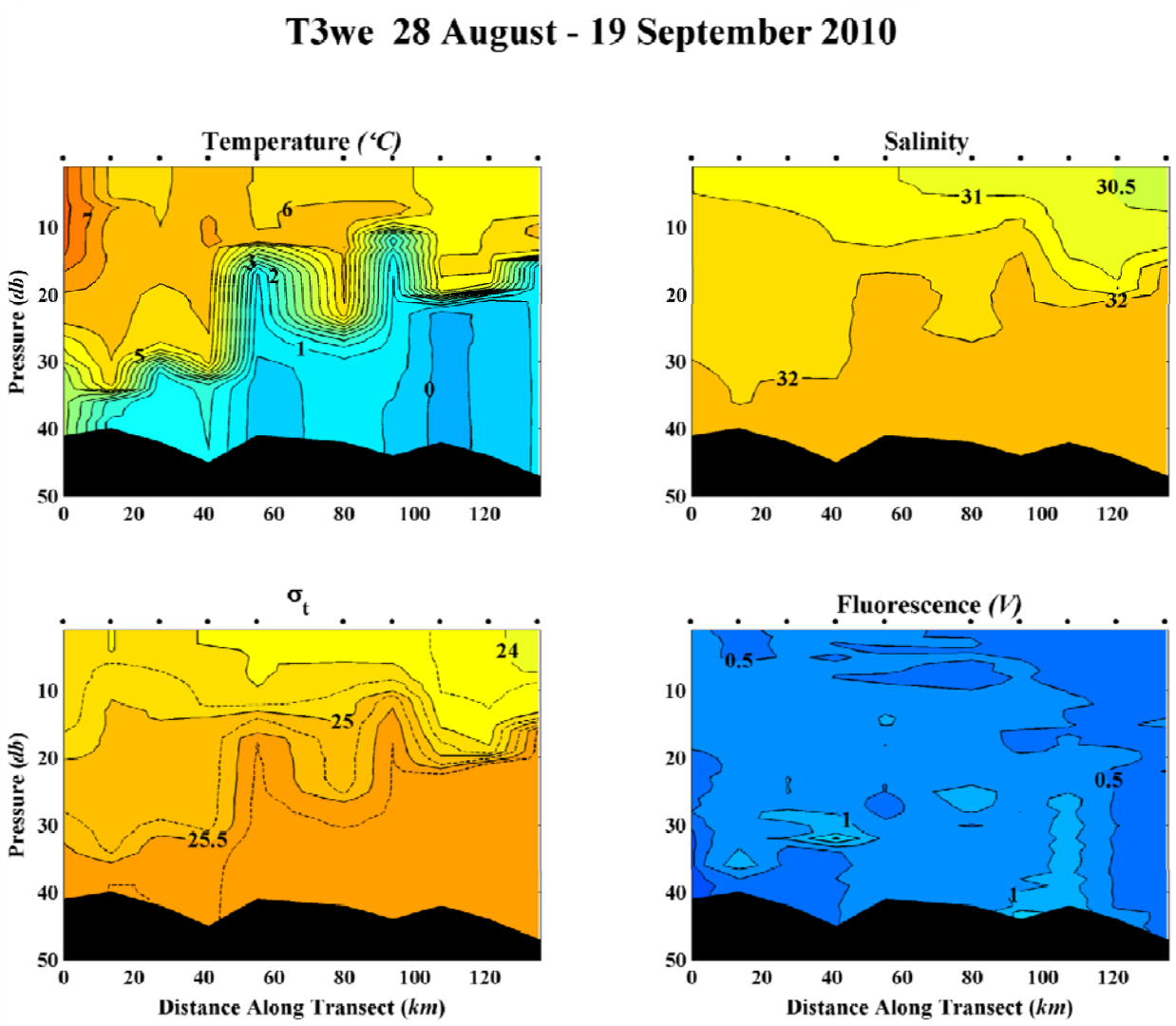

Figure 64. The west to east section of temperature (upper left), salinity (upper right), sigma-t (lower left), and fluorescence (lower right) from the 29 August – 9 September 2010 survey.

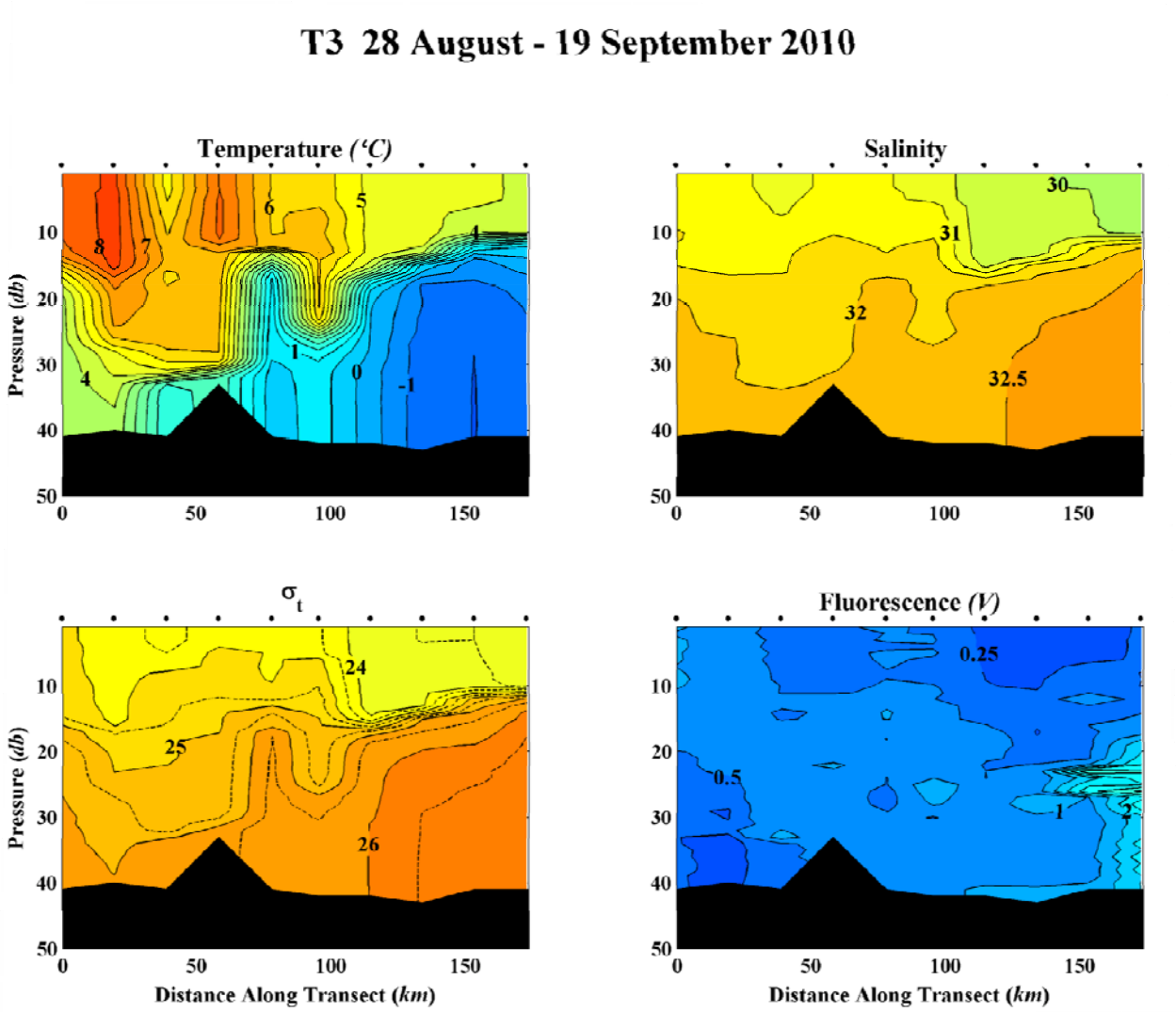

Figure 65. The southwest to northeast section of temperature (upper left), salinity (upper right), sigma-t (lower left), and fluorescence (lower right) from the 29 August – 9 September 2010 survey.

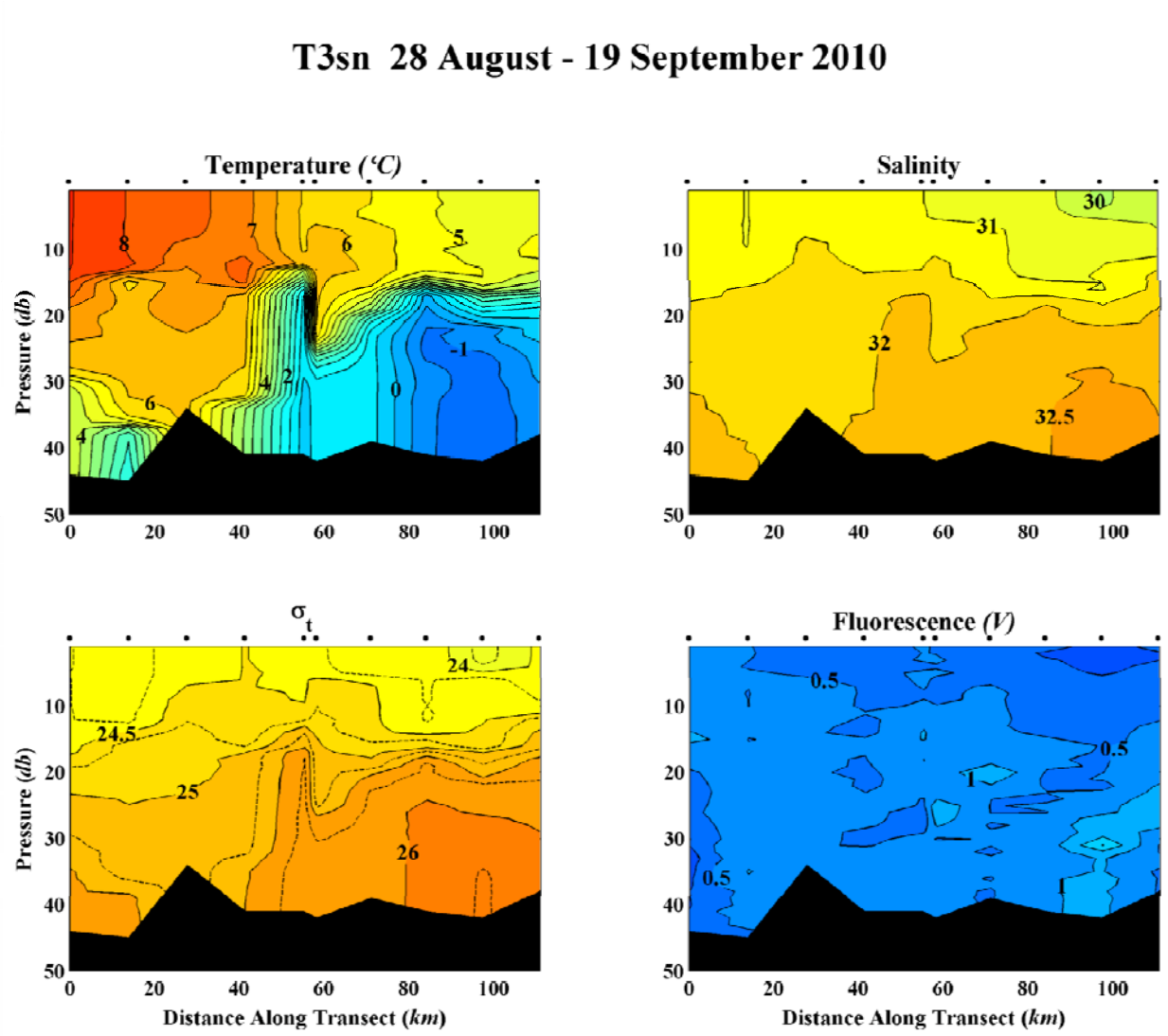

Figure 66. The north to south section of temperature (upper left), salinity (upper right), sigma-t (lower left), and fluorescence (lower right) from the 29 August – 9 September 2010 survey

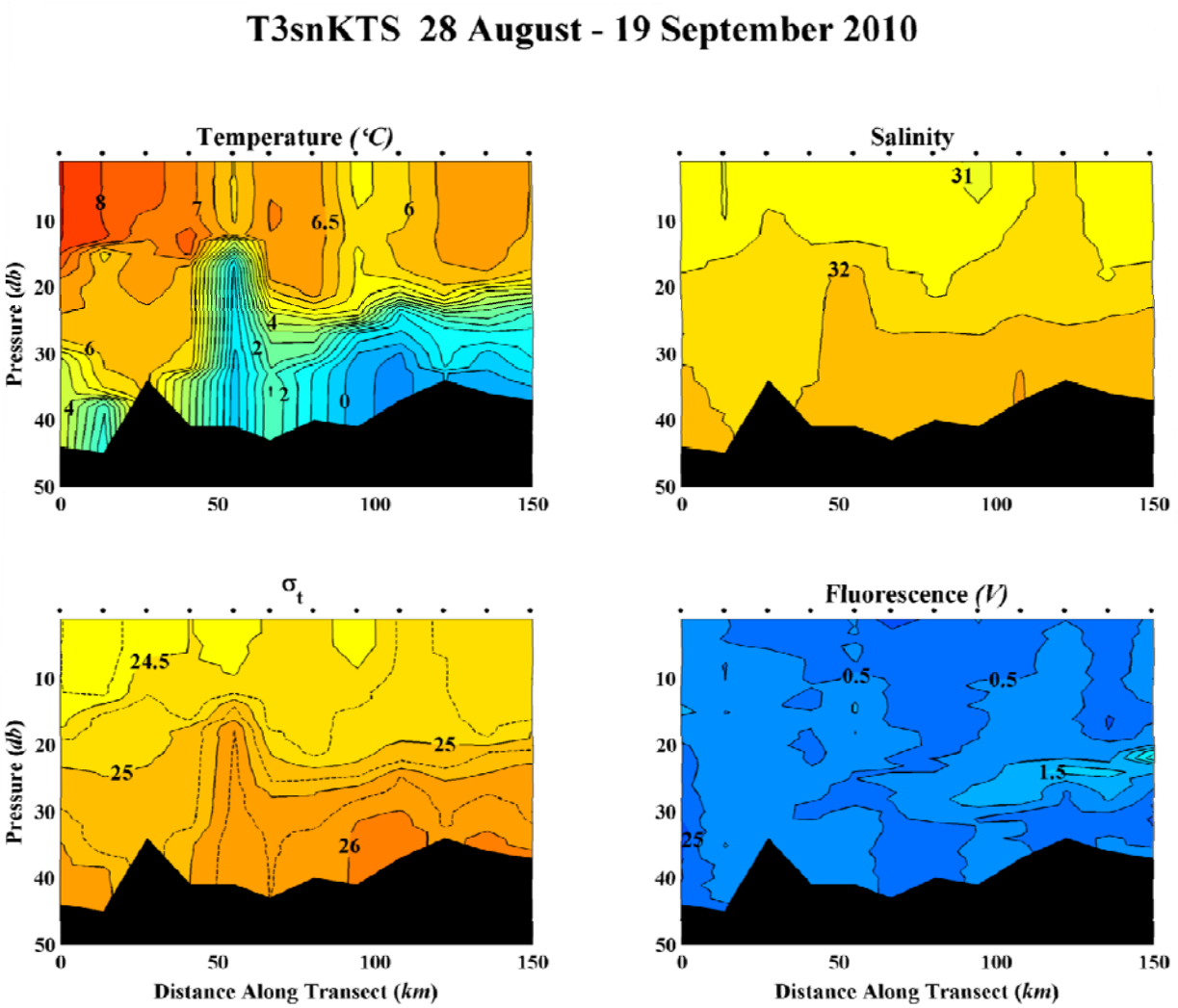

Figure 67. The south – north section connecting Klondike to the Statoil survey areas of temperature (upper left), salinity (upper right), sigma-t (lower left), and fluorescence (lower right) from the 29 August – 9 September 2010 survey.

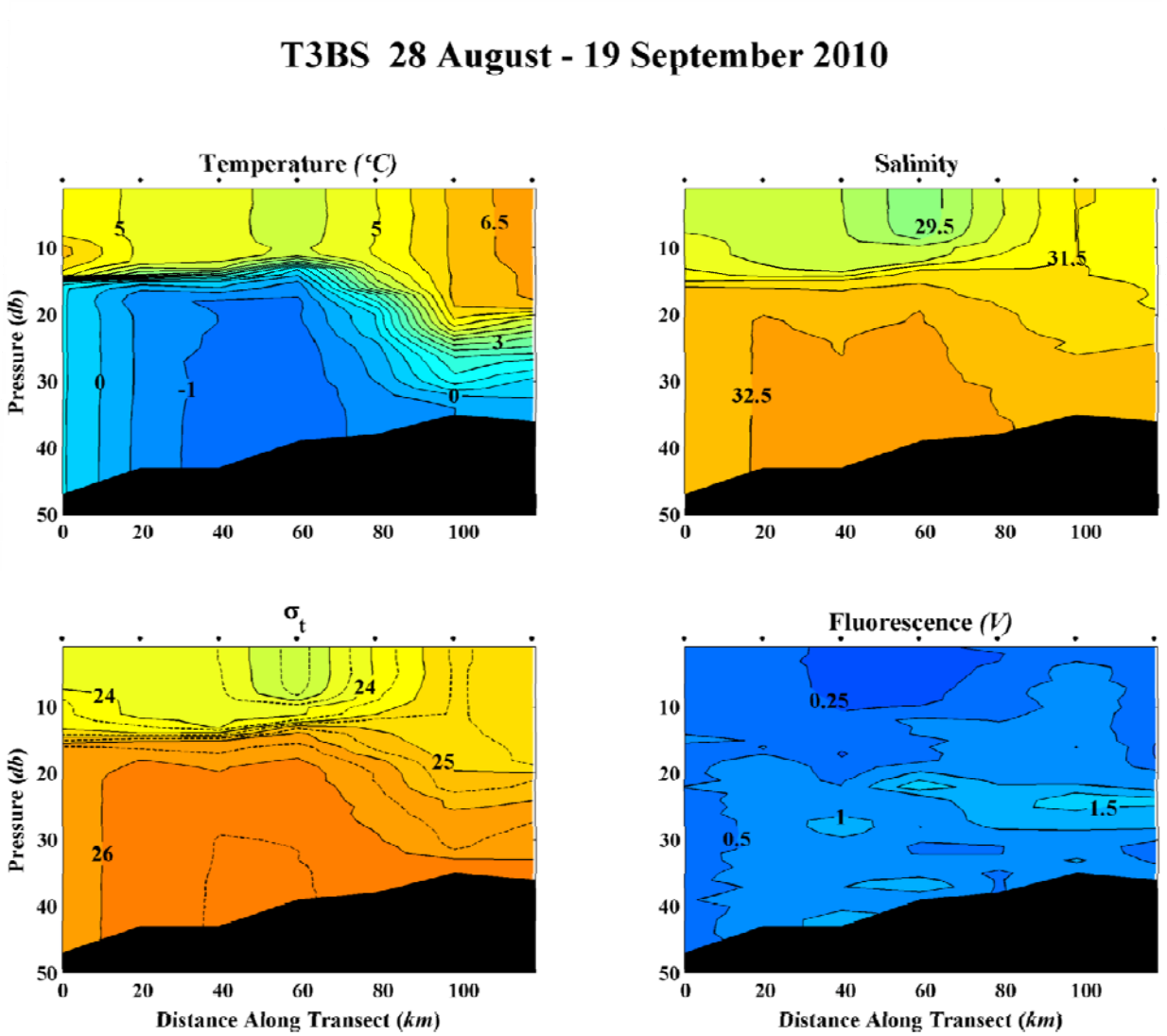

Figure 68. The southeast to northwest section connecting Burger and Statoil areas of temperature (upper left), salinity (upper right), sigma-t (lower left), and fluorescence (lower right) from the 29 August – 9 September 2010 survey.

Horizontal maps of temperature and salinity, averaged over the topmost and bottommost 10 m of the water column provide an alternative perspective on the seasonal evolution of water properties and their horizontal gradients. The surface maps are shown in **Figures 69** and **70** and the corresponding maps for the bottom 10 m are shown in **Figures 71** and 72. At the time of the 6 – 28 August survey there were two regions of cool, relatively fresh surface waters; one in the southwest corner of the grid and the other in the northeast corner. Both are likely remnants of ice melt. The patch in the northeast corner was seen in both the 2008 and 2009 surveys and is prominent over Burger southern flank of Hanna Shoal. The patch in the southwest corner was most likely associated with melting ice to the west of the survey region (see **Figure 17**) earlier in the summer. In fact it may have drifted eastward into the region from the vicinity of Herald Shoal in the central Chukchi Sea, since this shoal tends to trap ice and meltwater (*Martin and Drucker*, 200 ; *Weingartner et al.,* 2005). However, by the time of the second survey this

meltwater had vanished while that in the northeast corner of the grid had shrunk substantially in size. In addition, surface waters in the western half of the grid, including all of Klondike and most of the Statoil survey areas had warmed by 3 - 4°C. This warming was accompanied by an increase in salinity by 1 to 1.5 over much of the region. These same regions warmed and freshened at the bottom at the same time. Based on our notion of the mean flow, this change is likely due in part to northward advection of Bering Sea summer waters through the Central Channel (to the west of Klondike) and south of Klondike and its eastward spread into the region south and west of Hanna Shoal. (The ADCP data discussed below support this suggestion). As was evident in the section plots, these changes were accompanied by a decrease in stratification in the same areas. Although the third survey was limited to the Burger area, the horizontal maps show cooling at the surface (due to heat loss to the atmosphere) and a slight increase in salinity. By contrast bottom water temperatures hardly changed and salinity increased slightly.

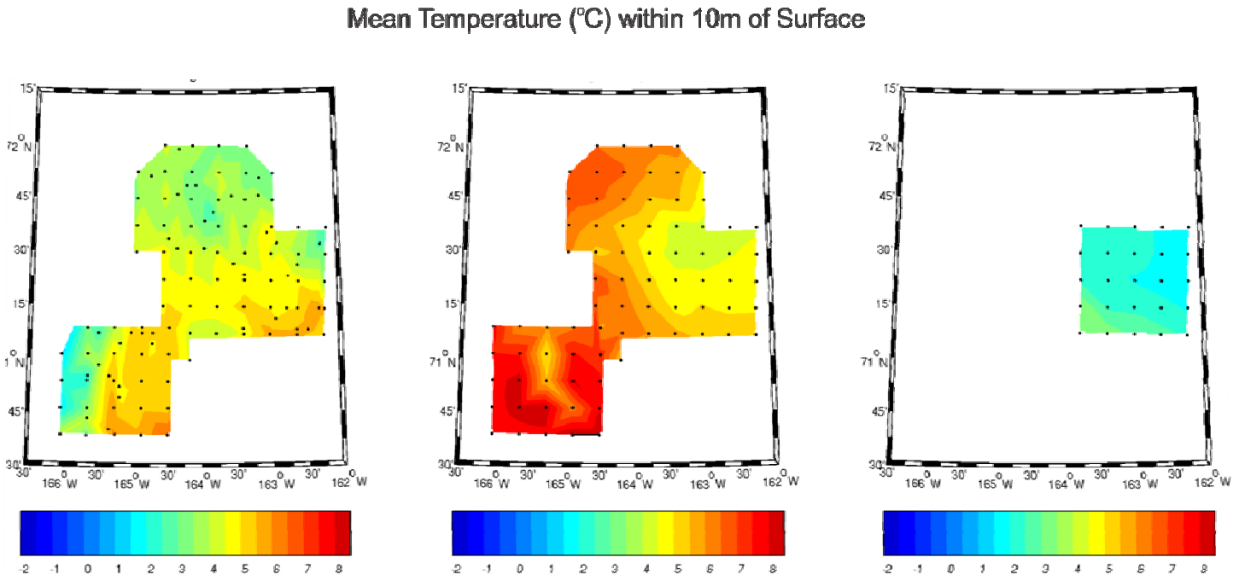

Figure 69. Plan view of the mean temperature over the upper 10 m of the water column for the 6 - 28 August survey (left), the 29 August - 19 September survey (middle) and the 1 - 6 October survey (right) in 2010.

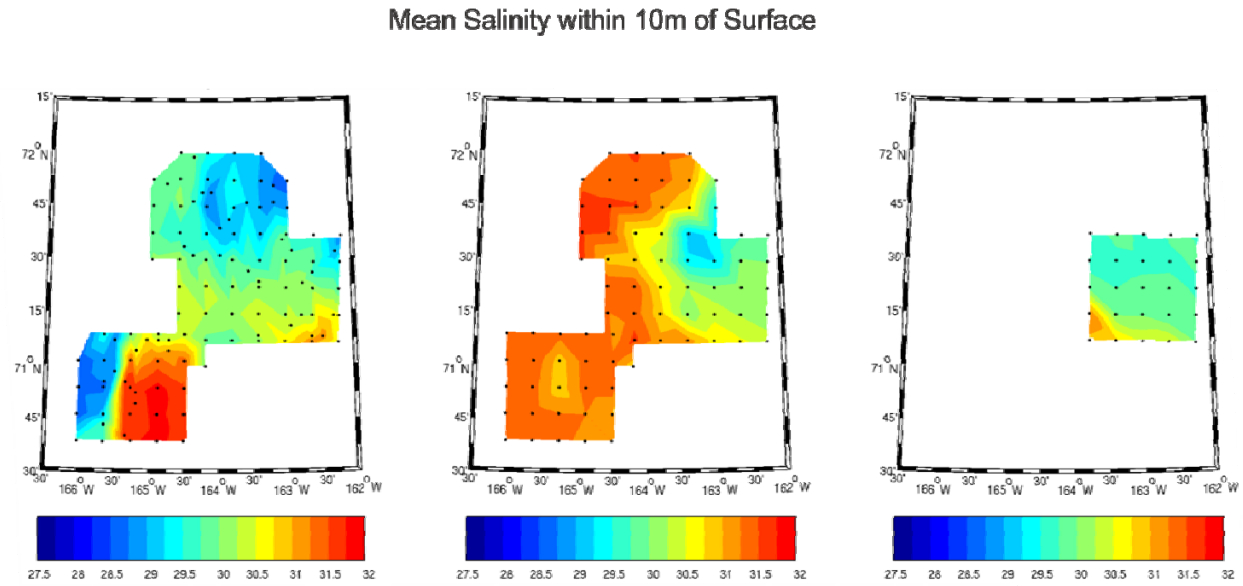

Figure 70. Plan view of the mean salinity over the upper 10 m of the water column for the 6 - 28 August survey (left), the 29 – August - 19 September survey (middle) and the 1 - 6 October survey (right) in 2010.

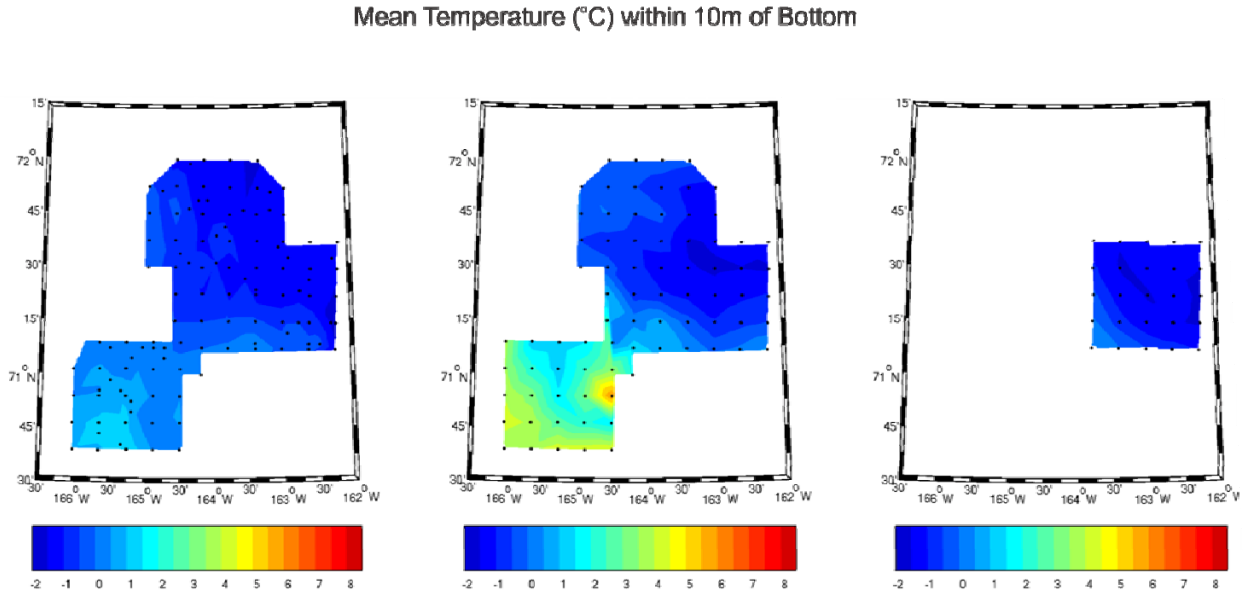

Figure 71. Plan view of the mean temperature within 10 m of the bottom of the water column for the 6 - 28 August survey (left), the 29 – August - 19 September survey (middle) and the 1 - 6 October survey (right) in 2010.

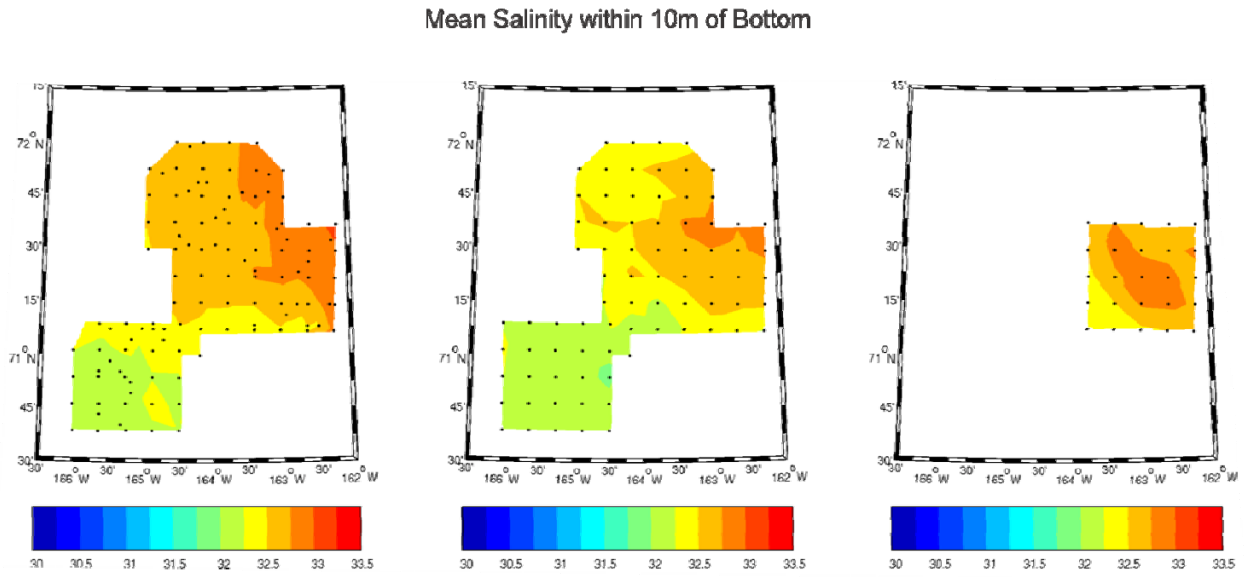

Figure 72. Plan view of the mean salinity within 10 m of the bottom of the water column for the 6 - 28 August survey (left), the 29 – August - 19 September survey (middle) and the 1 - 6 October survey (right) in 2010.

ADCP-derived current maps are shown for each cruise in **Figures 73 – 75**. These are based on 6-hourly averages of the ADCP vectors and are shown at two depths (11 and 27 m), chosen to provide the best spatial coverage. Wind and ADCP vectors are color-coded similarly to correspond to periods with approximately similar wind conditions. Caution needs to be exercised in interpreting these maps, since the data were collected over a broad time period. Hence the figures simply represent an instantaneous view of the currents at a given time and location and cannot be regarded as representative of the mean flow during the sampling period. Although there are some exceptions, in general the current vectors vary little in magnitude or direction with depth. Horizontal variations in flow speeds are considerable, however, and range from as a few cm s^{-1} to 35 cm s^{-1} For August and September (**Figures 73** and **74**), the vectors suggest southward/ southeastward flow between 71° 30' – 71° 45'N along ~164° W. The flow veers more eastward between 164°W. West of 164°W and south of 71 N, the flow is northeastward and eastward. The current patterns are such that they would tend to carry warmer water from the Statoil and Klondike regions into the western boundary of Burger. Since these warmer waters tend to be of moderate salinity (cf. (**Figures 69 - 72**), they would freshen the lower half of the water column and increase salinity in the upper half of the water column. The final survey was limited to Burger in early October (**Figure 75**) and the data were collected during a period of strong but variable winds. The currents in Burger at this time were generally weak and more variable in direction.

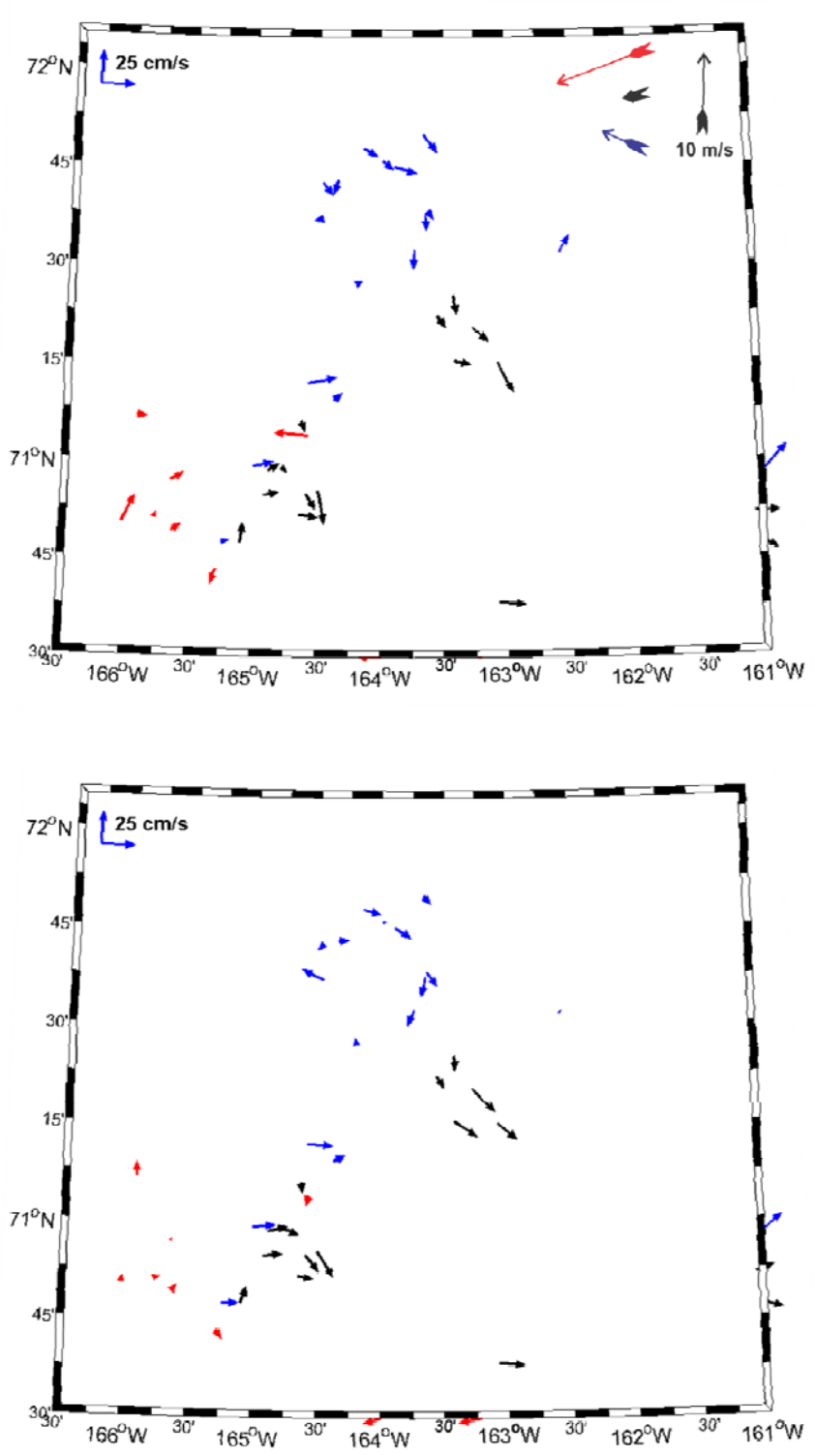

Figure 73. 6-hourly averaged current vectors for the period August 6 – 29, 2010. The upper (lower) panel shows the vectors at a depth of 11 (27) m. The vectors are color-coded and correspond to the periods: Aug. 6 – 11 (red), Aug. 12 – 20 (black) and Aug. 21 – 29 (blue), in accordance with variations in the winds. Wind vectors for each corresponding period are in the upper right-hand corner of the top panel.

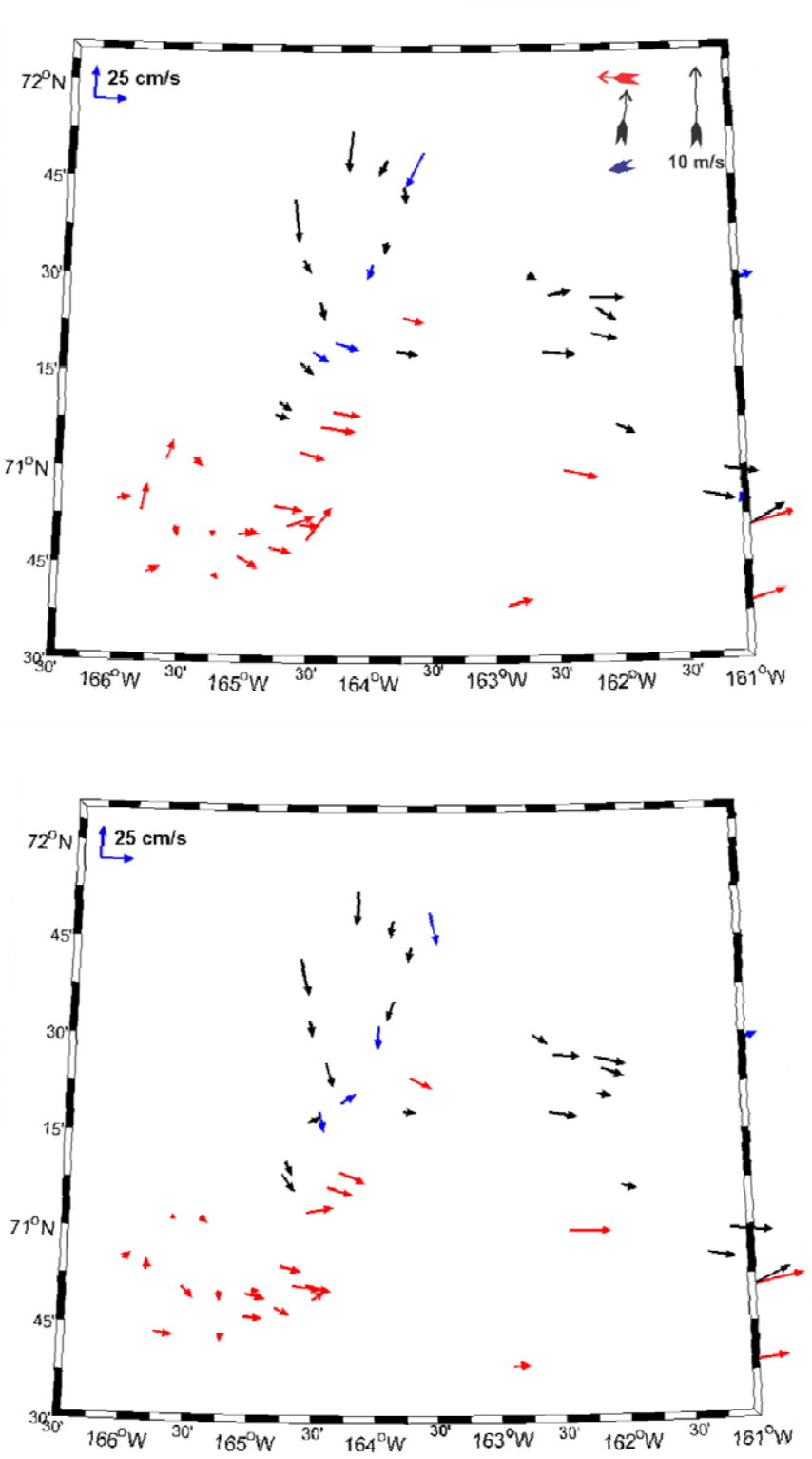

Figure 74. 6-hourly averaged current vectors for the period August 29 – September 21, 2010. The upper (lower) panel shows the vectors at a depth of 11 (27) m. The vectors are color-coded and correspond to the periods: Aug. 29 – Sept. 10 (red), Sept. 11 – 20 (black) and Sept. 18 - 21 (blue), in accordance with variations in the winds. Wind vectors for each corresponding period are in the upper right-hand corner of the top panel.

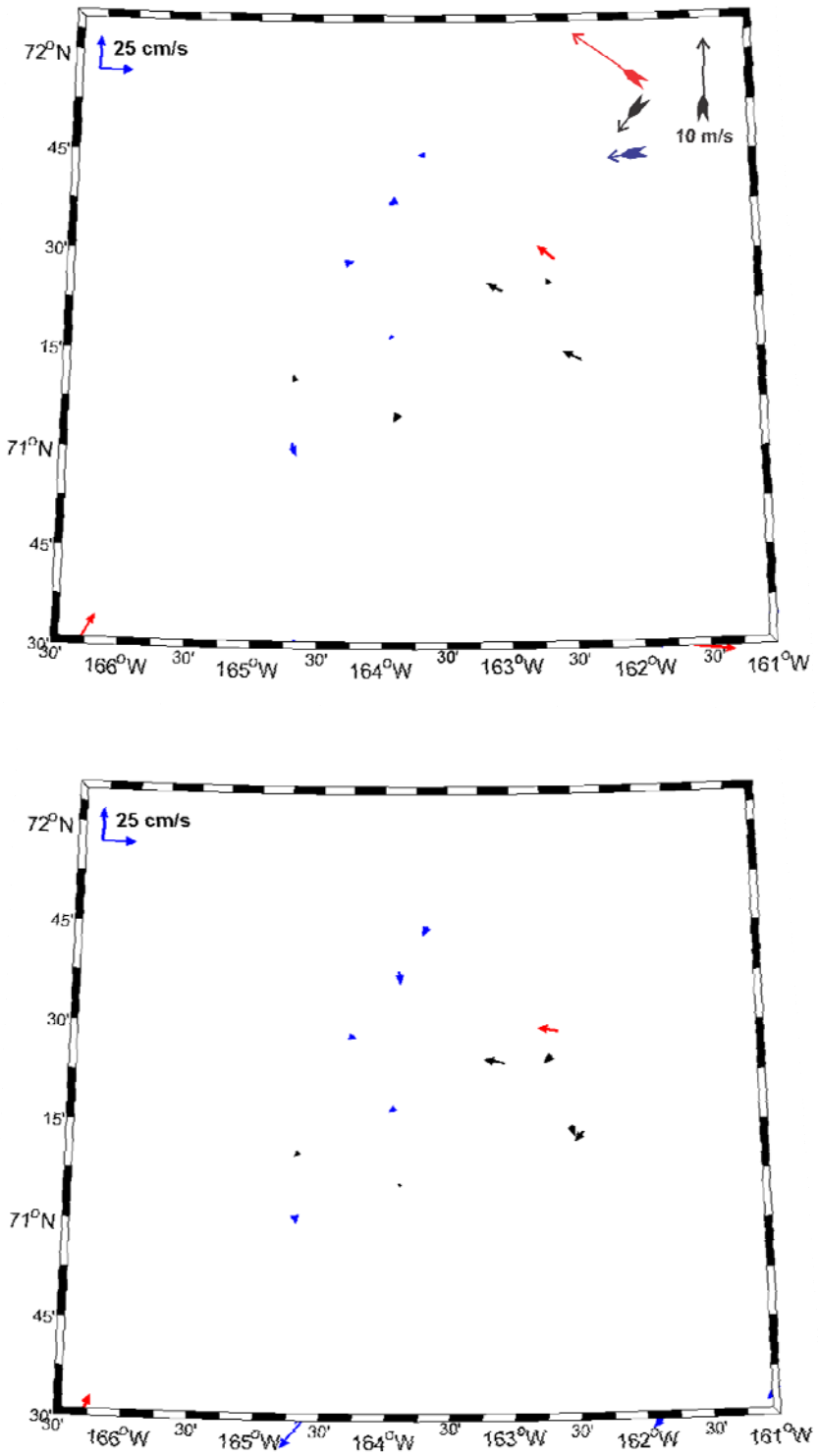

Figure 75. 6-hourly averaged current vectors for the period October 1 - 13, 2010. The upper (lower) panel shows the vectors at a depth of 11 (27) m. The vectors are color-coded and correspond to the periods: Oct. 2 – 5 (red), Oct. 6 – 8 (black) and Oct. 9 - 13 (blue), in accordance with variations in the winds. Wind vectors for each corresponding period are in the upper right-hand corner of the top panel.

Discussion

In a general sense, the results presented here for all years are consistent with prior notions of the circulation and hydrography of the northeast Chukchi Sea shelf as outlined in the introductory discussion surrounding **Figure 3**. In particular, the results suggest that the western edge of the Klondike study area lies along the eastern side of the Central Channel, where the flow is northward on average in summer at about 10 – 15 cm s^{-1} (*Weingartner et al.*, 2005). North of the channel the mean flow veers to the northeast, with the suggestion of water moving toward the west side of Hanna Shoal. Meanwhile, south of Hanna Shoal the flow is eastward at ~5 cm s^{-1}. These flows would tend to bring warm and moderately saline Bering Shelf water into the region in summer and gradually replacing the cold, saline bottom water formed the previous winter. In aggregate, the results from 2008 – 2010 suggests that there are considerable differences among years and survey areas. These differences are underscored by examining changes in the salt and heat content through time between Klondike and Burger.

Figure 76 depicts the mean salinity in the upper 20 m and lower 20 m of the water column on each survey of Klondike and Burger. (The dates of each point coincide with the starting date of each survey). Differences between dates reflect mean salinity changes in each layer through time. Note that in all years the surface layer salinity at Klondike is greater than that at Burger and reflects the fact that Burger contains more ice meltwater than Klondike, is closer to relatively fresh coastal water adjacent to the Alaskan coast, and/or meltwater to the north of Burger. In contrast, bottom water salinities are generally higher at Burger than in Klondike. This difference is due to the greater abundance at Burger of saline water remnant from the previous winter. Note also that the salinity range is larger in Burger than in Klondike. Hence the mean salinity in the upper 20 m at Burger ranges between ~29.1 (Oct. 2008) and 30.9 (Sept. 2009). The corresponding range at Klondike is between 31.7 (July 2008) and 30.3 (Sept. 2008).

The data indicate that 2008 salinities evolved quite differently than those in 2009 and 2010. In the latter two years, upper layer salinities increased by about 0.6 between the first and second cruises. In 2009, upper layer salinities then decreased by <0.1 between the second and third cruise at Klondike. At Burger salinities also decreased between the second and third cruise, by about 0.25 in 2009 and 0.65 in 2010. Lower layer salinities at Klondike were quite similar in 2009 and 2010 and in both years decreased by ~0.1 between the first and second cruise. At Burger, lower layer salinities were unchanged between the first and second cruise in both 2009 and 2010 and then decreased by ~0.2 (0.1) between the second and third cruise in 2009 (2010). By contrast, in 2008 salinities steadily declined in both areas and layers from August through September. These decreases were quite large, range from 0.65 in the lower layer at Klondike to ~1.7 in the upper layer of Burger. Hence, in 2008, the seasonal salinity changes at both sites differed substantially in magnitude and direction from those of 2009 and 2010. While the salinity differences and rates of change differed among years, the changes are either too large or of the wrong sign to be associated with vertical mixing or precipitation. They can only arise due to horizontal advection or horizontal mixing with water masses of different salinities.

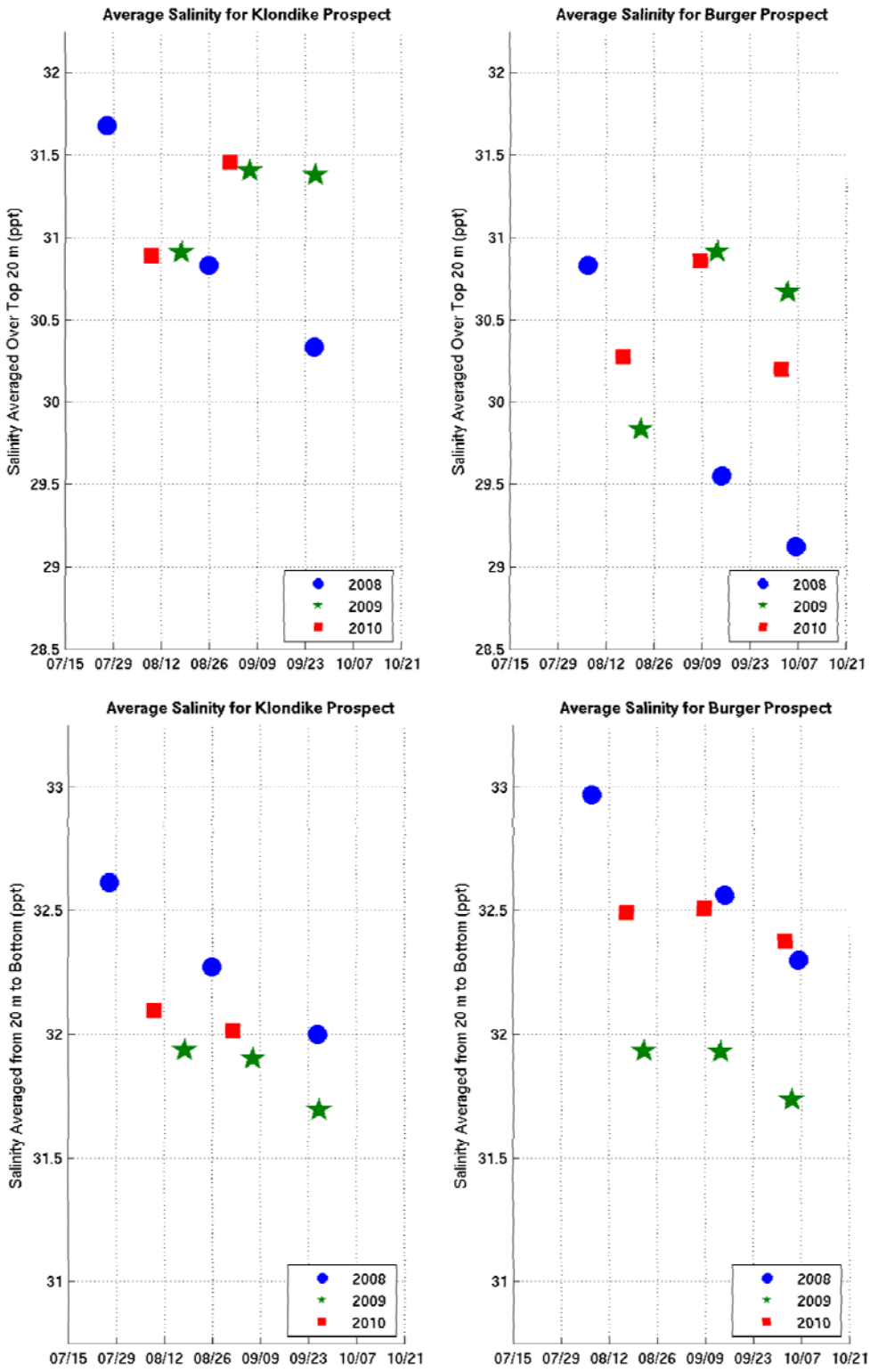

Figure 76. Average salt content between the surface and 20 m (top) and 20 m and the seabed (bottom) for Klondike (left) and Burger (right). The dates correspond to the start date of the sampling of each survey.

The heat content (Q, which reflects the depth and areally-averaged temperature) for each survey area and sampling period is shown in **Figure 77**. As expected based on earlier discussions of temperature, Q_{Burger} is generally less than $Q_{Klondike}$. This is particularly true in 2008 and 2010 when $Q_{Klondike}$ was 2 – 2.5 times greater than Q_{Burger}. In 2009 the differences in heat content between the two survey areas was only ~20% (with Klondike being warmer). Of more interest, however, is that the seasonal evolution in Q between the two areas bears little similarity with one another. For example, in 2008 $Q_{Klondike}$ builds steadily from early August through late September, whereas Q_{Burger} remains fairly constant throughout the survey period. In 2010, $Q_{Klondike}$ increased rapidly between August and September, while Q_{Burger} decreased during the same time period. In 2009, $Q_{Klondike}$ stayed more or less constant while Q_{Burger} increased and then decreased over the season. The figure also underscores the large interannual variations in both Q (especially between 2008 and the later years) and the seasonal changes in Q. For example, in 2008 and 2009 $Q_{Klondike}$ increased between the first two survey periods, whereas in 2009 there was little change in $Q_{Klondike}$ between the first two survey periods. Moreover, while $Q_{Klondike}$ decreased between the second and third surveys in 2009, it increased between the second and third surveys in 2008.

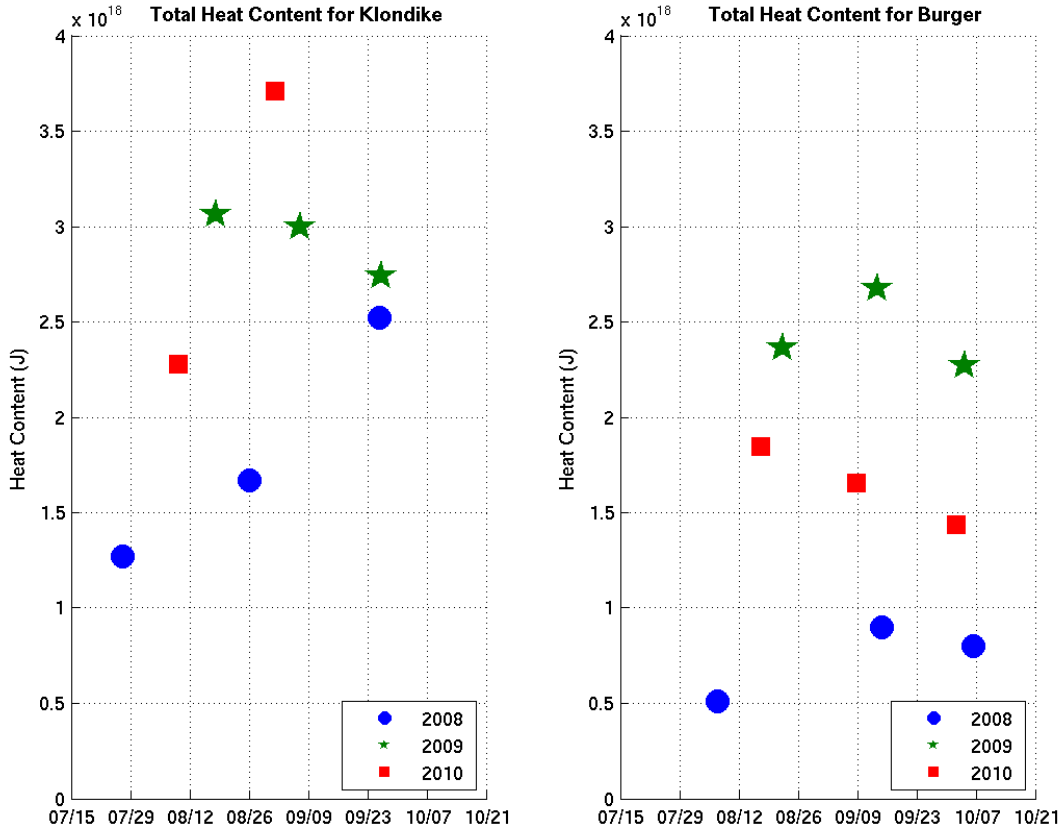

Figure 77. Total heat content in Klondike (left) and Burger (right) for each survey in all years.

Figures 76 and **77** also indicate that conditions at the beginning of each year were quite different from one another. Although some of this may reflect seasonal changes, we will argue that they are primarily a result of advective differences that occurred earlier in the spring and summer.

Figure 78 shows the mean daily values of the net (e.g., albedo-corrected ARM) shortwave radiation for each year between May 1 and October 8. Maximum values occur between late May and early July and decay thereafter due to shortening daylength and increased cloud cover. Although there is considerable day-to-day variability, the year-to-year differences in net radiation are actually quite small. This is illustrated in **Figure 79**, which shows the cumulative net solar radiation between June and early October. The first point on each curve is the cumulative May net solar radiation and each point thereafter represents the sum of the net radiation between May 1 and the end of the week indicated. Week-to-week and seasonal differences are small and generally less than 15%. Hence the large differences in heat content within the survey areas cannot be due solely to interannual differences in solar radiation.

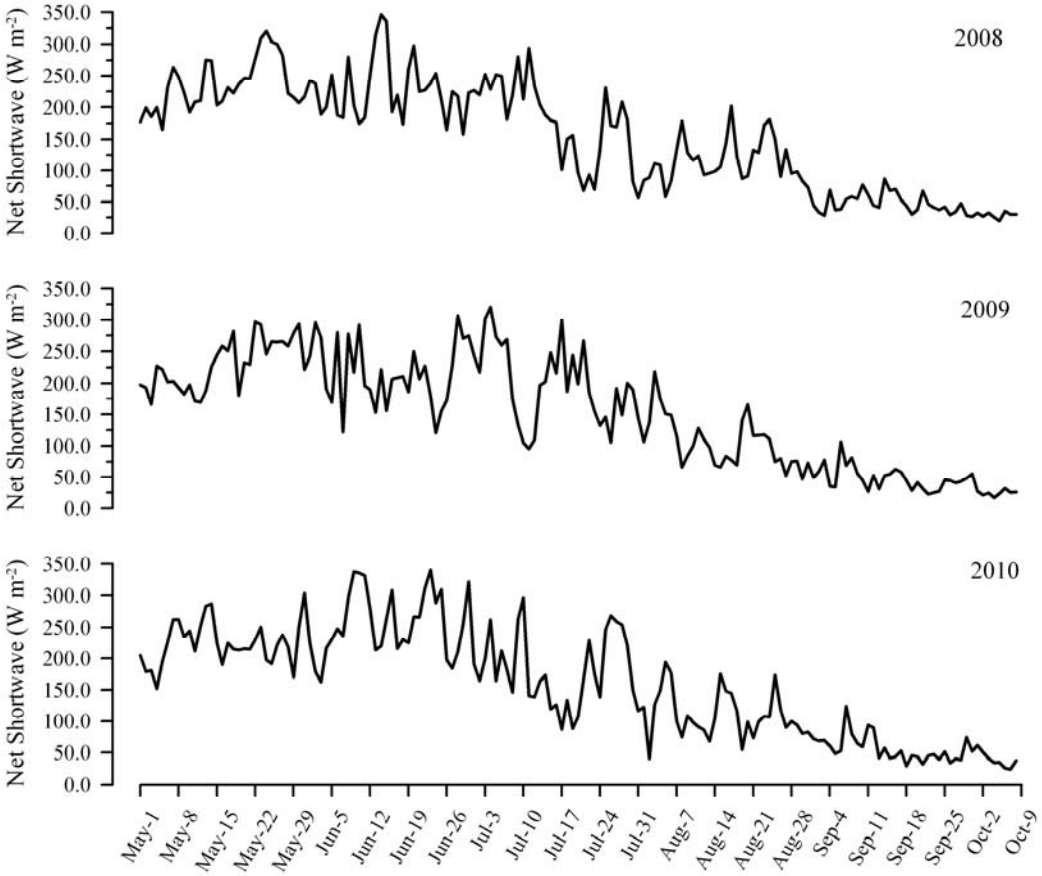

Figure 78. Mean daily net solar radiation May 1 – October 9 for 2008 (top), 2009 (middle) and 2010 (bottom). The measurements are from the ARM site in Barrow and have been corrected for an assumed albedo of 0.07 for open water.

Indeed, these differences can only be due to advection. This is illustrated simply by considering what the mean temperatures would be in a 40 m deep water column if air-sea heat exchange were the sole terms in the heat budget. The mean daily net solar radiation from May through June in 2008 and 2010 (when open water areas in the northeast Chukchi Sea were comparable) were 215 and 220 W m^{-2}, respectively. Our calculation assumes negligible latent and sensible heat fluxes and a mean daily longwave loss of 60 W m^{-2}, and an initial water temperature of -1^{o}C. Under these assumptions the upper layer temperatures would have been ~6.5^{o}C by the end of July. By

contrast mean temperatures in Klondike were ~0°C and 2.5°C in August of 2008 and 2010, respectively.

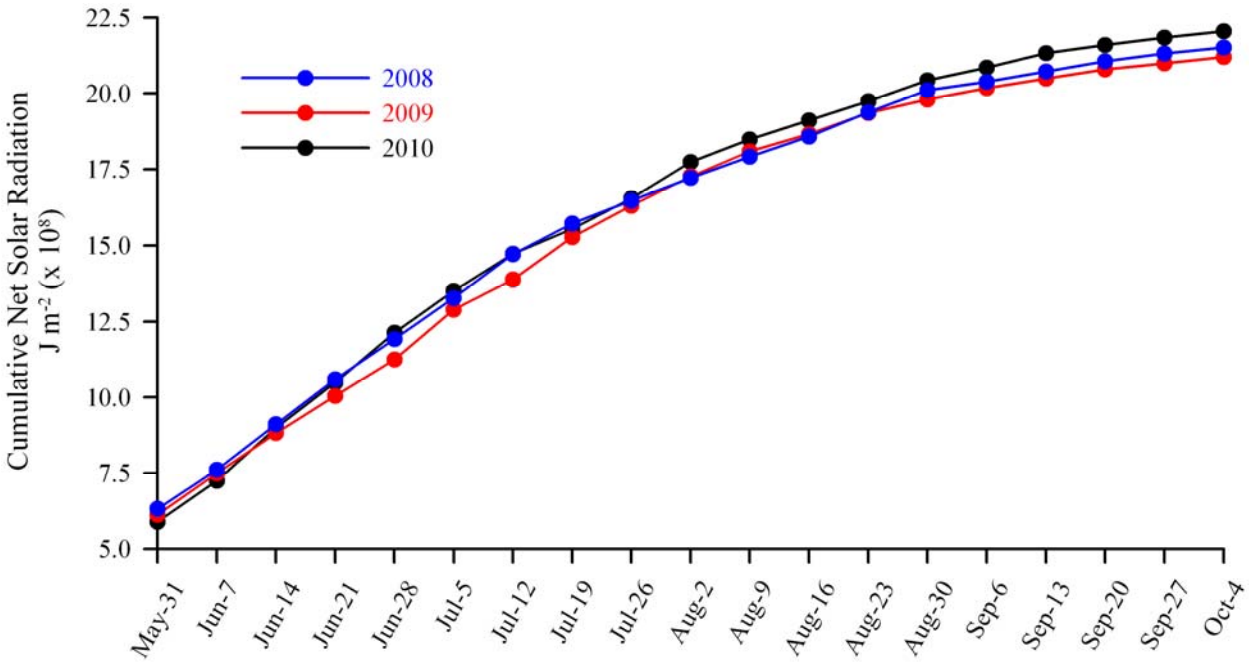

Figure 79. The cumulative net solar radiation for 2008, 2009, and 2010. The first point plotted represents the May value. Each point thereafter is plotted at weekly intervals.

Additional evidence indicating the importance of advection can be gleaned from the heat budget for each area. **Table 4** summarizes the estimates of the various air-sea heat flux terms for each sampling period. Note that the net longwave radiation term is fairly constant in all years and seasons, since this depends largely upon the sea surface temperature. The latent heat flux (evaporative cooling; Q_{latent}) is always negative (ocean cooling), while the sensible heat flux warms the ocean slightly in August, when air temperatures are warmer than sea surface temperatures, but cools the ocean in fall when air temperatures are less than sea temperatures. The net air-sea heat flux (last column of **Table 4**) suggests that the net air-sea heat exchange warms the ocean through August and cools the ocean in September. In September 2009 and 2010 net air-sea cooling rates were ~-120 W m^{-2}, whereas in September 2008 the net air-sea cooling was ~-37 W m^{-2}. These differences were largely due to differences in the sum of the latent and sensible heat fluxes, which were -27 W m^{-2} in September 2008 compared to -96 W m^{-2} and -119 W m^{-2}in 2009 and 2010, respectively. Both fluxes vary linearly with the air-sea temperature difference and with the wind speed squared. Much of the difference among years can be ascribed to the wind speeds which averaged 6 m s^{-1} in September 2008, and 7.3 m s^{-1} and 8 m s^{-1}, in September of 2009 and 2010, respectively.

Table 4. The estimated air-sea heat fluxes (W m^{-2}) for each sampling period. The sum of columns 2 – 5 yields the net air-sea heat flux ($Q_{air-sea}$) in column 6.

Sampling Period	$(1-\alpha)Q_{solar}$ +	$Q_{net\ longwave}$ +	Q_{latent} +	$Q_{sensible}$ =	$Q_{air-sea}$
8/3 – 9/3/2008	109	-58	-9	12	54
9/3 – 9/29/2008	48	-58	-25	-2	-37
8/22 – 9/13/2009	64	-60	-35	-11	-42
9/13 – 10/3/2009	39	-61	-56	-40	-118
8/17 - 9/8/2010	86	-58	-2	18	44
9/8 -10/3/2010	50	-58	-71	-48	-127

The difference between the observed heat gain (or loss) between sampling periods and the net air-sea heat exchange yields the required oceanic heat flux ($Q_{oceanic}$) contribution to maintain balance. **Table 5** summarizes these results. $Q_{oceanic}$ is highly variable between sites, sampling periods, and across years. For example, $Q_{oceanic}$ was a heat source for Klondike at all times except August 2008 when it cooled the area at a rate of -6 W m^{-2}. Advective heating at Klondike varied substantially and ranged from of 32 W m^{-2} from late August through early September 2009 to a maximum of 193 W m^{-2} over the same period in 2010. The ocean circulation also tended to warm Burger, although the circulation in August 2008 and from mid-August to early September 2010 cooled Burger. There is also no apparent relation between the ocean heat flux tendencies at Burger and Klondike. For example, from mid-August to early September 2010 the $Q_{oceanic}$ cooled Burger at -13 W m^{-2}, while it heate Klondike at 193 W m^{-2}.

Table 5. Heat budget terms (W m^{-2}) for each site and survey period. The second column is the rate of heat loss during the indicated period. This term minus the air-sea heat flux (column 3) yields the contribution by ocean heat fluxes (column 4) required for balance.

Survey Area/Date	$(\Delta Q/\Delta t)$ –	$Q_{air-sea}$ =	$Q_{oceanic}$
Klondike			
8/3 – 9/3/2008	47	54	-6
9/3 – 9/29/2008	120	-37	159
8/22 – 9/13/2009	-12	-42	32
9/13 – 10/3/2009	-47	-118	71
8/17 - 9/8/2010	235	44	193
Burger			
8/3 – 9/3/2008	46	54	-8
9/3 – 9/29/2008	-14	-37	23
8/22 – 9/13/2009	43	-42	85
9/13 – 10/3/2009	-54	-118	64
8/17 - 9/8/2010	31	44	-13
9/8 -10/3/2010	-33	-127	94

We may further partition $Q_{oceanic} = Q_{Ekman} + Q_{other\ advection}$ as described previously and use this relation to evaluate $Q_{other\ advection}$. **Table 6** summarizes these results. Based on the satellite-derived sea surface temperature gradients and the wind-driven Ekman transports (assumed

limited to the upper 15 m of the water column), we find that the cross-shelf Ekman heat fluxes act to cool both Burger and Klondike in 2008 and 2009. (Note that satellite information is not available for 2010. However, glider measurements made in late September 2010 indicate that the cross-shelf temperature gradient was such that the Ekman transport was a source of heat for Burger and Klondike. We have not included these results since they are too few in number to regard as representative of the sampling period.) Q_{Ekman} varies between -20 and -48 W m^{-2}.

Table 6. Summary of $Q_{oceanic}$, the cross-shelf Ekman heat flux (Q_{Ekman}) and $Q_{other\ advection}$. Also included are the cross-shelf Ekman current speed (u_E) and $\partial T/\partial x$, the cross-shelf temperature gradient. A negative $\partial T/\partial x$ implies colder water to the east of Klondike or Burger. Negative u_E implies westward cross-shelf flow. $Q_{oceanic} = Q_{other\ advection}$ for 2010 and these values are italicized.

Survey Area/Date	$Q_{oceanic}$ (W m^{-2})	u_E (m s^{-1})	$\partial T/\partial x$ (10^{-5} °C m^{-1})	Q_{Ekman} (W m^{-2})	$Q_{other\ advection}$ (W m^{-2})
Klondike					
8/3 – 9/3/2008	-6	-0.04	-1.8	-45	39
9/3 – 9/29/2008	159	-0.04	-2.0	-48	207
8/22 – 9/13/2009	32	0	-5.3	0	32
9/13 – 10/3/2009	71	-0.06	-0.5	-20	91
8/17 - 9/8/2010	193	-0.03	Na	na	*193*
Burger					
8/3 – 9/3/2008	-8	-0.04	-1.8	-45	37
9/3 – 9/29/2008	23	-0.04	-1.6	-40	63
8/22 – 9/13/2009	85	0	-5.0	0	85
9/13 – 10/3/2009	64	-0.06	-0.6	-22	86
8/17 - 9/8/2010	-13	-0.03	Na	na	*-13*
9/8 -10/3/2010	94	-0.01	Na	na	*94*

It is not feasible to attempt to partition $Q_{other\ advection}$ further except to note that it would include the northward and/or eastward (from the Central Channel) transports of heat into either Burger or Klondike as suggested by the mean flows in **Figure 3**, and the previously described water property distributions and ADCP data. We can estimate the range in northward velocities (v) required to satisfy this term for various meridional temperature gradients ($\partial T/\partial y$). The latter are likely to range from 1 - 3°C/2° latitude (with temperature decreasing to the north). Thus we set:

$Q_{other\ advection} = \rho C_p h_T v \partial T/\partial y$ and solve for v, e.g.,

$$\frac{Q_{other\ advection}}{\rho C_p h_T\, \partial T/\partial y} = v$$

Table 7 summarizes these calculations assuming a uniform velocity over a water depth of h_T = 40 m. For the 2010 sampling periods we evaluate v using $Q_{oceanic}$. Values derived from this term are italicized in **Table 7** and represent averages for the period of interest. The derived values of v appear reasonable except those in Klondike for the periods of Sept. 3 - 29, 2008 and Aug 17 – Sept. 8, 2010 for an assumed south-north temperature gradient of -0.9 x 10^{-5} °Cm^{-1} (e.g., 1°C/2° latitude). For these cases the velocities exceed 0.25 m-s^{-1}, which seems to be an unreasonably

large average for the periods of time considered. While these calculations do not prove that these were the conditions experienced during the various sampling dates, they underscore the sensitivity of thermal conditions in Klondike and Burger to relatively small changes in velocity and/or temperature gradients. The estimated flows are northward on average for each period with the exception of the period from 8/17 – 9/8 in 2010 at Burger. At this time, we find that $Q_{other\ advection}$ was -13 W m^{-2} so that oceanic heat fluxes acted to cool Burger, while other oceanic heat sources were warming Klondike.

Table 7. The partitioning of $Q_{oceanic}$ into the cross-shelf Ekman heat flux and $Q_{other\ advection}$. Also included are the cross-shelf Ekman current speed (u_E) and $\partial T/\partial x$, the cross-shelf temperature gradient. Negative values of $\partial T/\partial x$ imply colder water to the east of Klondike or Burger. Negative values of u_E imply westward cross-shelf flow. Italicized values are periods when there was no data available for estimating the zonal temperature gradient.

Survey Area/Date	$Q_{other\ advection}$ (W m^{-2})	v (m s^{-1}) for $\partial T/\partial y = -1.35x10^{-5o}Cm^{-1}$	v (m s^{-1}) for $\partial T/\partial y = -0.9x10^{-5\ o}Cm^{-1}$
Klondike			
8/3 – 9/3/2008	35	0.02	0.06
9/3 – 9/29/2008	207	0.09	0.28
8/22 – 9/13/2009	32	0.01	0.03
9/13 – 10/3/2009	91	0.04	0.12
8/17 - 9/8/2010	*193*	0.09	0.27
Burger			
8/3 – 9/3/2008	37	0.02	0.06
9/3 – 9/29/2008	63	0.03	0.09
8/22 – 9/13/2009	85	0.04	0.12
9/13 – 10/3/2009	86	0.04	0.12
8/17 - 9/8/2010	*-13*	*-0.01*	*-0.03*
9/8 -10/3/2010	*94*	*0.04*	*0.12*

The heat budget results are summarized diagrammatically for each period and study area in **Figure 80**.

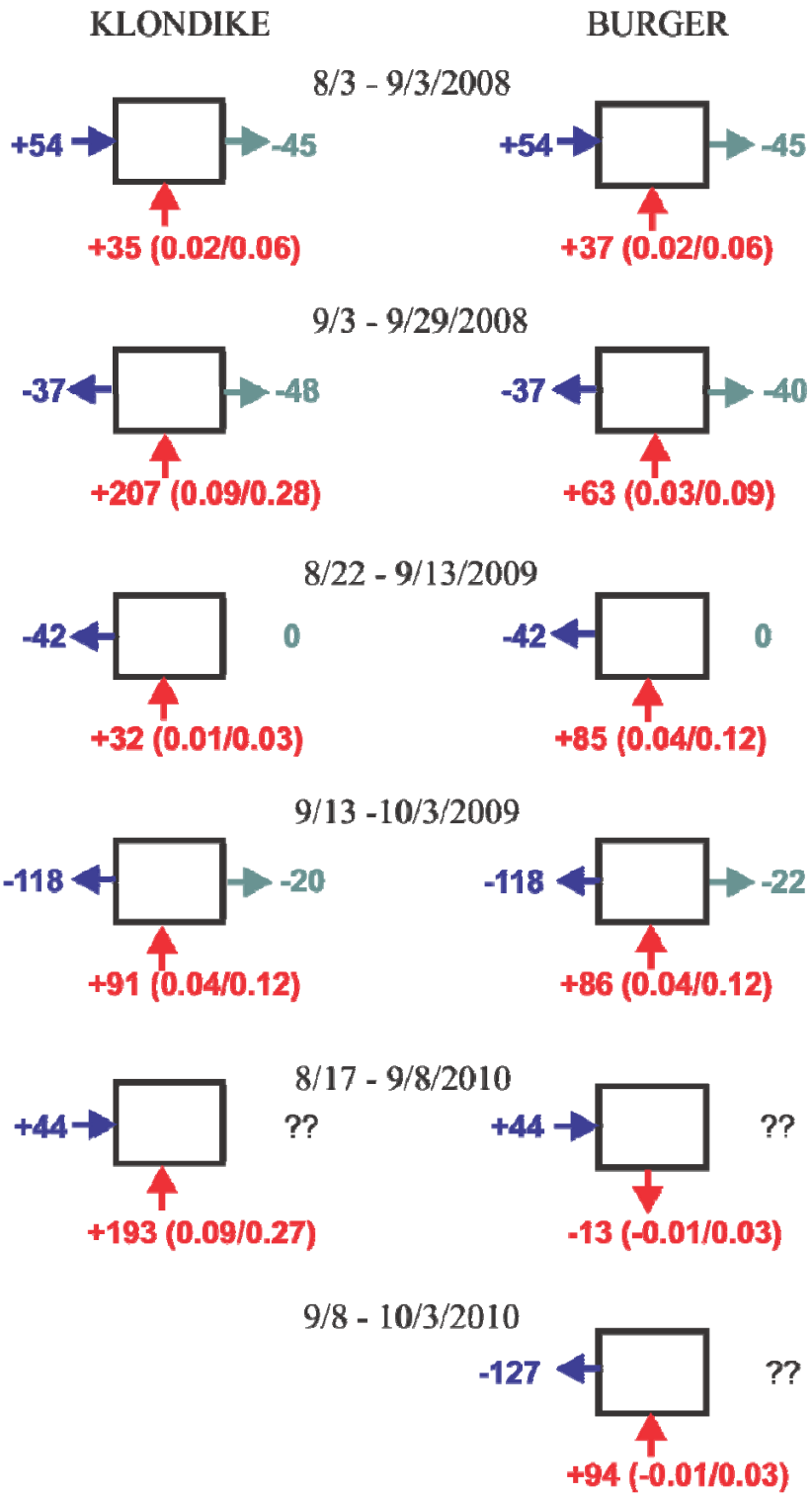

Figure 80. Summary of the heat gains (arrows pointing into the box) and losses (arrows pointing out of the box) due to air-sea heat exchange (blue), Cross-shelf Ekman heat flux (green) and other ocean heat fluxes (red). Red numbers in parentheses are estimated mean meridional velocities assuming that the other ocean heat fluxes are due to meridional advection for two different choices of the meridional temperature gradient (see **Table 4** for details).

Summary

This analysis of three years (2008 – 2010) of wind, sea ice distributions, air-sea heat exchanges, and hydrographic data underscores the large interannual and spatial variability in conditions over the northeast Chukchi Sea shelf, particularly within the Klondike and Burger study areas.

Spring-summer sea ice retreat differed substantially among these years. In May 2008 and 2010, large expanses of open water spread westward across the northeast and central Chukchi shelf from the NW coast of Alaska apparently due to strong westward winds. This development occurred well-before late May when sea ice began to retreat northward through Bering Strait. Hence in these years, the ice initially retreated from east to west in spring. By contrast, sea ice began retreating northward through Bering Strait in early May 2009, with the retreat primarily occurring from south to north. In fact, the northeast shelf did not open substantially until similarly strong westward winds developed in late June 2009. Differential ice-retreat patterns may have important biological consequences, since patterns of primary production will depend upon the ice cover. Hence ice retreat in May over the northeast shelf provides pelagic phytoplankton with abundant light levels at the same time that marine nutrient concentrations are high (Codispoti, 2005). Such conditions can support a vigorous, open-water spring bloom as apparently occurred in May 2008. Much of this production is likely carried to the sediments to support benthic communities, since zooplankton populations are probably small at this time. By contrast, the ice conditions in May and June 2009, would favor ice algal production well into June.

Although our analysis is limited, it does not appear that the spring ice retreat is a harbinger of late summer ice conditions. While ice retreated more slowly in 2009 than in the other years, the northeast shelf was effectively ice-free by mid-August. This portion of the shelf was similarly ice-free by mid-August 2010. By contrast, substantial ice remained trapped over Hanna Shoal in 2008. The proximal reasons for these differences are the more persistent winds from the northeast in August 2008 compared to 2009 and 2010. The winds presumably delayed ice retreat by forcing ice southward. They may also have retarded oceanic heat transport into the Burger area, which would reduce ice melting.

We find little interannual variability in the net solar radiation between May and mid-August (when the other air-sea heat fluxes are relatively small). This period effectively defines the "heating" season for the ocean in terms of air-sea heat fluxes. Given the consistency in net solar radiation amongst years, one might expect that the early ice retreat in May 2008 and 2010 might have led warmer temperatures than in 2009. However, this was not the case. August 2008 temperatures in both Klondike and Burger were the coldest observed. In spite of the delayed ice retreat in 2009, August temperatures in Klondike were the warmest observed and the mean August temperatures in Burger were only slightly warmer in 2010 compared to 2009. These results suggest that variations in summer heat content in these areas of the shelf are relatively insensitive to the seasonal patterns of ice retreat. Instead, it appears that the August water properties are largely set by the properties of water masses transported northward from Bering Strait from May through July.

Our results show that atmospheric cooling begins in late August/early September over the central Chukchi Sea shelf. These cooling rates can differ substantially from year-to-year as exemplified by the fourfold difference in cooling between September 2009 (-118 W m^{-2}) and September 2008 (-37 W m^{-2}). However, northward heat transport of waters from the Bering Strait may continue well into September at rates that exceed the cooling rates associated with air-sea heat fluxes.

The following paragraphs summarize our findings for each year. For simplicity we will use the term "northward advection" herein, emphasizing that this advection may include transport from the west, e.g., the Central Channel and its extension to the north as suggested by the 2010 results.

In August of 2008, both Klondike and Burger were colder and saltier than in 2009 and 2010. During this month Klondike experienced a net heat gain due to air-sea heat exchange, primarily solar radiation. On balance, the ocean circulation acted act to cool Klondike. The net cooling by oceanic advection was due to westward wind-driven Ekman transport that brought cooler coastal water into the region. Cooling by Ekman transport was buffered somewhat by other advective processes, most likely northward advection of warm water into the area from Bering Strait. At this time Klondike also freshened, with the freshening due to the gradual replacement of saline winter water by lower salinity water advected northward and/or carried westward in the surface Ekman transport. During the same period Burger also warmed and freshened by the same combination of mechanisms. These changes also led to an increase in stratification at both locations between the first and second surveys.

In September of 2008, Klondike warmed substantially, while Burger cooled slightly. Throughout the month, both regions lost heat to the atmosphere and were cooled by cross-shelf Ekman heat transport. We ascribe these different responses to the much larger northward advection of heat into Klondike compared to Burger. The net effects of advection contributed to a further decrease in salinity at both locations. Stratification remained essentially unchanged between the second and last surveys in 2008.

In 2009, air-sea heat exchange cooled the shelf between the first and second surveys. This cooling was nearly buffered by northward advection of heat at Klondike. Oceanic heat advection was even greater during this time at Burger. Advection also increased the salinity at the surface but freshened the deeper layer at both locations at this time. Again this is consistent with the gradual replacement of saline deep water and fresher surface water by more moderate salinity water advected from the south. Cross-shelf Ekman transport still tended to cool both regions, but it was substantially smaller in 2009 compared to 2008, due to the reduction in winds from the northeast. In contrast to 2008, stratification substantially decreased at both locations between the two surveys.

Between the second and third surveys of 2009, strong atmospheric cooling ensued, but the effects of this cooling were nearly offset by continued northward advection of warmer water into both areas. Upper layer salinities remained virtually unchanged at Klondike during this period, but decreased substantially at Burger due to surface water advection from the northeast (**Figures 54 – 56**). At both locations lower layer salinities also decreased, again due to replacement of saline, winter water by more moderate-saline waters. Stratification continued to decrease at Klondike, while it remained virtually the same at Burger.

Klondike warmed rapidly between the first two surveys in 2010. This warming was largely due to oceanic advection which was nearly 5 times larger than the net heat flux from the ocean to the atmosphere. As in 2009, this warming was accompanied by an increase in salinity in the upper layer and a slight salinity decrease in the lower layer. In contrast, Burger cooled over the same time period due to ocean advection. The cold water had to have been transported from the east or northeast since temperatures to the west and south were substantially warmer. Moreover, salinity increased in the surface layer at Burger and was largely unchanged in the lower layer. It thus appears that the flow fields between these two regions were substantially different during these sampling periods. Stratification decreased at both sites between these two periods.

Between the second and third surveys, the ocean lost heat to the atmosphere. Within Burger, this cooling was buffered somewhat by an influx of warm water from the south and the west. Warming was also accompanied by a salinity decrease in both the surface and bottom layers, which led to a reduction in stratification.

The analysis of these data continues. We anticipate refining these calculations using radar data from 2010 and, if possible, the mooring data obtained by ConocoPhillips and Shell from the Klondike and Burger prospects for each year.

Acknowledgements

The authors thank the captains and crews of the vessels that efficiently collected the CTD and ADCP data sets discussed herein. We also thank Jeff Hastings and Sheyna Wisdom for their efficient co-ordination in the planning and execution of the field programs and planning meetings. This work benefited from many interesting discussions with R. H. Day, program Chief Scientist, R. Hopcroft, and A. Blanchard.

References

Aagaard, K., Current, CTD, and pressure measurements in possible dispersal regions of the Chukchi Sea, Outer Continental Shelf Environmental Research Program, Final Rep., Princ. Invest. 57, pp. 255-333. Dept., of Commerce/Dept. of Interior, Anchorage, AK, 1988.

Aagaard and Roach, Arctic ocean-shelf exchange: Measurements in Barrow Canyon, *J. Geophys. Res.*, 95: 18163-18175, 1990.

Aagaard, K., C. H. Pease, A. T. Roach, and S. A. Salo, *Beaufort Sea Mesoscale Circulation Study – Final Report*, NOAA Tech. Mem, ERL PMEL-90, 114 p., 1989.

Aagaard, K., J.H. Swift, and E.C. Carmack, Thermohaline circulation in the Arctic Mediterranean seas, *J. Geophys. Res*., 90, 4833-4846, 1985.

AMAP Arctic Pollution 2002: Persistent Organic Pollutants, Heavy Metals, Radioactivity, Human Health, Changing Pathways. Arctic Monitoring and Assessment Programme (AMAP), Oslo, Norway, xii+112 pp., 2003.

Bignami, F., R. Santoleri, M. Schiano, and S. Marullo, 1991. Net longwave radiation in the Westwern Mediterranean Sea, Poster Session at the 20th General Assemby of the International Union of Geodesy and Geophysisc, IAPSO, Vienna, August, 1991.

Brower, Jr., W.A. R.G. Baldwin, Jr., C.N. Williams, J. L. Wise, and L.D. Leslie. 1988. *Climate atlas of the outer continental shelf waters and coastal regions of Alaska*, volume 1, Gulf of Alaska. Asheville, NC: National Climatic Data Center.

Carmack, E. C., Circulation and mixing in ice-covered waters, in *The Geophysics of Sea Ice*, edited by N. Unstersteiner, pp. 641 – 712, Plenum, New York, 1986.

Carmack, E,C., and D. C. Chapman, Wind-driven shelf/basin exchange on an Arctic shelf: the joint roles of ice cover extent shelf-break bathymetry. *Geophys. Res. Lett*., 30(14): 1778 doi: 10.1029/203GL017526, 2003.

Coachman, L.K., Aagaard, K., and Tripp, R.B., *Bering Strait: The Regional Physical Oceanography*, 172 pp., University of Washington Press, Seattle, Washington, 1975.

Codispoti, L., C. Flagg, V. Kully, and J. H. Swift (2005), Hydrographic conditions during the 2002 SBI process experiments. *Deep-Sea Res., II*, 52 (24-26): 3199 – 3226.

Cooper, L. W., J. Grebmeier, T. Whitledge, and T. Weingartner, The nutrient, salinity, and stable oxygen isotope composition of Bering and Chukchi sea waters in and near Bering Strait, *J. Geophys. Res*., 102: 12563 – 12578, 1997.

Danielson, S. L., K. Aagaard, T. Weingartner, S. Martin, P. Winsor, G. Gawarkiewicz, and D. Quadfasel. 2006. The St. Lawrence polynya and the Bering shelf circulation: New observations and a model comparison. *J.Geophys. Res., 111*. C09023, doi:10.1029/2005JC003268.

Gawarkiewicz G and D. C. Chapman, A numerical study of dense water formation and transport on a shallow, sloping continental shelf, *J. Geophys. Res*., 100: 4489-4508, 1995.

Gawarkiewicz, G., T. Weingartner, and D. Chapman, Sea Ice Processes and Water Mass Modification and Transport over Arctic Shelves. pp. 171-190 *in* K. H. Brink and A. R. Robinson, (eds.), *The Sea: Ideas and Observations on Progress in the Study of the Seas*, Vol. 10, John Wiley and Sons, New York, 1998, 604 p.

Hansell, D., T.E. Whitledge, and J.J. Georing, Patterns of nitrate utilization and new production over the Bering-Chukchi shelf, *Cont. Shelf Res*., 13, 601 – 627, 1993.

Liu, A. K., C. Y. Peng, and T. J. Weingartner, Ocean-ice interaction in the marginal ice zone using SAR. *J. Geophys. Res*., 99, 22391 – 22400, 1994.

Martin, S., amd R. Drucker, 1997, The effect of possible Taylor columns on the summer sea ice retreat in the Chukchi Sea *J. Geophys. Res*., 102, 10,473-10,482.

Muench, R. D., Mesoscale Phenomena in the Polar Oceans. pp 223-286 *in* W.O. Smith, Jr., (ed.), *Polar Oceanography, Part A: Physical Science*, Academic Press, New York, 1990, 406 p.

Muench, R. D., C. H. Pease, and S.A. Salo, Oceanographic and meteorological effects on autumn sea-ice distribution in the western Arctic. *Ann. Glaciol*., 15: 171-177, 1991.

Münchow, A., E. C. Carmack, and D. A. Huntley, Synoptic density and velocity observations of slope waters in the Chukchi and East Siberian Seas, *J. Geophys. Res*., 105: 14103-14119, 2000.

Münchow, A., T. Weingartner, and L. Cooper, The summer hydrography and surface circulation of the East Siberian Shelf Sea, *J. Phys. Oceanogr*., 29: 2167 – 2182, 1999.

Münchow, A. and E. C. Carmack, Synoptic flow and density observations near an Arctic shelfbreak, *J. Phys. Oceanogr*., 6, 461 - 470, 1997.

Nikolopoulos, A., R.S. Pickart, P.S. Fratantoni, K. Shimada, D.J. Torres, and E.P. Jones. 2009. The western Arctic boundary current at 152°W: Structure, variability, and transport. *Deep-Sea Research II* 56: 1164-81.

Spreen, G., L. Kaleschke, and G.Heygster (2008), Sea ice remote sensing using AMSR-E 89 GHz channels. *J. Geophys. Res.*, 113, C02S03, doi:10.1029/2005JC003384.

Paquette, R. G., and R. H. Bourke, Ocean circulation and fronts as related to ice melt-back in the Chukchi Sea, *J. Geophys. Res*., *86*, 4215-4230, 1981.

Walsh, J. E., W. L. Chapman, D. H. Portis, 2009: Arctic Cloud Fraction and Radiative Fluxes in Atmospheric Reanalyses. *J. Climate*, **22**, 2316–2334. doi: 10.1175/2008JCLI2213.1

Walsh, J.J., C.P. McRoy, L.K. Coachman, J.J. Goering, J.J. Nihoul, T.E. Whitledge, T.H. Blackburn, P.L. Parker, C.D. Wirick, P.G. Shuert, J.M. Grebmeier, A.M. Springer, R.D. Tripp, D.A. Hansell, S. Djenedi, E. Deleersnijder, K. Henriksen, B.A. Lund, P. Andersen, F.E. Müller-Karger, and K. Dean, Carbon and nitrogen cycling within the Bering/Chukchi seas: Source regions for organic matter affecting AOU demands of the Arctic Ocean, *Progr. Oceanogr*., 22, 277-359, 1989.

Walsh, J.J., D.A. Dieterle, F.E. Muller-Karger, K. Aagaard, A.T. Roach, T.E. Whitledge, and D. Stockwell, CO2 cycling in the coastal ocean. II. Seasonal organic loading of the Arctic Ocean from source waters in the Bering Sea, *Cont. Shelf Res*., 17,1-36, 1997.

Weingartner, T. J., Seth L. Danielson, Jeremy L. Kasper and, Stephen R. Okkonen. Circulation and Water Property Variations in the Nearshore Alaskan Beaufort Sea, Final Report, OCS Study MMS 2005-028, 155 p., 2009.

Weingartner, T.J., S. Danielson, and T. C. Royer. Freshwater Variability and Predictability in the Alaska Coastal Current *Deep-Sea Research*, 52: 169 – 192, 2005a.

Weingartner, T., K. Aagaard, R. Woodgate, S. Danielson, Y. Sasaki, and D. Cavalieri, Circulation on the North Central Chukchi Sea Shelf, *Deep-Sea Res., Pt. II*, 52: 3150-3174, 2005b.

Weingartner, T.J., S. Danielson, Y. Sasaki, V. Pavlov, and M. Kulakov, The Siberian Coastal Current: A wind- and buoyancy-forced Arctic coast current *J. Geophys. Res*., 104: 26697 – 29713, 1999.

Weingartner, T.J., D.J. Cavalieri, K. Aagaard, and Y. Sasaki, Circulation, dense water formation, and outflow on the northeast Chukchi shelf, *J. Geophys. Res*., 103: 7647 – 7661, 1998.

Winsor, P., and D. C. Chapman (2004), Pathways of Pacific Water across the Chukchi Sea: A numerical model study. *Journal of Geophysical Research*, 109, C03002, doi: 1029/2003JC001962.

Woodgate, R.A., K. Aagaard, Weingartner, T. J., Changes in the Bering Strait fluxes of volume, heat and freshwater between 1991 and 2004. (in press, *Geophys. Res. Lett*.)

Woodgate, R. A. and K. Aagaard, Revising the Bering Strait Freshwater flux into the Arctic Ocean *Geophys. Res. Lett*., L02602, doi:10.1029/2004GL021747, 2005.

Woodgate, R. A., K. Aagaard, and T. Weingartner, Monthly temperature, salinity, transport variability for the Bering Strait. throughflow. *Geophys. Res. Lett*., 32, L04601, doi:10.1029/2004GL021880, 2005.

Woodgate, R. A., K. Aagaard, and T. Weingartner, A Year in the Physical Oceanography of the Chukchi Sea: moored measurements from autumn 1990-91, *Deep-Sea Res., Pt II*, 52, 3116-3149, 2005.